SEDIMENTOLOGY AND STRATIGRAPHY OF A MATRIX-POOR TO MATRIX-RICH DEPOSITIONAL CONTINUUM IN PROXIMAL BASIN FLOOR STRATA, UPPER KAZA GROUP, WINDERMERE SUPERGROUP, B.C., CANADA.

Nataša Popović

Thesis submitted to the
Faculty of Graduate and Postdoctoral Studies
in partial fulfillment of the requirements
for the M.Sc. degree in Earth Sciences

Ottawa-Carleton Geoscience Centre
Faculty of Science
University of Ottawa

©Nataša Popović, Ottawa, Canada, 2016

Abstract

Matrix-rich strata (20-70% mud matrix) have been increasingly recognized in deep-marine systems. These beds are thought to be deposited from mud-rich flows in a distal basin-floor setting; however they remain poorly understood, partly because details of lateral lithological changes are poorly known. In this study, matrix-rich strata are common in proximal basin-floor strata of the Neoproterozoic Windermere Supergroup. The objective of this thesis is to provide detailed description and interpretation of the lithological and mineralogical make-up and lateral facies trends of matrix-rich strata in in a unit 40 m thick and 800 m wide. Here, stratigraphic and petrographic analyses identified five facies: classic turbidites; sandstones; clayey sandstones; sandy claystones and fine-grained banded couplets, which laterally are arranged systematically from matrix-poor sandstones to thin-bedded turbidites. This lateral change is interpreted to represent a depositional continuum along the margins of an efflux jet that formed immediately downflow of an avulsion node.

Acknowledgements

First and foremost, I would like to whole-heartedly thank my supervisor, Dr. Bill Arnott, for the opportunity to work on such an amazing project and for all of his countless hours of support, guidance and mentoring. Your positive energy and love of geology is contagious, and I am ever thankful to have been surrounded by such brilliance and enthusiasm.

This project would not have been possible without all those involved in the Windermere Consortium: NSERC, BP, Chevron, Statoil, Canadian Natural, Nexen, Apache, Anadarko and Husky Energy – Thank you for making the field work and this project possible and for your continued support.

To the Windy crew: Viktor, Mike, Dave, Lindsay, Gerry, Lillian, Katrina, Anika, Derrick, Curran, Dylan, Omar, Michelle, Thomas…without you guys I would have been a lonely island, thank you for being the best research group ever… for the countless advice, for listening during our long meetings, for all the memories, geology and beers shared. I would especially like to thank Michelle, Thomas, Alex and Kim for all of their help in the field and for making each day a fun adventure.

I would also like to thank the support staff at UOttawa: Hélène, Lisa and Caroline. Thank you for always answering my many questions and for always making the department feel like home. A special thanks goes to my friend George Mrazek for preparing and cutting some wonderful thin sections that were so instrumental in my thesis – Děkuji!

To my Ottawa famjam: words cannot describe how grateful I am to have had you all by my side during this experience. Gujaničići- Hvala! For always being there and for helping me find my way in Ottawa. To my FG KOLO girls: thank you, for literally holding my hands through all of this, for being my weekly pick me up, for supporting me and for all of the folki love. Boškovići: Thank you doesn’t even begin to express my love and gratitude for you guys. I am forever grateful to you for opening your home and hearts up to me, I’m so happy to be part of the Bošković famjam.

To my sisters, Dragana and Melanija: Tenk Ju, for all your support, for dealing with all my ups and downs and for always being there for me and believing in me – especially when I didn’t believe in myself. And of course, to my mama and tata: Thank you for always pushing me to be the best version of myself, for always supporting me (through everything) and for allowing me to chase after my dreams.

Lastly, I would like to dedicate this thesis to my baba Milka and deda Srećo. You were the first people to open my eyes and mind to the joy of learning and always encouraged my curiosity…that curiosity is what led me to this field and to my passion. I would not be the geoscientist or woman I am today without your love and guidance.

Table of Contents

List of Figures

the layers exchange momentum as a result of turbulent diffusion. Where the viscous sublayer itself shows strong particle grading, the bed may essentially grade upwards into the flow, and the velocity profile may appear convex upwards near the bed (profile 2). (C) Increasing viscosity and strength in the viscous sublayer result in the appearance of a dynamic interface at the top of or within the upper part of the viscous sublayer. Below this interface, the cohesive strength of the viscous sublayer prevents settling of mud, quartz and feldspar grains, whereas above this interface, denser grains, mainly quartz and feldspar, are still settling towards the bed. Sediment accumulation at this interface initiates plug formation within the flow and deposition of light- band plug sediment on top of the viscous sublayer. Foundering of these early deposited light- band sediments into the underlying, still- shearing sublayer increases the particle content and strength of the upper part of the sublayer. Freezing of the sediment- charged upper part of the viscous sublayer may also contribute to plug development. Schematic velocity profiles 1–3 show velocity evolution within the flow and viscous sublayer as the plug forms and, later, as sediment accumulates on and thickens the plug, in part by forcing compaction and freezing in the underlying shearing sublayer (profiles 2 and 3). (D) Settling mud and sand continue to accumulate on top of the plug. Brief working as bed load beneath the overlying turbulent flow forms the crudely layered sandstone of light bands. This current- deposited sandstone continues to load into the underlying mud- rich plug/viscous sublayer. Deposition on top of the plug eventually causes collapse, freezing and deposition of the entire viscous sublayer. At this point, the bed surface

Chapter 1: Thesis Introduction

1.1 Thesis Rational

The deep marine basin floor is the most distal and final depositional site for clastic sediment. Here the largest (volumetric) sediment bodies on earth, termed submarine fans, are currently being investigated by both academe and industry — the latter because of their proven hydrocarbon potential (Talling et al., 2012). However their remote and deep-water location has for many years made scientific investigation problematic. Recent advances in seismic imaging, in particular, a more voluminous library of drill core, have provided many new insights into the deep-sea sedimentary record. However, due to the limited vertical resolution of seismic, the wide spacing of wells, and short length of most cores many of the vertical, but perhaps more importantly, lateral centimeter-to decameter-scale stratal trends remain poorly understood. These data are typically obtained by studying well-exposed ancient deep-marine, seismic-scale outcrop analogues to bridge the gap between low resolution, large-scale 2D and 3D seismic data and high resolution 1D core observations.

It is widely known that sediment-gravity flows (i.e. turbidity currents and debris flows) are the main agents that transport and deposit sediment in the deep marine (Middleton and Hampton, 1976; Lowe, 1979, 1982). Work by geologists for the past several decades has been devoted almost exclusively to the sand-rich part of the deep-marine sedimentary record. Recently, however, sandstones with high matrix content (>30%) have been increasingly recognized and debated, especially in terms of the physical behavior of the flow and the depositional processes that emplace these beds. Matrix-rich beds are generally thought to represent deposition from a changing or transitioning flow state from laminar to turbulent flow and have been referred to by a variety of terms, including: “slurry deposits” (Lowe and Guy, 2000; Lowe et al, 2003), “linked debrites” (Haughton et al. 2003; Amy and Talling 2006; Haughton et al. 2009), “cogenetic debrite-turbidite beds” (Talling et al, 2004) and “hybrid event beds” (Hodgson, 2009; Pyles and Jennette, 2009), and typically are reported from the distal and lateral parts of basin-floor turbidite systems. In this study, however, matrix rich deposits, hereafter termed “matrix-rich strata” or “sandy claystones”, crop out in strata interpreted to have been deposited not only on the proximal part of the basin floor, but also were deposited by processes that contrast significantly to those proposed by earlier authors.

At the Castle Creek study area, strata of the Upper Kaza Group are well exposed and provide a remarkable and unique opportunity to document the centimeter to meter scale vertical and lateral changes of matrix-rich deposits. The objective of this thesis is to provide a detailed description and interpretation of the lithological, textural and mineralogical make-up and lateral facies trends in matrix-rich strata of the Upper Kaza Group. From an industry perspective, understanding their lithological make-up and facies trends, in addition to their relationship with genetically related matrix-poor sandstones, will provide important input for building more accurate reservoir models.

1.2 Geologic History and Regional Stratigraphy

1.2.1 Overview of the Windermere Supergroup

The Neoproterozoic Windermere Supergroup (WSG) crops out extensively throughout western North America forming a discontinuous outcrop belt that extends from the Sonoran Desert (Northern Mexico) to the Yukon-Alaska boarder; a strike length of approximately 4000 km (Ross, 1991; Figure 1.1). In Mexico and the southwestern United States strata of the WSG consists of continental and shallow-marine sedimentary siliciclastic and subordinate carbonate rocks (Link, 1993). Further north in the southern Canadian cordillera, deep-marine slope and basin-floor siliciclastic strata crop out superbly over an area of approximately 35 000 km^2 (without palinspastic restoration) (Ross, 1995). Still further north in the Mackenzie Mountains (Yukon Territory) strata consists of shelf and upper-slope facies (Terlaky, 2014; Ross, 1995). Collectively, the WSG is interpreted to represent deposition along the continental margin of Laurentia (ancestral North America) as it prograded into the paleo-Pacific (Figure 1.2; Bell et al., 1987; Ross, 1991; Ross et al., 1995; Karlstrom et al., 2001; Ross and Arnott, 2007). This thesis focuses on deep-water siliciclastic rocks of the WSG that crop out in the Castle Creek study area, Cariboo Mountains, southern Canadian cordillera, British Columbia, Canada.

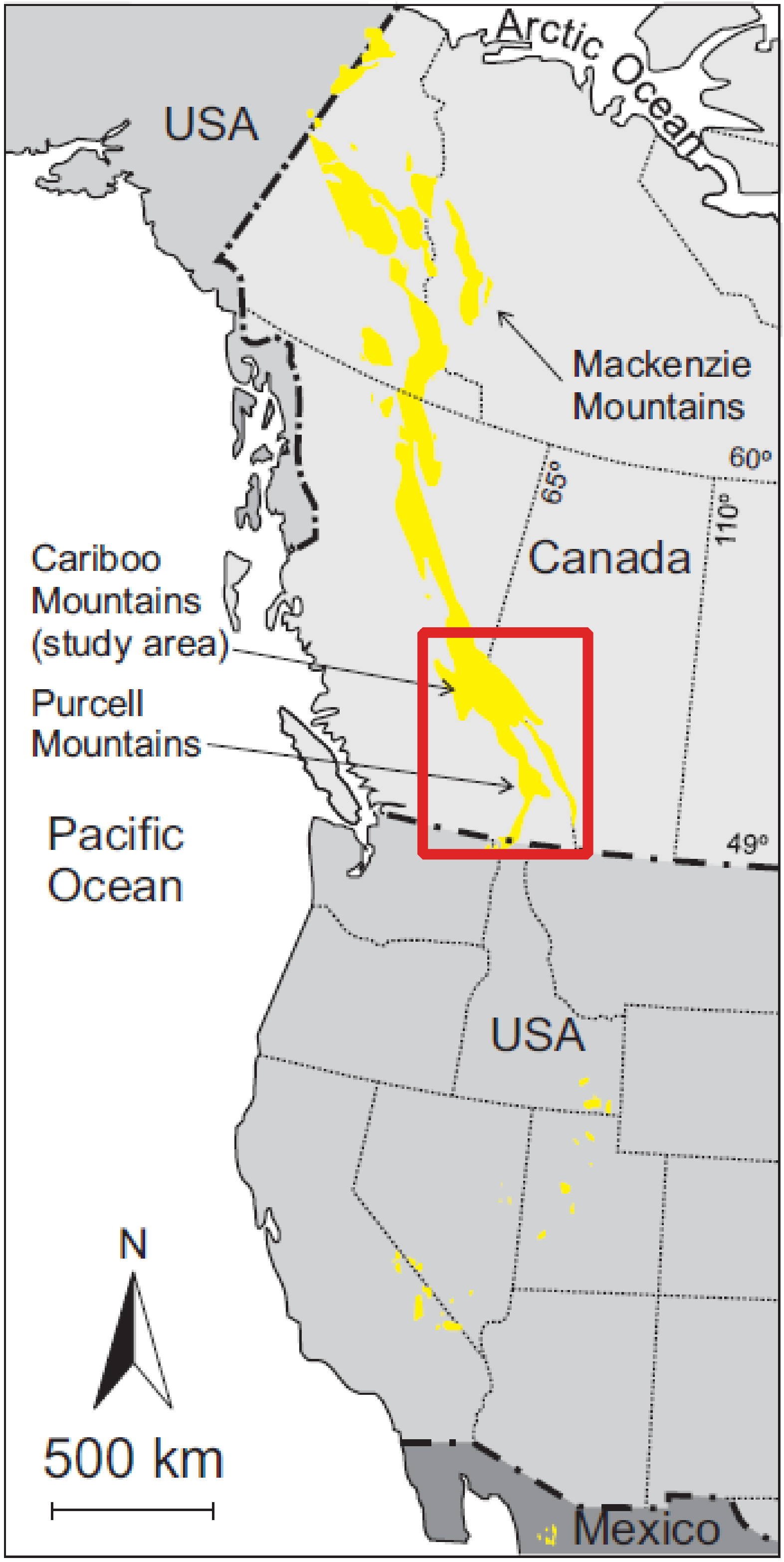

Figure 1.1: Location of exposed strata of the Windermere Supergroup (yellow) in western North America. The red rectangle shows the location of generally well-exposed deep-water rocks in the southern Canadian Cordillera (after Ross, 1991).

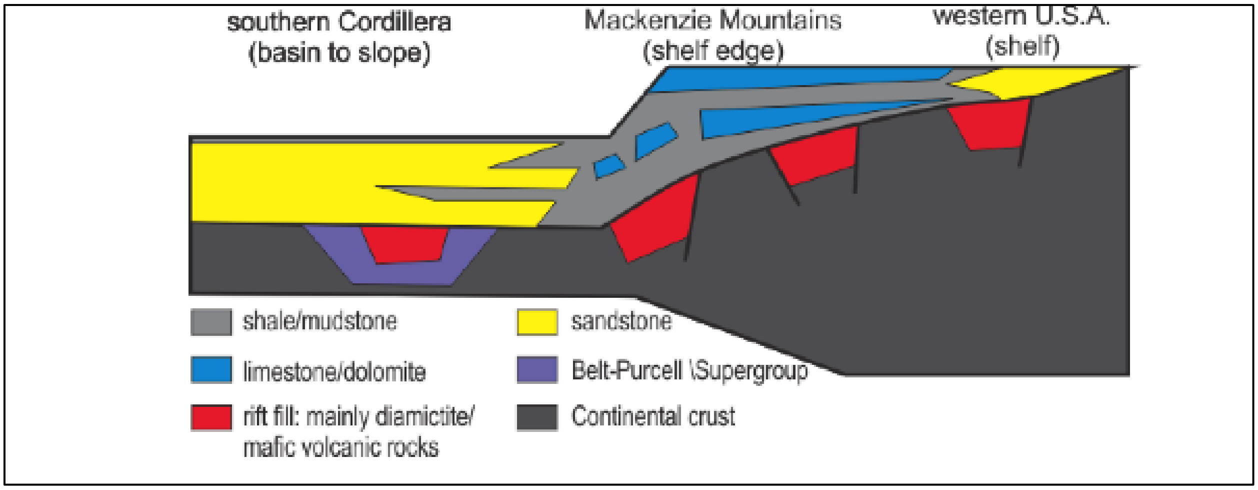

Figure 1.2: Schematic cross-section of western North America ca. 600 Ma (redrawn by Khan, 2011; from Ross, 1991). The correlation of shelf strata in the southwestern USA with deep-water rocks in the Canadian Cordillera are unknown, but age and continuity of major stratigraphic elements (e.g. glaciogenic diamictites and mafic volcanic rocks) suggest a once continuous basin (Eisbacher, 1985; Ross, 1991). Erosion related to the sub-Cambrian unconformity has removed shallow- water strata in the southern Canadian Cordillera (Ross, 1988).

1.2.2 Southern Canadian Cordillera

During the Neoproterozoic (755 – 569 Ma) Laurentia (ancestral North America) separated from the supercontinent Rodinia and created a passive margin along its ancestral western coast (Bell et al, 1987; Ross, 1991; Ross et al, 1995; Ross and Arnott, 2007). Separation of a continental landmass from the western margin of Laurentia resulted in the creation of the proto-Pacific Ocean and growth of an extensive passive continental margin (Ross et al, 1995). Along this margin, and in the present day position of the southern Canadian cordillera, was the deposition of mostly deep-water deposits of the Windermere Supergroup (Figure 1.3). In this area, the lower part of the WSG consists of an intercalated assemblage made up of the Toby (continental coarse-grained siliciclastics) and Irene (mafic volcanics) formations that accumulated in localized rift basins coincident with the fragmentation of Rodinia (Stewart, 1972; Ross, 1991). At present, timing of rifting in the southern Canadian Cordillera is constrained by a

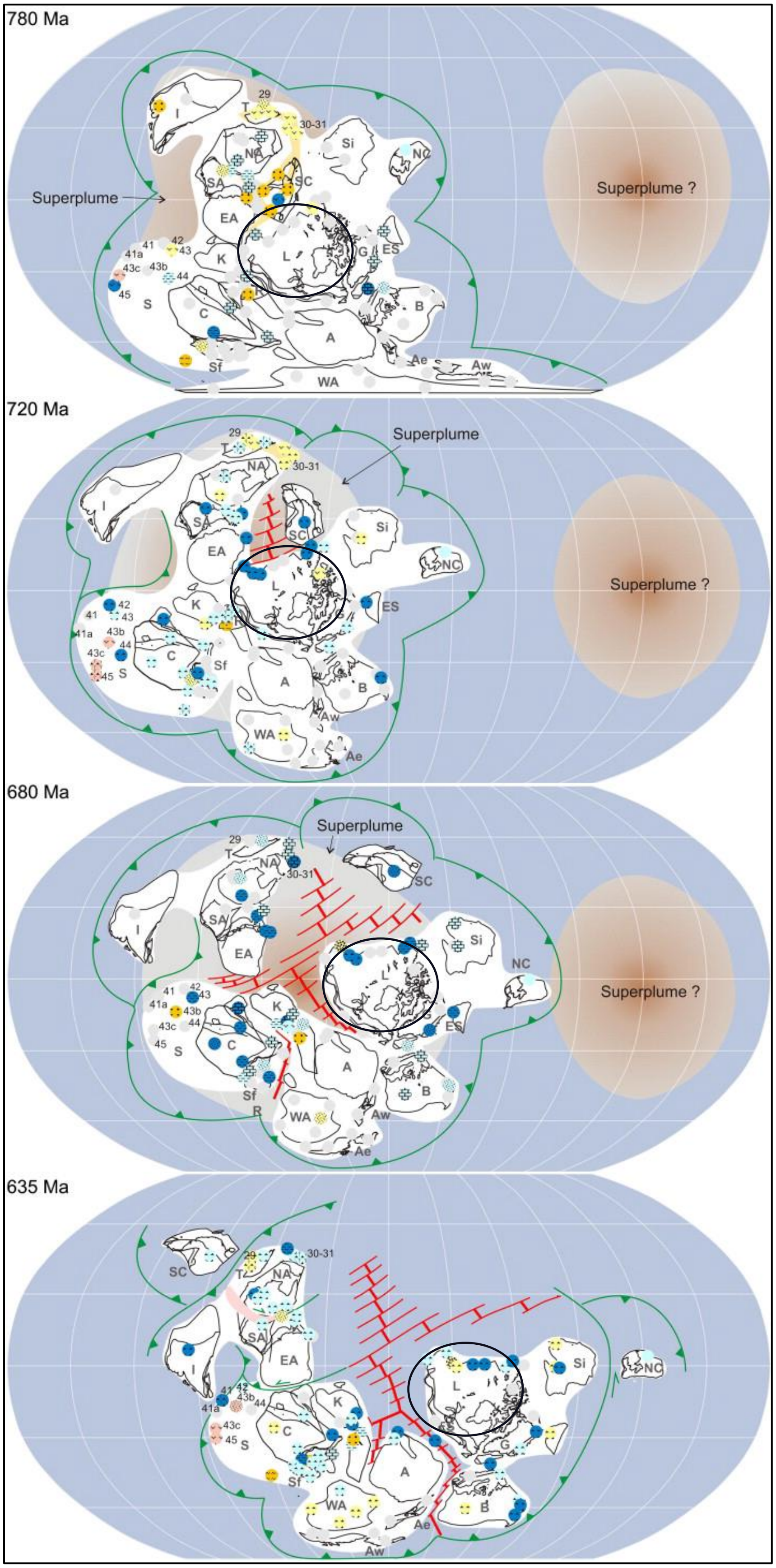

Figure 1.3: Global paleo-reconstructions illustrating the breakup of Rodinia (spreading ridge depicted by red lines) and the temporal development of Laurentia (ancestral North America) circled in black. 780 Ma: showing the full development of Rodinia; 720 Ma: the onset of the breakup of Rodinia. Note the spreading center immediately to the north of Laurentia; 680 Ma: Expansion of spreading ridge complexes, continued breakup of Rodinia and the creation of the Proto-pacific ocean; 635: Ma nearly complete breakup of Rodinia and the formation of a fully-developed continental margin along the north-facing margin of Laurentia (present-day western North America). Figure modified from Li et al, 2013.

single Sm-Nd age of 762 ± 44 Ma from mafic volcanic rocks of the Irene Formation (Devlin et al., 1988). However dates from igneous rocks interpreted to be correlative with the Irene Formation in northern British Columbia and Idaho provide dates that range from 762-684 Ma (Ferri et al., 1999; Fanning and Link, 2004). Later and as a result of thermally driven subsidence, a ~6 km thick succession of deep marine sedimentary rocks that transition stratigraphically upwards from deep marine to continental shelf strata accumulated in the newly formed basin. This post-rift succession is termed the Miette Group in the western Rocky Mountains (Charlesworth et al., 1967), Horsethief Creek Group in the Purcell Mountains (Resson, 1973) and the Kaza and Cariboo groups in the Cariboo Mountains (Campbell et al, 1973). This kilometer scale upward-shoaling succession is interpreted to represent progradation of the Laurentian passive continental margin into the proto-Pacific (Ross and Arnott 2007). During the Early Paleozoic, a second major tectonic event occurred, which in western Canada resulted in the formation of the Western Canadian Sedimentary Basin and the eventual accumulation of over 10 km of mostly shallow marine carbonate rocks (Hein and McMechan, 1994). Sedimentation along the passive margin terminated in the Jurassic as the margin was converted into a tectonically active margin forming a continental arc system. Accretion of allochthonous micro-continents and related deformational events led to the creation of the Canadian Cordillera (Reid et al., 2002), which from east to west comprises five distinct northwest-southeast trending morphological belts: the Rocky Mountain, Omineca Crystalline, Intermontane, Coast Plutonic and Insular belts (Figure 1.5). The Rocky Mountain and Omineca Crystalline belts are composed of autochthonous deformed Proterozoic and.

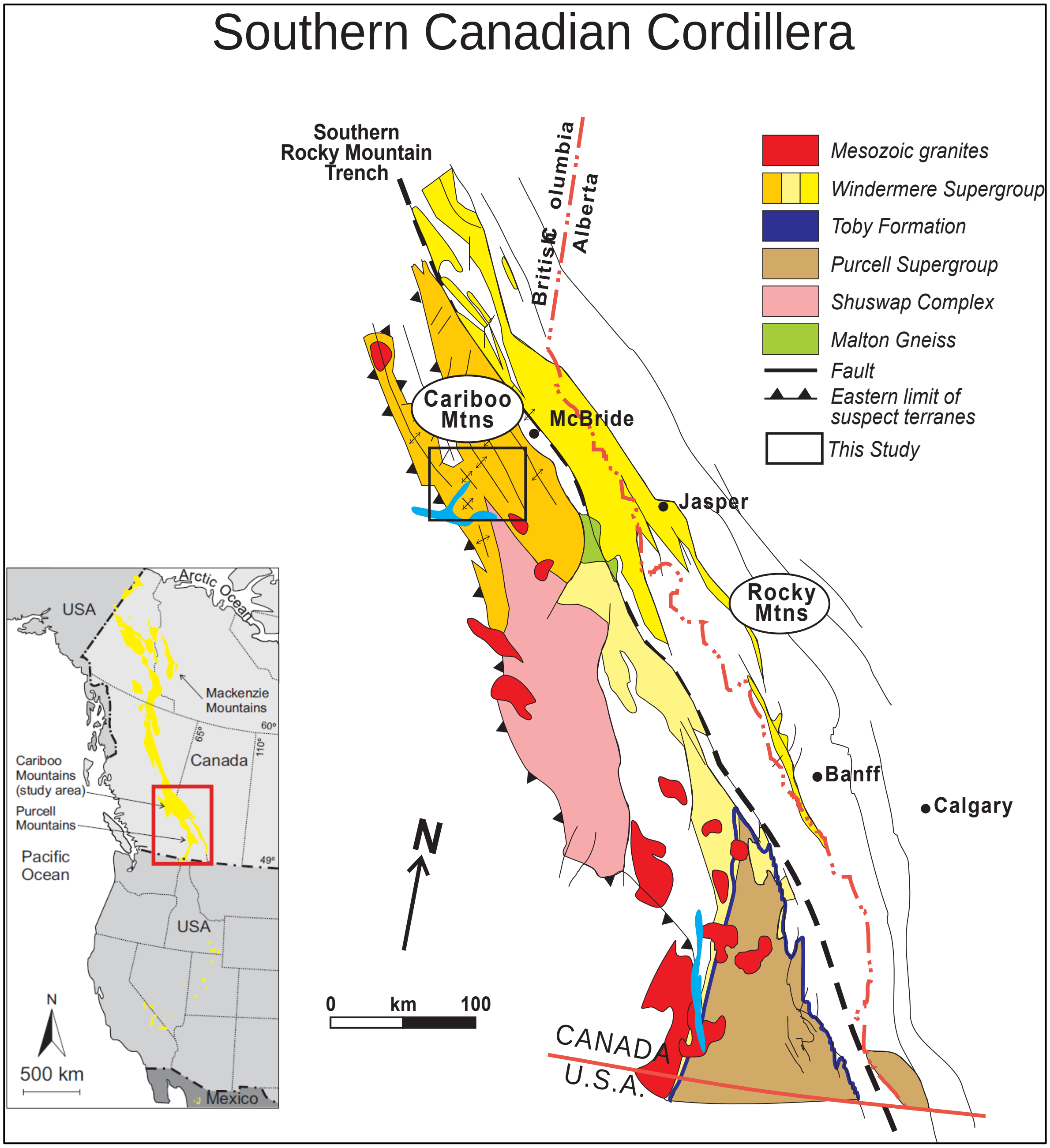

Figure 1.4: Simplified geological map of the deep-water unit of the Windermere Supergroup and surrounding units in the southern Canadian Cordillera. Modified from Ross and Arnott, 2007.

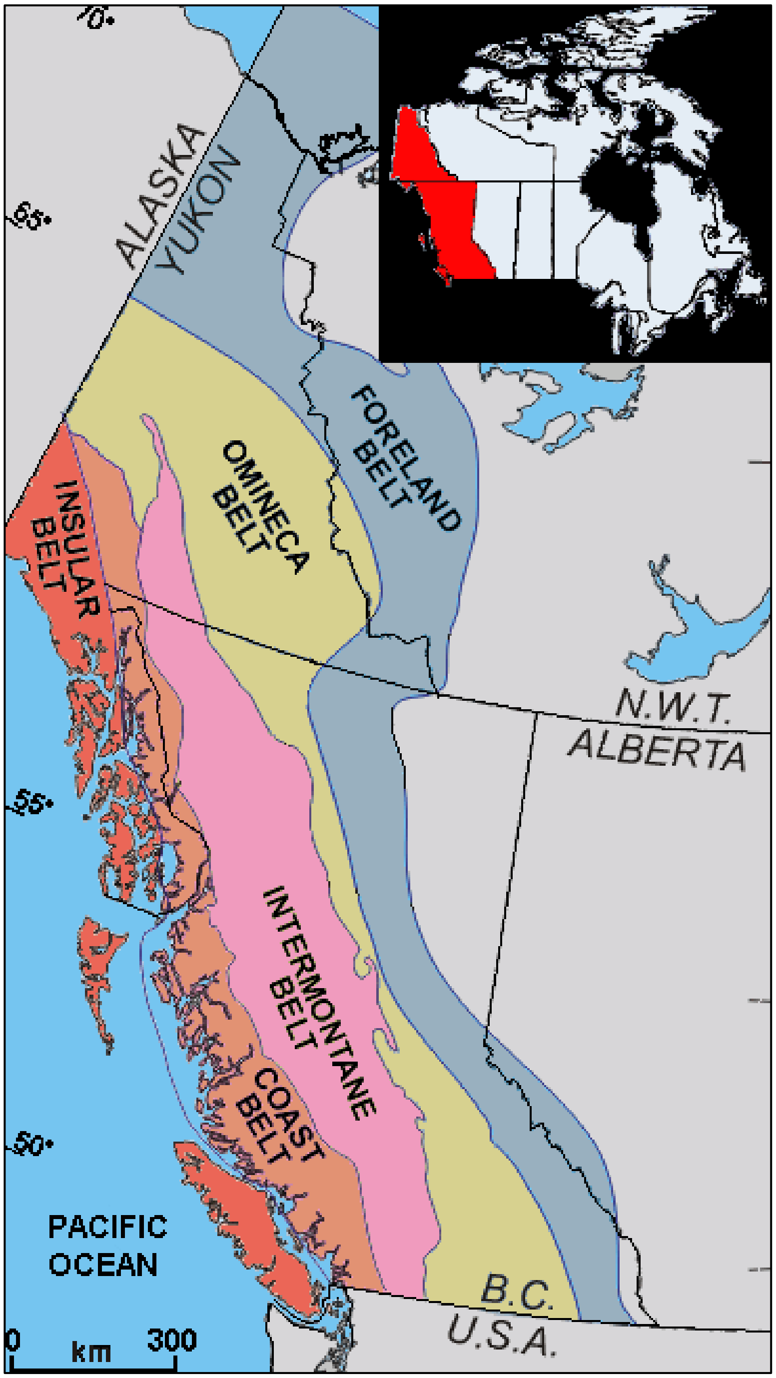

Figure 1.5: The Western Canadian Cordillera comprises five morpho-tectonic belts. From east to west they include the Foreland Belt, Omineca Belt, Intermontane Belt, Coast Belt and Insular Belt. The northwest-southeast trending belts reflect mountain building processes related to collisional tectonism and accretion of allochtonous terranes along the western margin of Laurentia between the Mid-Jurassic (185 Ma) and Early Cenozoic (50 Ma; Price, 2000). Map after Wheeler and McFeely, 1991.

Paleozoic mostly marine sedimentary rocks, whereas the Intermontane, Coast Plutonic, and Insular belts are made up of allochthonous micro-accretionary terraces and subduction-related magmatism associated with mountain building

1.2.3 Regional Stratigraphy of the Cariboo Mountains

The study area is located in the Cariboo Mountains (the northernmost sub-range of the Columbia Mountains in east-central British Columbia), which forms part of the Omineca Belt in the southern Canadian cordillera. Here, kilometer-scale Jurassic folds dominate the local structure and are confined by a series of strike-slip faults (Reid et al., 2002). The metamorphic grade in the Cariboo Mountains ranges from sub-greenschist in the northern part and increases to greenschist towards the south. Neoproterozoic rocks of the WSG comprise the Kaza and Cariboo groups. The Kaza Group is subdivided into Lower, Middle and Upper parts, whereas the Cariboo Group is subdivided, stratigraphically upwards, into the Isaac, Cunningham and Yankee Bell formations (Campbell et al, 1973; Figure 1.6). The Kaza Group is a few kilometers thick and consists mostly of coarse-grained sandstone and conglomerate, interbedded with fine-grained sandstone, siltstone and shale. The Kaza Group is interpreted to represent stacked depositional lobes in a basin floor setting (Terlaky and Arnott, 2014). It is important to note that the Kaza Group includes the only regionally extensive marker unit within the WSG: the Old Point Fort Formation. Conformably overlying the Kaza Group is the Isaac Formation composed mostly of mudstone, siltstone and shale interbedded with thick units of sandstone or conglomerate. The Isaac Formation is interpreted to represent the deposits of slope leveed-channel complexes (Khan and Arnott, 2012). It then is overlain by the 800 m thick Cunningham Formation dominated by oolitic-intraclastic limestone interpreted as carbonate-rich upper slope to outer shelf deposits (Khan and Arnott, 2012). Lastly, the Yankee Bell Formation is a ~ 900 m thick succession of alternating carbonate and siliciclastic rocks interpreted to represent deposition on a high-energy continental shelf (Khan and Arnott, 2012).

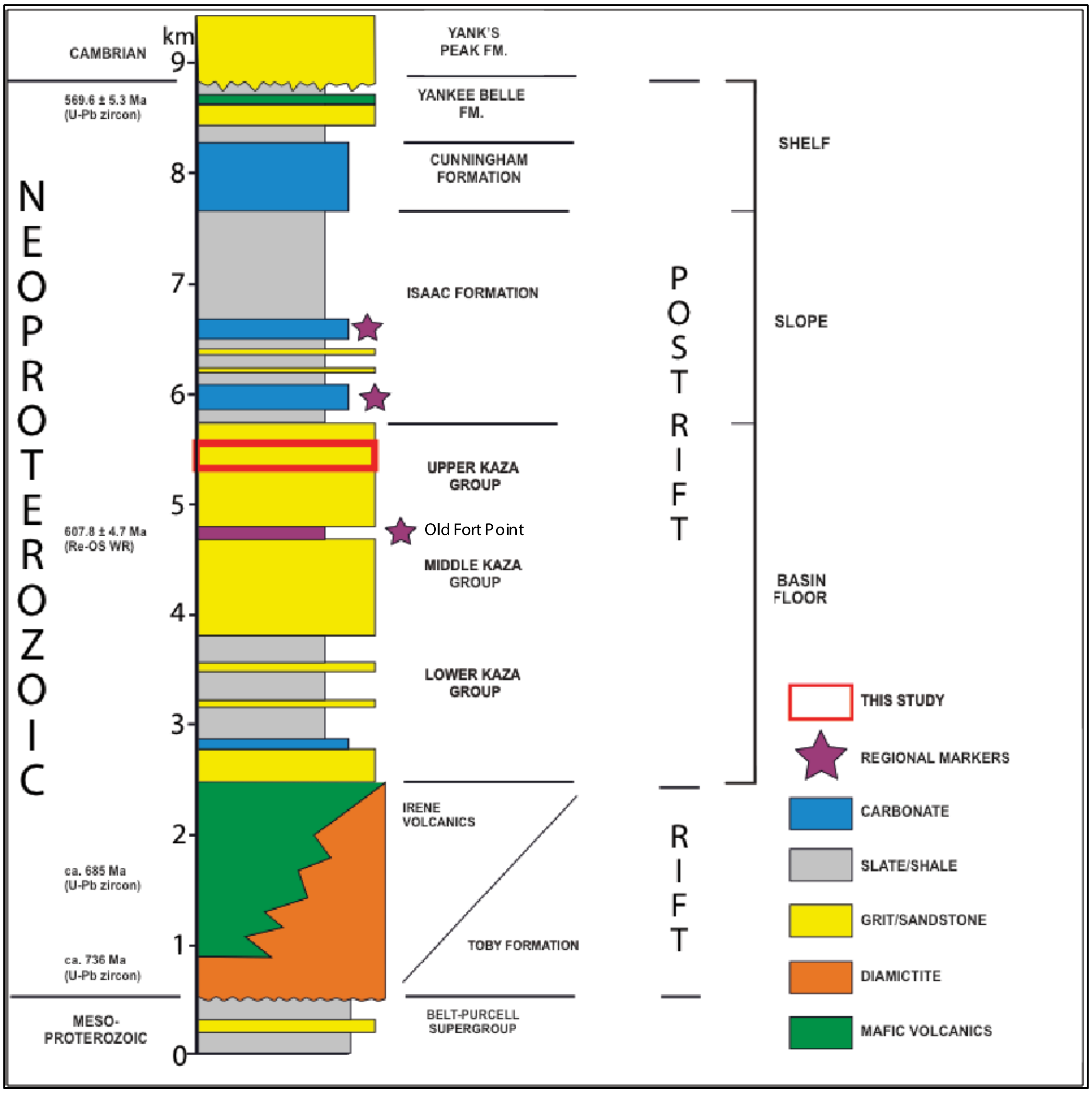

Figure 1.6: Regional stratigraphy of the Windermere Supergroup in the southern Canadian cordillera. This study focuses on the Upper Kaza Group, which is highlighted by the red rectangle (modified from Ross and Arnott 2007). Geochronological dates from Ross *et al*. (1995), Lund *et al*. (2003), Kendall *et al*. (2004) and Colpron *et al*. (2002).

1.2.4 Age Constraints and Sediment Provenance of the Windermere Supergroup in the southern Canadian cordillera

The minimum and maximum age of WSG deposition is constrained by ages obtained from rocks that unconformably underlie and overlie the WSG sedimentary succession. Based on U-Pb dating, crystalline basement rocks that underlie the WSG range from 740-728 Ma, thus providing a maximum age for WSG sedimentation (Armstrong, 1953; Parrish and Armstrong, 1983; Evenchick et al, 1984). The minimum age of WSG sedimentation is 569.6±5.3 Ma and is based on U-Pb dating of volcanic rhyolites from the Lower Cambrian Gog Group that unconformably overlie the WSG (Colpron et al, 2002).

Although, biostratigraphic control is absent, regional correlations are made possible by a small number of regionally extensive lithostratigraphic markers. The most widespread and visually distinct in the field is the Old Fort Point Formation (OFP). The OFP separates the Lower and Middle Kaza groups and crops out across the entire southern Canadian cordillera. Here it forms an up to 450 m thick, geochemically distinct deep marine succession comprising three units (Smith et al, 2009; 2014a, b; Figure 1.7). The basal unit termed the Mount Temple Member, is 50-125 m thick and consists of purple, green and grey siltstone-mudstone base that grades upwards into rhythmic limestone-siltstone couplets. The middle unit, the Geikie Siding Member, is 2-15 m thick and consists of distinct grey to black organic-rich mudstones interpreted to represent a period of deep-ocean anoxia and a maximum flooding surface (Kendall, 2004). The Whitehorn Mountain Member forms the uppermost unit, which is 0.5-165 m thick and composed of a lithologically diverse assortment of re-sedimented siliciclastic and carbonate strata (Smith et al, 2014a). The Isaac Formation contains two less aerially-extensive markers informally termed the first and second Isaac carbonates. These units range from 10 m to 250 m thick and consist of interstratified thin-to-medium bedded calciturbidites and subordinate conglomerate breccia and slump blocks. These lithostratigraphic markers are interpreted to represent re-sedimented carbonate sediment sourced from a continental shelf that became flooded during periods of sea level highstand (Ross, 1995; Ross and Arnott 2007; Khan and Arnott, 2012). The only direct age within the deep-water sedimentary pile of the WSG comes from a Re-Os date from organic rich shales in the Geikie Siding Member, and provides an age of 607.8 ± 4.7 Ma (Kendall, 2004; Ross and Arnott, 2007). Within the southern Canadian cordillera, detrital zircon populations in deep-water strata of the WSG show a distinctly bimodal age distribution of 1.9-1.75 Ga and 2.6 Ga (Ross and Bowring, 1990; Ross and Parrish, 1991), suggesting that sediment sources remained stable and were confined to the southern Canadian Shield and the northwestern part of the United States (Ross et al, 1995; Ross and Arnott, 2007). Moreover, regional paleoflow shows a general trend towards the northwest (Ross et al, 1995; Ross and Arnott, 2007) although local deviations, most likely related to local topographic effects, are observed (Khan and Arnott, 2012). Based on regional correlations, map patterns and the homogeneity of detrital zircon provenance, deep-water siliciclastic rocks of the WSG are interpreted to have been deposited by a single, deep-water, turbidite system of substantial dimensions. Currently in the southern Canadian cordillera, deep-water sedimentary rocks of the WSG crop out over an area of approximately 35 000 km^2 and are 6-9 km thick. However, taking into account tectonic shortening and faulting associated with the Mesozoic

Cordilleran Orogeny, the palinspatically restored WSG may have been at least 80 000 km^2 (Ross and Arnott, 2007), which then would make it one of the world's largest ancient turbidite systems and also dimensionally similar in to modern-day systems like the Amazon and Mississippi turbidite systems (Figure 1.8)

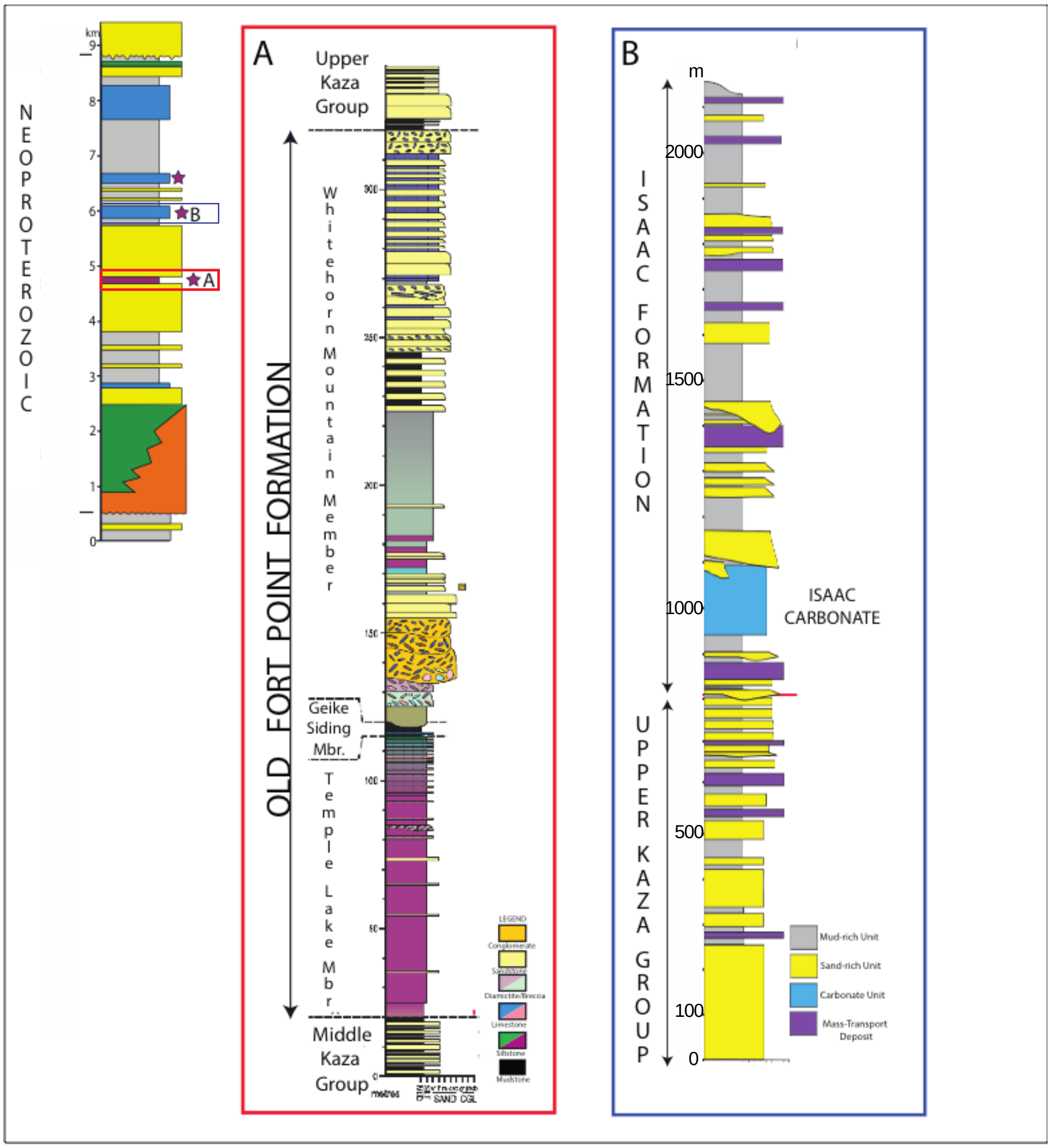

Figure 1.7: A: Generalized stratigraphic column of the regionally extensive Old Fort Point Formation and its three stratal constituents: Mount Temple Lake, Geikie Siding and the Whitehorn Mountain members. Modified from Smith et al., 2014. B: Generalized stratigraphic column of the Castle Creek study area showing the location of the first Isaac carbonate unit. Modified from Ross and Arnott, 2007.

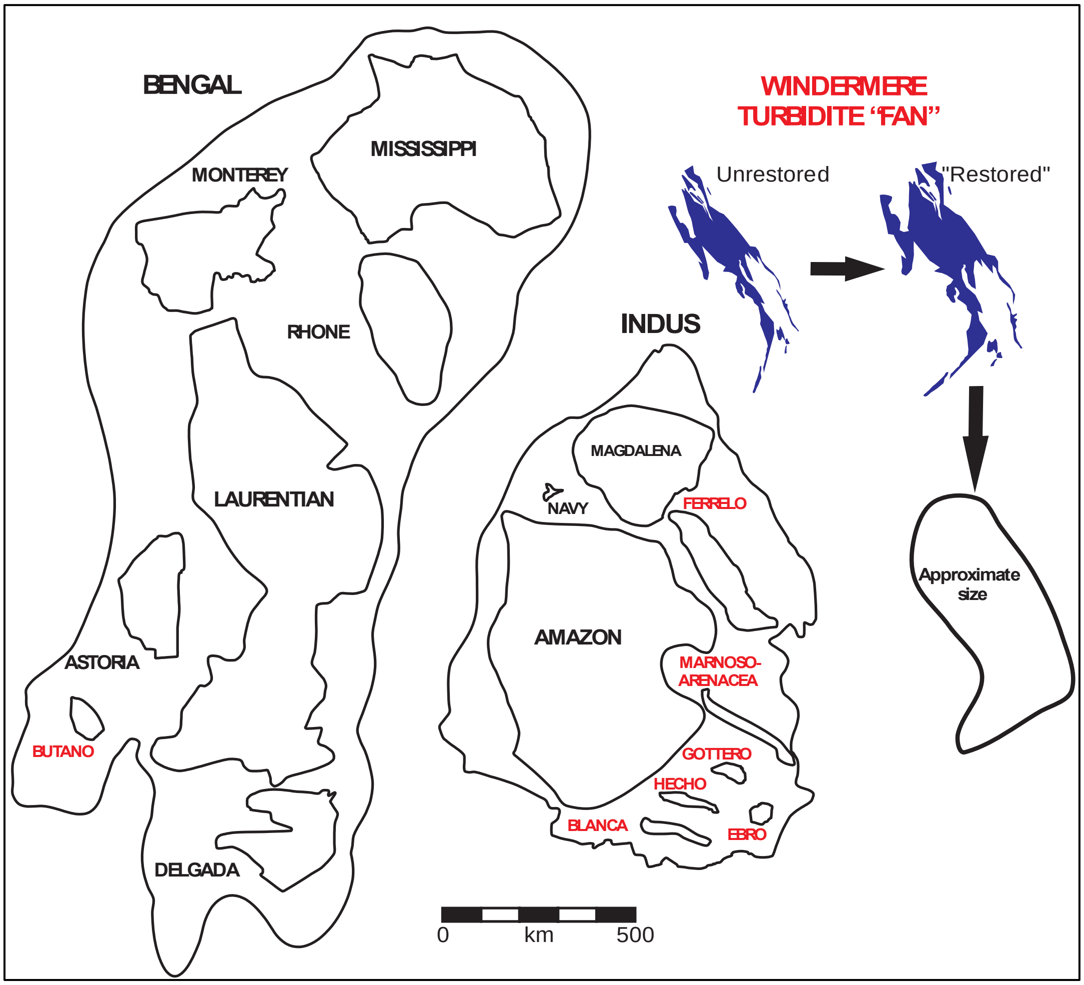

Figure 1.8: Hypothetical reconstruction of the Windermere turbidite system in relation to other modern (in black text) and ancient (in red text) turbidite systems (from Khan and Arnott, 2012).

1.2.5 Castle Creek Outcrop and Stratigraphy

The Castle Creek study area is located in the Cariboo Mountains of east-central British Columbia near the headwaters of Castle Creek (~53º03‟N, 120º26‟W; Figure 1.9). Here, strata of the WSG are well-exposed on the vertically-dipping limb of a major southwest-verging anticline along the eastern side of the Isaac Synclinorium (Ross and Arnott, 2007). The Castle Creek area has been affected by at least four phases of deformation (Murphy and Rees, 1983; Reid et al, 2002; Khan and Arnott, 2012).

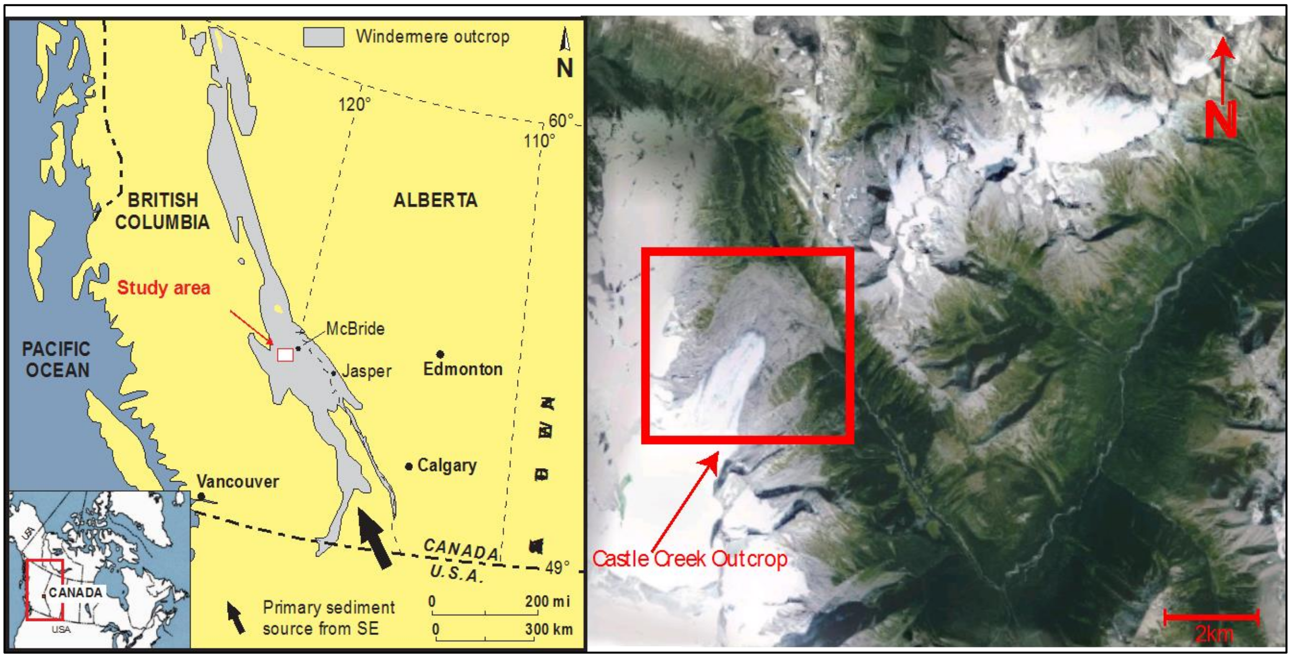

Figure 1.9: Location of the Castle Creek outcrop (Cariboo Mountains, British Columbia) where strata of the Upper Kaza Group and Isaac Formation of the Windermere Supergroup are superbly exposed. Right image from Terlaky, 2014; Left image from ©2015 Province of British Columbia, Cnes/Spot Image, Map data ©2015 Google.

The first deformation event (D1) resulted in east-verging, meter-scale folds and a cleavage (S1) that locally sub-parallels bedding. The second event (D2) formed kilometer-scale southwest-verging folds that represent the dominant regional structural grain preserved in the area – the major fold (anticline) at Castle Creek is related to this event. This deformational event also resulted in an axial-planar cleavage (S2) and a prevalent crenulation cleavage throughout the area (Murphy, 1987a). The minimum age of D1 and D2 is provided by cross-cutting intrusive igneous rocks dated at 174 Ma (Pigage, 1977; Gerasimoff, 1988). The third deformational event (D3) resulted in dextral strike-slip faulting, kilometer-scale folds (northwestern-verging) and an axial planar cleavage that crenulates S2 cleavage (Reid et al., 2002). The fourth deformation event (D4) resulted in local meter-thick upright kink folds. Murphy (1987a) postulated that metamorphism in the area began during or shortly after D1 and peaked during D2–D3 resulting in sub-greenschist to greenschist grade metamorphism. Nevertheless, despite a complex history of deformation and metamorphism, primary sedimentary structures in strata at Castle Creek are still well preserved, even at the millimeter scale. As a result, sedimentary rather than metamorphic nomenclature is used to classify these rocks (Ross and Arnott, 2007).

The Castle Creek outcrop is 7 km wide (parallel to bedding) and 2.5 km thick (perpendicular to bedding) (Khan and Arnott, 2010) (Figure 1.10). Within the area is a small, rapidly retreating glacier that has polished and smoothed the strata forming freshly exposed surfaces with little to no vegetation, lichen or moss. This, in addition to the vertically-dipping attitude of the stratigraphy, allows beds to be walked out for hundreds of meters laterally and therein the opportunity to carefully document the nature of lithological changes. Exposed at Castle Creek are strata of the Upper Kaza Group and Lower Isaac Formation. Here, the Upper Kaza Group is ~800 m thick and composed of laterally continuous, decameter thick units of normally graded, quartzofeldspathic, coarse-grained sandstone, with lesser granule conglomerate interbedded with thin-bedded turbidites. The ratio of sandstone to mudstone is ~75:25 (Arnott et al., 2011). Sheet-like sandstones are up to 40 m thick and in many cases >800 m wide (width of the outcrop) and are interpreted to represent deposition in basin-floor lobes by poorly confined turbidity currents. The much more mudstone-rich Isaac Formation (sandstone: mudstone ratio of 25:75) conformably overlies the sand-dominated Upper Kaza Group. At Castle Creek, the Isaac Formation is composed of mudstones interstratified with decameter-thick sandstones, conglomerates and uncommon carbonates (Arnott et al., 2011). The mudstone units consist of thinly-bedded, fine-grained T_{cde}/T_{de} turbidites interpreted to represent levee deposits bounding channels filled with the coarse-grained sandstone units (Khan and Arnott, 2012). In addition, common slide, slump and debris flow deposits within the Isaac Formation are interpreted to be a consequence of gravitational instability characteristic of deep-water slope to base-of-slope settings (Khan and Arnott, 2012).

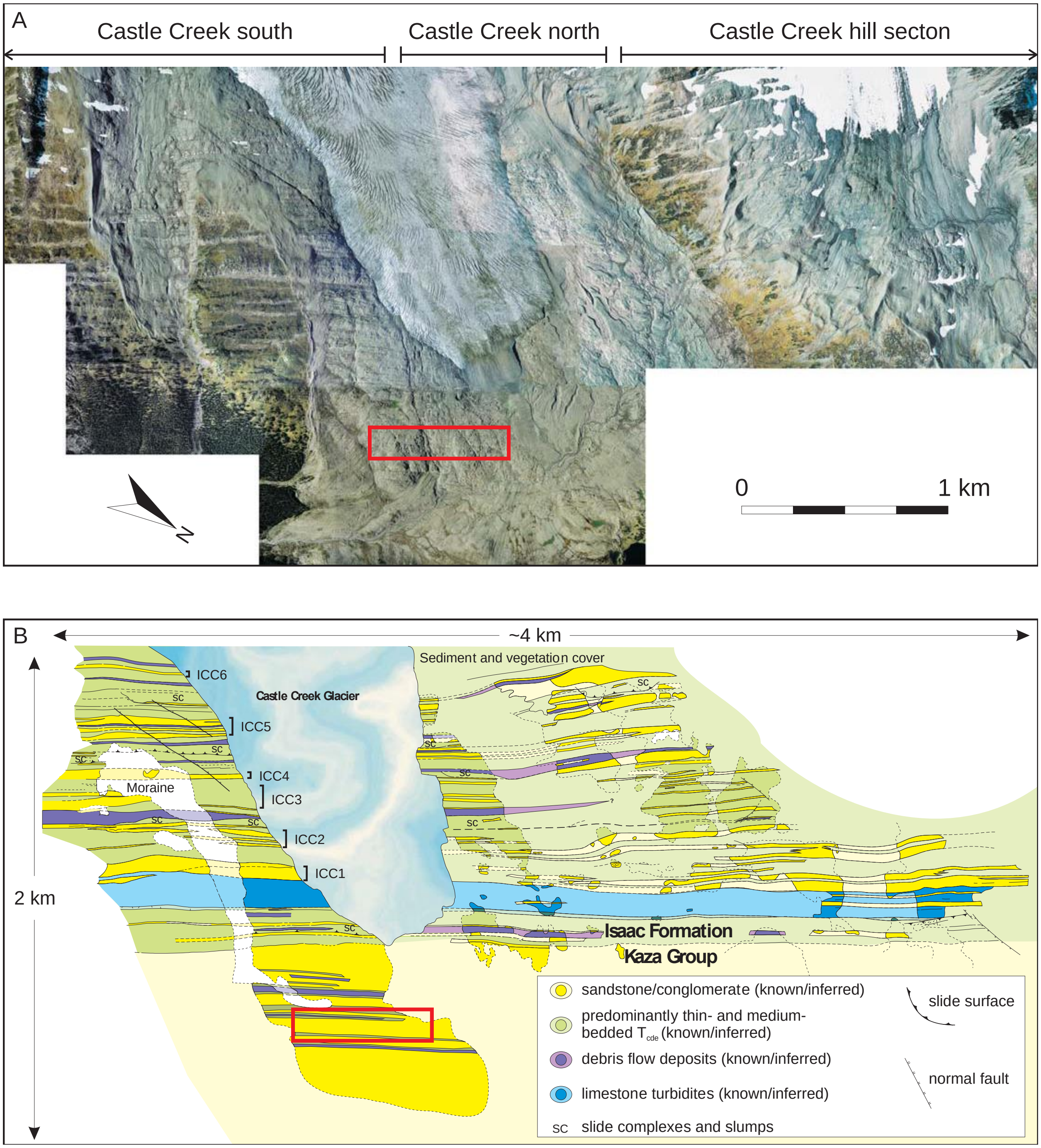

Figure 1.10: A) Photomosaic of the Castle Creek study area. B) Interpreted geological map of the Castle Creek study area with the area of this study indicated by red rectangle. For the location of previous studies conducted at Castle Creek see figure 5B in Ross and Arnott, 2007. Figure modified from Ross and Arnott, 2007.

1.3 Previous Work

The regional stratigraphy, deformation and metamorphism was first described in the geologic work of Campbell et al. (1973) that also produced a 1:250,000 regional map. In 2003, Ross and Ferguson published a 1:50,000 map that included the Castle Creek study area (Figure 1.11). Numerous other studies focusing on the regional geology and structure of the Cariboo Mountains have been published, notably: Murphy and Rees (1983); Murphy (1987a, b); Ross and Murphy (1988); Ross (1991; 2000); Gabrielse and Campbell (1991); Hein and McMechan (1994); Ross et al., (1995); Reid et al, (2002); Reid (2003).

1.3.2 Previous work by the Windermere Consortium

This study is part of a larger research effort (Windermere Consortium) based at the University of Ottawa and supervised by Dr. Bill Arnott. Since its inception in 2001, the Windermere Consortium has been focused on documenting the stratigraphy and architecture of deep-water sedimentary rocks. In the Castle Creek study area work on basin floor deposits of the Upper Kaza Group were first described by Meyer (2004) and Meyer and Ross (2007a, b). Thereafter, smaller areas of the Upper Kaza were described in sedimentological detail by Rocheleau (2011); English (2013); Al Mufti (2013) and Lockwood (2014) and the more regional study by Terlaky (2014). Of particular note is that these studies were the first to recognize and briefly describe matrix-rich strata in the Upper Kaza Group, and therein the impetus for this study.

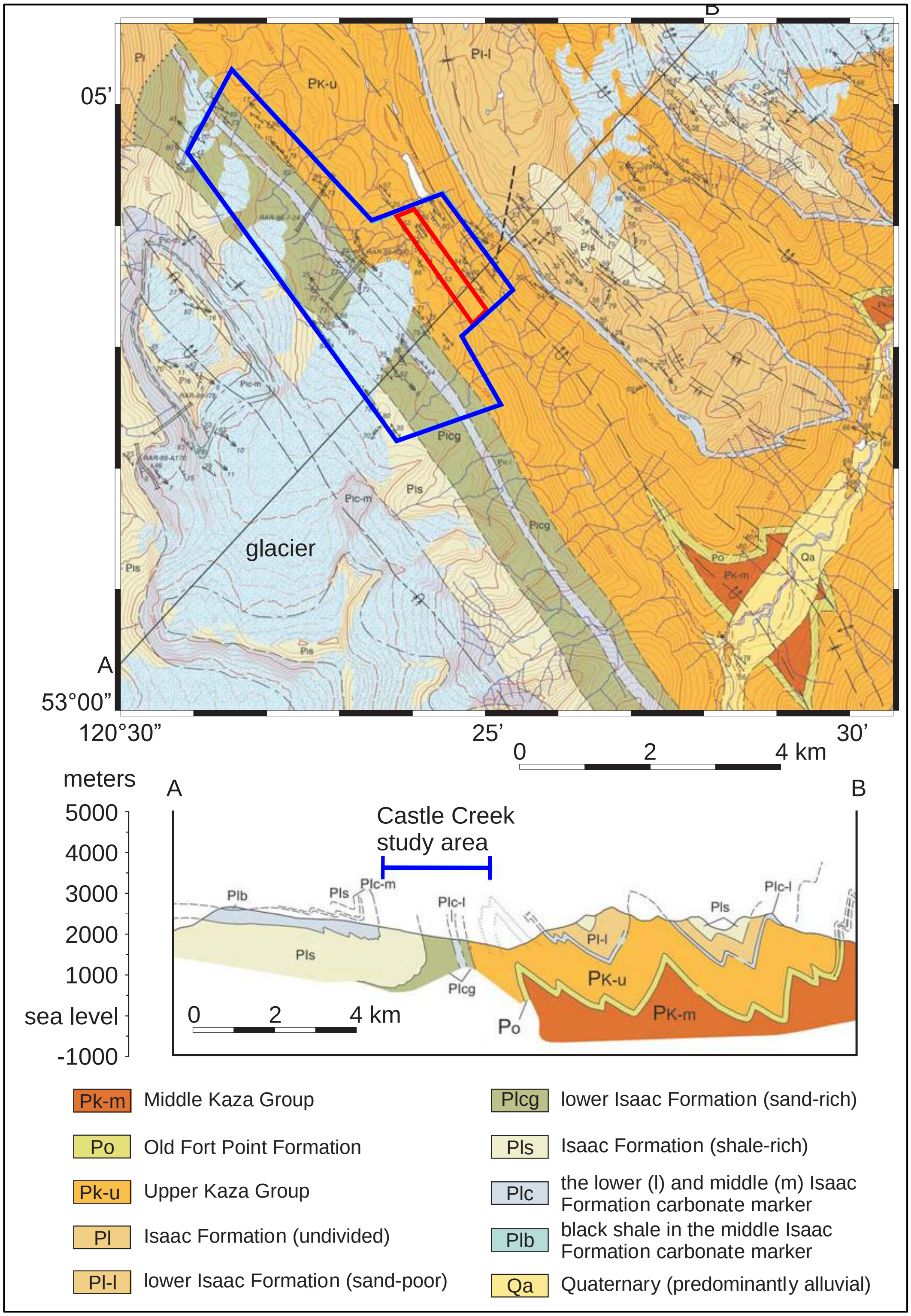

Figure 1.11: Regional geology of the Castle Creek study area and surrounding area (excerpt from the Eddy 1:50,000 map area: Ross and Ferguson, 2003). The general Castle Creek field area is highlighted by the blue polygon; this study focuses on the area in the red rectangle.

1.4 Study Area and Methodology

This thesis is based primarily on fieldwork conducted over two six week periods from mid-July to late August 2012 and 2013. Emphasis was placed on careful bed-by-bed, centimeter-to-meter scale description of the textural and sedimentological character of strata cropping out in 36 vertical stratigraphic sections that range from 15 m to 30 m in length and are spaced laterally over a distance (parallel to bedding) of about 800 m in the middle part of the Upper Kaza outcrop at Castle Creek (Figure 1.12). The distance between logs ranges from 20 m to 100 m depending on the quality of exposure and the character of lateral lithological change. In addition, stratigraphic correlations were mostly “walked-out” in the field (due to excellent outcrop exposure) and aided by the use of high-resolution (1:300) aerial photographs, on which some beds could be confidently identified and traced laterally. These data were then used to create a number of correlation panels (at various scales) to further illustrate lateral and vertical lithological trends within the study area (Appendix A).

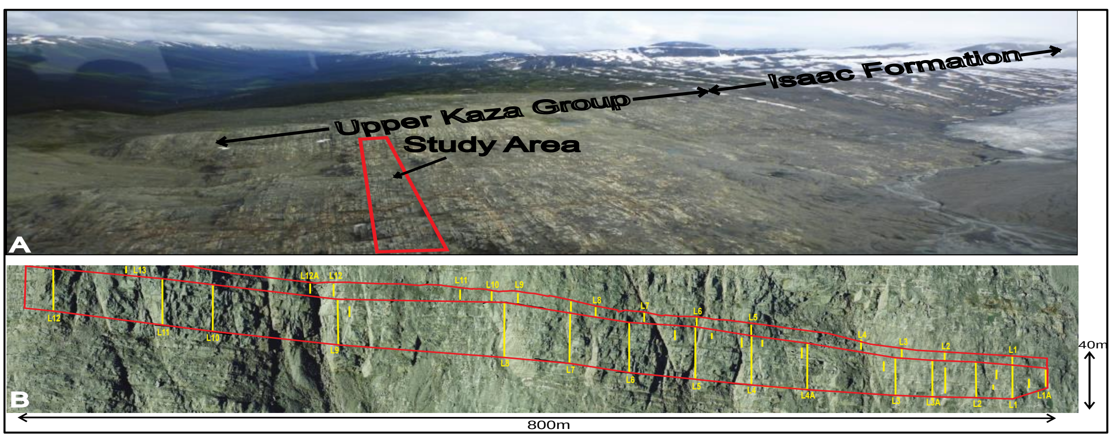

Figure 1.12: A) Panoramic view of a portion of the Castle Creek outcrop with the study area outlined in red rectangle. B) High-resolution aerial photograph showing the location of all 36 stratigraphic logs in yellow and the boundaries of the study area in red.

A total of 42 samples were collected from strategic locations across the study area and made into thin-sections for a more detailed description of grain size, grain sorting and mineralogy (for a complete list of samples and sample descriptions see Appendix B). Samples from clay sandstones (F3) and sandy claystones (F4) beds were collected systematically from the bottom, middle and top of beds to capture any upward change. Detailed manual point-counting of 420-560 grains per sample was carried out using a quadrant point-counting method wherein ~70 points were systematically counted from each quadrant using a grid (note: 6 quadrants per thin-section; Figure 1.13). The following classification scheme was used:

$$\text{Total} = \text{Framework Grains} + \text{Matrix} + \text{Altered Grains} \pm \text{Cement}$$

$$T = [Q_S + F_S + L_S + O_S] + [M_{QS} + M_{RXC}] + [RXC + RXC_{SG}] \pm C_{C/CM}$$

Where:

Q_S – sand-sized (or coarser) quartz grains;

F_S – sand-sized (or coarser) feldspar grains;

L_S – sand-sized (or coarser) lithic grains;

O_S – sand-sized (or coarser) other minerals (i.e. muscovite);

M_{QS} – (quartz) silt matrix;

M_{RXC} - recrystallized matrix (composed of muscovite and chlorite);

RXC - recrystallized medium sand-sized quartz (or coarser) with visible evidence of grain-boundary migration;

RXC_{SG} - recrystallized fine-grained quartz subgrains with prevalent subgrain rotation or bulging recrystallization;

$C_{C/CM}$ - calcite or clay mineral cements (uncommon).

This study is one of the first of the many studies at Castle Creek to use detailed petrographic analysis to quantitatively differentiate detrital matrix and framework grains, and therein quantitatively capture the textural differences between matrix-rich versus matrix-poor strata –The results and implications of petrographic analysis are described in the facies (Chapter 3) and discussion (Chapter 5) sections of this thesis.

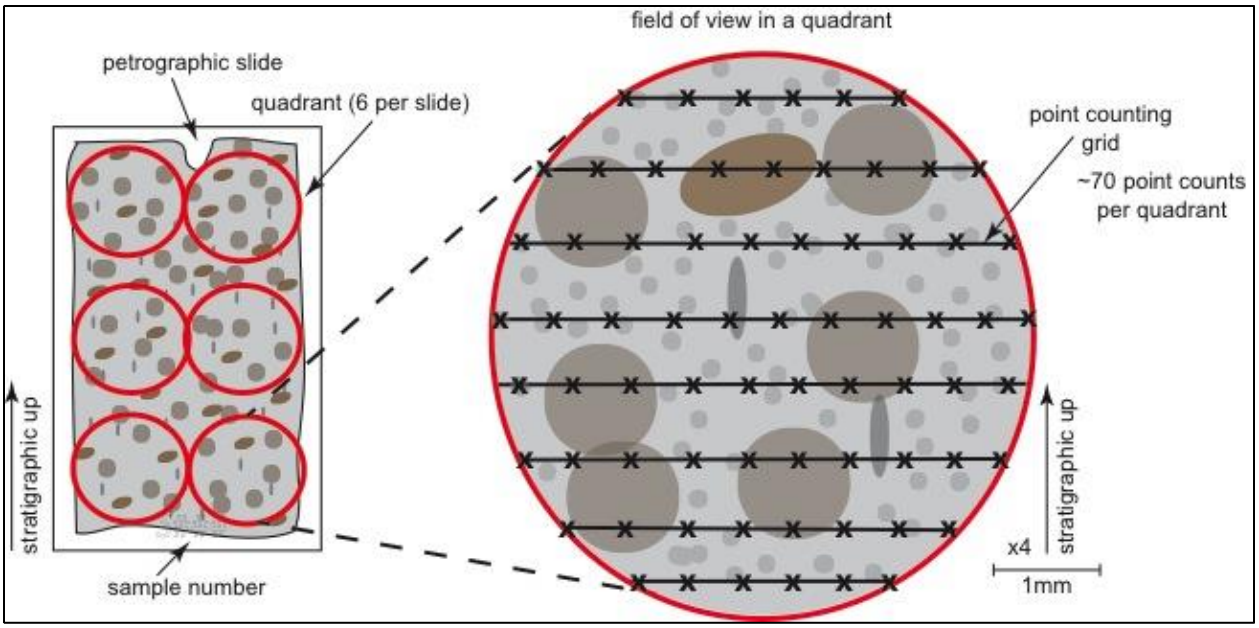

Figure 1.13: Schematic of the quadrant point-counting method used in this study.

Chapter 2: Literature Review

To aid in the understanding and interpretation of strata described in this thesis a brief overview of submarine sediment-gravity flows, their processes and resultant deposits is first presented. This is followed by a brief review of the types of dynamic quartz recrystallization associated with regional tectonism.

2.1 Introduction

The great depth and isolated location of the deep sea has always lead to unanswered questions about the processes occurring at the bottom of the ocean. Even into the 19th century very little was known about the sedimentological processes of the deep ocean. The Challenger Expedition (1872–1876) was a scientific exploration that made many important discoveries and laid the foundation of deep-marine research at the time. From this expedition it was postulated that the deep ocean was a calm setting where sediment accumulated by slow pelagic fallout and biological processes (Murray and Renard, 1891), and remained the general opinion of the scientific community up until about the 1930's. Moreover, it was assumed that sand was confined to shelf and shallow marine settings. During the past several decades, however, significant advances in deep-sea exploration, research and laboratory experiments have shown that the processes that transport large volumes of clastic material into the deep-marine are complex and their associated deposits accumulate in an environment that is anything but calm. These sediment-transport mechanisms are termed sediment-gravity flows and are volumetrically the most important flows operating on Earth (Talling et al., 2012).

2.2 Sediment-gravity Flows

Sediment-gravity flows are mixtures of sediment and fluid driven principally by gravity. In many cases flows are initiated when the shear strength of an accumulated sediment pile is exceeded by the downward force of gravity. During movement the sediment mass becomes expanded and disaggregated, eventually forming a more fluid, commonly fast-moving sediment-gravity flow. The loss of shear strength in the initial sediment mass is commonly manifested as a failure along the continental shelf edge (Shanmugan, 2006) and is a consequence of one or more of the following triggering mechanisms: 1) oversteepening and high slope angle (e.g. near the mouth of the Magdalena River, Colombia (Heezen, 1956), 2) seismic loading and/or earthquake disruption (e.g. 1929 Grand Banks tremors, east coast Canada; (Heezen and Ewing, 1952), 3) rapid sediment accumulation and under-consolidation (e.g. the Mississippi delta front, Gulf of Mexico; Coleman and Prior, 1982), 4) storm-wave loading (e.g. Henkel, 1970), 5) gas charging and gas hydrate dissociation (e.g. Scripps submarine canyon head, west coast U.S.A; Dill, 1964), 6) tsunamis (e.g. Gutenberg, 1939), 7) glacial loading (e.g. Scotian margin, North Atlantic; Mosher et al., 2004) 8) low tides, 9) seepage and 10) volcanic island processes moving downslope until friction along the base and top of the moving sediment mass exceeds the gravitational component. Once formed, sediment-gravity flows can transport over 100 km^3 of sediment (Rothwell et al., 1998; Piper et al., 1999; Talling et al., 2007), travel at speeds up to between 60-100 km/h as measured by submarine cable breaks (Heezen and Ewing, 1952; Piper et al., 1999a; Hsu et al., 2008) and have run-out distances in excess of 1500 km across the almost horizontal ocean floor (Klaucke et al, 1998; Wynn et al., 2002b; Talling et al., 2007; Frenz et al., 2008). In general, deep-marine sediment transport processes can be separated into two end-member kinds: mass-movements and sediment-gravity flows (Figure 2.1). Mass movements (e.g. slumps and slides) consist of coherent but contorted sediment masses that typically are confined to the proximal parts of the sedimentary system (e.g. continental slope and submarine canyon heads) and require a slope to initiate and maintain movement (Shanmugan, 2006). Sediment-gravity flows, on the other hand, consists of cohesion-less sediment-water mixtures that can be further subdivided into two common end-member kinds based on the principal particle support mechanism: cohesive flows (e.g. debris flows) and frictional flows (e.g. turbidity currents) (Middleton and Hampton, 1976; Lowe, 1979, 1982; Mulder and Alexander, 2001; Talling et al., 2012). In debris flows sediment is maintained in suspension principally by cohesive forces aided by buoyancy effects, dispersive pressure, elevated pore pressure, and hindered settling (Middleton and Hampton, 1973; Hampton, 1975; Pierson, 1981). In turbidity currents sediment particles are supported mostly, at least by definition, by fluid turbulence, but in most sand-transporting currents buoyancy effects, dispersive pressure, and hindered settling are also important (Sanders, 1965; Leeder, 1999; Shanmugam, 2006).

Strata in this study are interpreted to have been deposited on the (proximal) basin-floor (Figure 2.2), by fluidal, and hence relatively far-distance-travelled sediment-gravity flows. The following discussion, then, will focus on turbidity currents, but also flows that exhibit transitional characteristics between laminar and fully turbulent flow behaviour, and especially those with high sediment concentration and a significant fine-grained component (e.g. Mulder and Alexander, 2001; Baas et al., 2009, 2011; Talling et al., 2012; Talling, 2013).

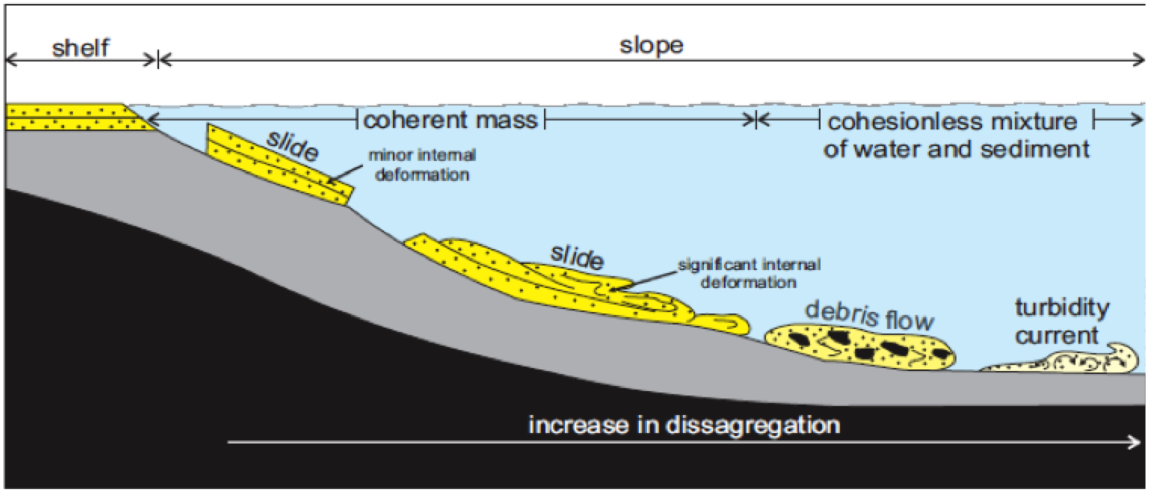

Figure 2.1: Downslope evolution of sediment gravity flows. Initially sediment failure at the shelf edge forms coherent slides and slumps, which transform downflow into debris flows and ultimately turbidity currents. Modified from Shanmugam et al., 1994

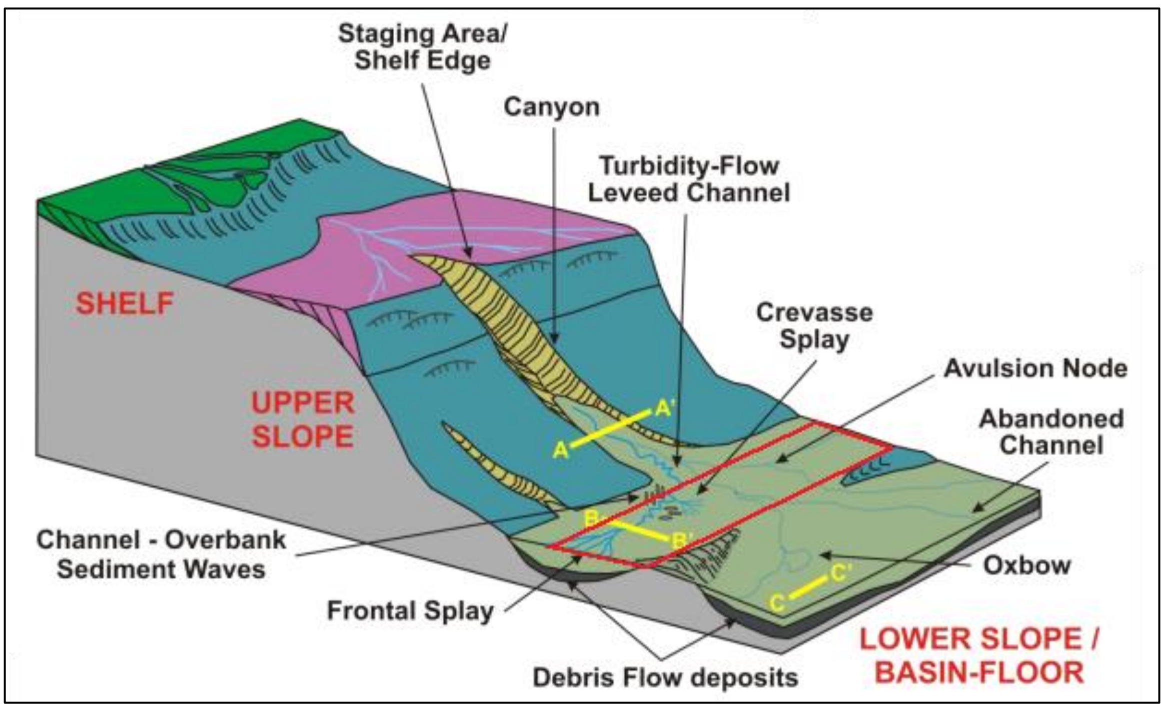

Figure 2.2: Generalized schematic of the principal depositional elements in deep-water settings. The red box outlines the proximal basin-floor and the approximate overall position of the strata in this study. Modified from Posamentier and Kolla, 2003.

2.2.1 Classification

As a consequence of their infrequent and unpredictable occurrence, plus powerful and destructive nature, few in-situ measurements have been made of modern turbidity currents, although exceptions exist: Zaire deep sea fan (Khripounoff et al., 2003); coastal fjord in British Columbia (Prior et al., 1987), and in several submarine canyons offshore California (e.g. Inman et al, 1976; Parsons et al., 2003; Paull et al., 2003). As a consequence, the classification of submarine sediment flows is based largely on field studies and laboratory experiments. Commonly, field studies interpret flow characteristics based on lithological characteristics (e.g. Pickering et al., 1989; Guibaudo, 1992; Stow and Johansson, 2000; Mulder and Alexander 2001; Talling et al., 2012 and references within) whereas laboratory studies measure flow characteristics directly (e.g. Best et al., 2001; Tilston et al., 2015). As a result, several classification schemes and varying terminologies have been proposed (Lowe 1982; Kneller and Branney, 1995; Mulder and Alexander, 2001; Sumner, 2008 among others). Mulder and Alexander (2001) produced a comprehensive classification scheme that differentiates between cohesive and non-cohesive (frictional flows), the latter further subdivided into hyperconcentrated flows, concentrated flows and turbidity currents based on particle cohesion, flow duration, sediment concentration and particle-support mechanisms (Figure 2.3). In this classification scheme cohesive flows have plastic rheology and a laminar flow state and typically deposit mud-rich deposits termed debrites. Hyperconcentrated and concentrated flows grains are supported by a combination of grain-support mechanisms, including: grain-to-grain interaction, matrix-strength, hindered settling, buoyancy and disperse pressure. Hyperconcentrated flows are dominated by particle-

particle interaction, buoyancy and minor matrix strength effects, collectively resulting in reduced differential grain settling and hence generally ungraded sand-rich stratal textures. In contrast, more extensive differential grain settling in concentrated flows results in typically normally graded sand-rich deposits (termed Lowe sequences by Mulder and Alexander, 2001). Lastly, grains in turbidity currents are fully supported by the upward component of turbulence and produce graded Bouma sequences (Bouma, 1962). In addition to these three types there are a number of transitional types, and it is these that are interpreted to deposit the matrix-rich strata described in this study. Talling (2012) combined the laboratory results of Baas et al. (2009) and Sumner et al. (2009) to produce a phase diagram (Figure 2.4) depicting the relation between flow speed, mud concentration, flow structure and the final deposit. Experiments by Baas et al. (2009), Sumner et al. 2009 (and later Tilston, 2015) imply that even a small fraction of cohesive mud can cause an initially highly turbulent flow to evolve into a laminar plug flow. Below, an expanded review of turbidity currents and various matrix-rich transitional flow deposits is presented.

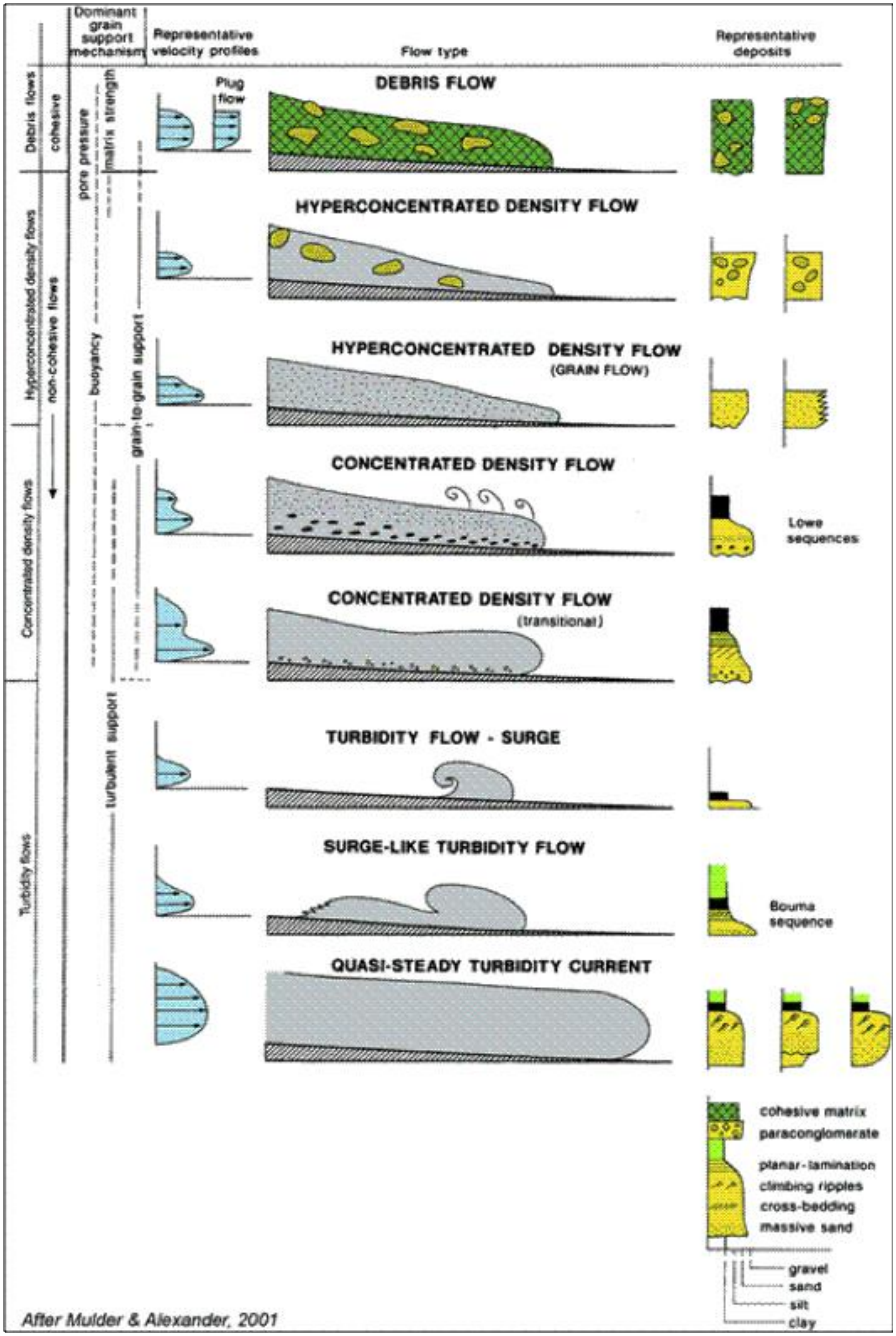

Figure 2.3: Sediment gravity flow types (from Mulder and Alexander, 2001).

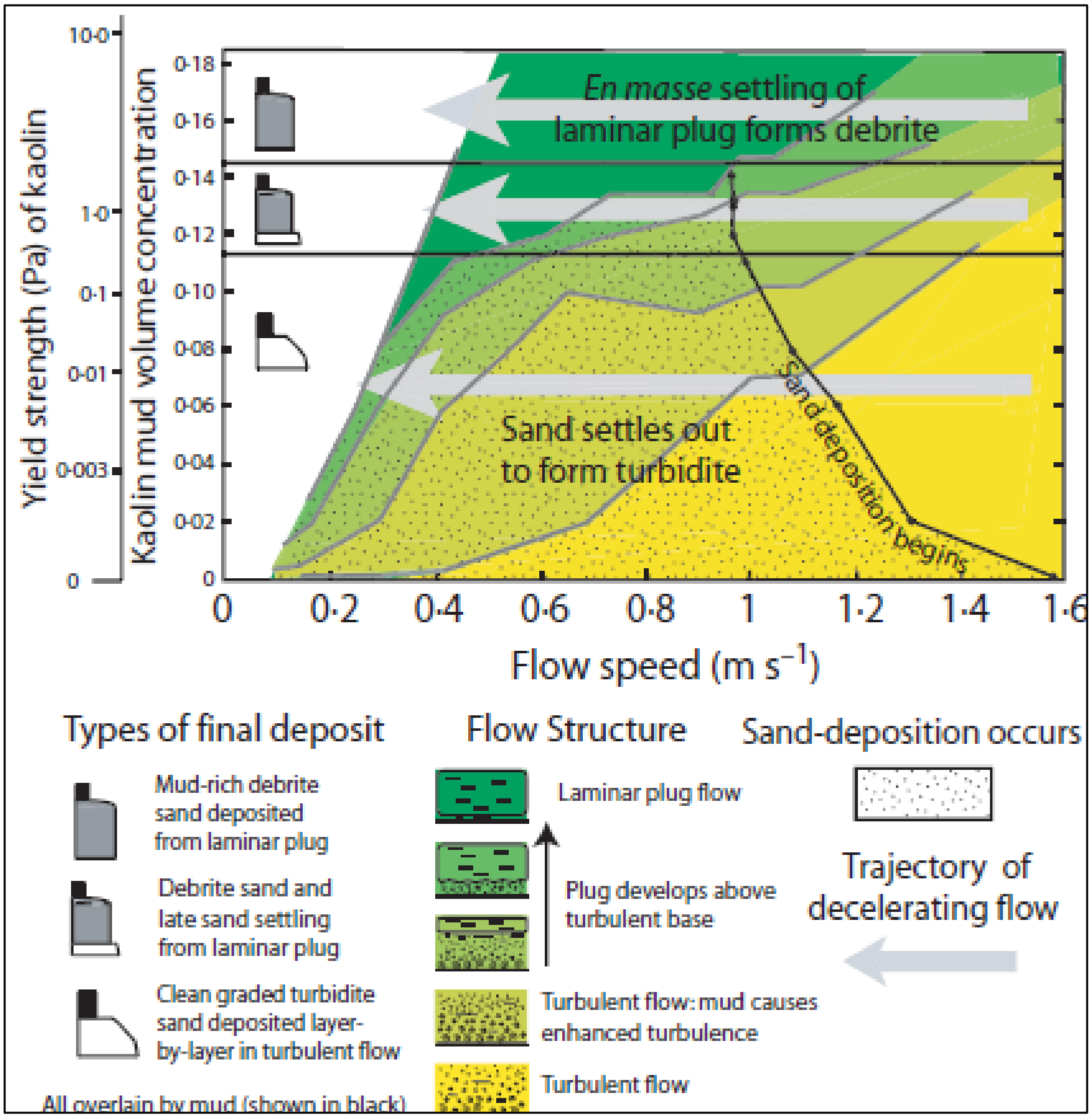

Figure 2.4: Phase diagram showing the relationship between flow speed and volume concentration cohesive mud in an initially fully turbulent sediment suspension which then decelerates (indicated by the thick grey arrows) (after Sumner et al., 2009). The figure combines results from the recirculating flume experiments of Baas et al. (2009), which described characteristics of vertical flow structure, and annular flume experiments by Sumner et al., 2009 that documented the lithological character of the deposits. Both sets of experiments involved mixtures of kaolin and water, with sand being added to the Sumner et al. experiments. Depending on mud content flow deceleration can lead to development of a non-shearing laminar plug, which in turn controls which of the three different types of deposit form. At low mud content, sand settles through the turbulent suspension and gradually builds up a clean, graded sandy turbidite. At high mud contents (>14.25% kaolin clay), en masse consolidation of a laminar plug that extends from the top to the base of the flow forms an ungraded, mud-rich sandy debrite. At intermediate concentrations, late-stage settling of sand from the laminar plug results in a thin, sand-rich basal layer beneath a sandy, mud-rich plug deposit. Sufficiently high mud fractions will support small mud clasts, and at even higher sediment concentrations large mud clasts can become buoyant. From Talling et al. (2012).

2.2.2 Turbidity Currents

Turbidity currents were first documented during the late nineteenth century by Forel (1885) who postulated that subaqueous canyons in Lake Geneva were produced by the underflow of the Rhone River. Later, Daly (1936) and Johnson (1939) proposed a 'similar mechanism', termed a turbidity current by Johnson (1939), to be the origin of continental submarine canyons (eroded during periods of sea-level lowstand). However, the modern concept of the term turbidity current as being the principal agent for transporting and depositing clastic sediment in the deep-sea originated from the experimental work of Kuenen and Migliorini (1950) who suggested that normally graded sandstone beds, such as those documented in the Italian Apennines, were deposited by decelerating turbidity currents.

As discussed above, turbidity currents can be initiated by a variety of single or combined causes. For example, turbidity currents may initiate directly from fluvial discharge, especially during sea-level lowstand when sediment is deposited directly on the upper continental slope. Over time this induces oversteepening, gravitational instabilities and eventually failure, which potentially may spawn a turbidity current (Kneller and Buckee, 2000). Similarly, slope failure can be initiated when sediment becomes destabilized and remobilized through seismic shaking (Normark and Piper, 1991). Moreover, turbidity currents may evolve due to the degradation of a slump, slide or debris flow (Figure 2.1); Kneller and Buckee, 2000; Shanmugan, 2006). An outstanding example of a turbidity current is the Grand Banks failure of 1929, where an earthquake generated a large slump that is interpreted to have progressively disintegrated downslope into a debris flow that then evolved into a turbidity current (Piper et al., 1985).

The path and speed of the current could be quantified by the sequential breaking of submarine telegraph cables, the last breaking 13 hours after the upflow initiation of the flow. The flow travelled up to 70 km/hr, was upwards of several hundred meters thick, and deposited a bed with a volume of about 185 km^3 (Piper and Aksu, 1987; Piper et al., 1988; Hugues-Clarke et al. 1990).

As mentioned earlier, turbidity currents are a fast-flowing, sediment-gravity flow in which sediment is suspended largely by the upward directed component of fluid turbulence (Bagnold, 1966; Middleton and Hampton 1973). This creates a sediment-water mixture denser than the surrounding ambient (marine) fluid, and as a consequence causes it to move downslope under the influence if gravity. These flows are non-conservative in that they may exchange sediment with the lower boundary (i.e. sediment bed) though suspension or deposition and may exchange fluid with the surrounding ambient fluid through entrainment or detrainment (Meiburg and Kneller, 2009). Commonly, these factors (along with sediment concentration and grain size) influence the runout distances and termination of the flow. Through the means of extensive mixing within the flow and the variability in settling rates for different grain sizes, turbidity currents become vertically and horizontally sorted. Vertical stratification results in grain concentration and flow velocity being highest near the base of the flow and decreasing exponentially upwards (Mulder and Alexander, 2001). Horizontal (longitudinal) stratification is made evident by the distinctive structure of a turbidity current, which consists of a well-developed head, body and tail (Figure 2.5). Typically, the highest sediment concentration and coarsest sediment occurs in the head whereas the tail is commonly the most dilute and fine grained. Furthermore, the head is commonly the thickest part of the flow, and moves slower than the body of the flow. This contrast in flow speed facilitates the faster flowing body of the current to continuously feed sediment into the head of the current, which helps counterbalance boundary friction effects and density loss due to ambient fluid entrainment (Hiscott, 2003). Additionally, the head of the flow has an overhanging nose that develops in response to frictional forces along the lower and upper boundaries of the flow. Furthermore, and assemblage of lobes and clefts forms at the contact between the lower boundary and the overhanging nose (Simpson, 1972). Ambient fluid is entrained into the flow through the clefts that separate the lobes (Figure 2.6). However, entrainment beneath the head of the flow is considerably less than that along the upper and lateral surfaces of the flow where Kelvin-Helmholtz instabilities can result in extensive mixing (Britter and Simpson, 1978; Figure 2.7, 2.8). Recent experimental work by Tilston et al., (2015) revealed that the amount of ambient fluid entrainment (i.e. the scale of Kelvin-Helmholtz instabilities) is related to the density structure of the flow. Typically, an exponential density structure forms in coarse-grained flows, which in turn produces large Kelvin-Helmholtz instabilities and extensive entrainment of ambient fluid leading to energy loss and disintegration of the flow. In contrast, a plug-like density structure is characteristic of fine-grained flows. In these flows small Kelvin-Helmholtz instabilities are generated and accordingly minor ambient fluid entrainment – the end result being reduced energy loss and longer run-out distances (Figure 2.7).

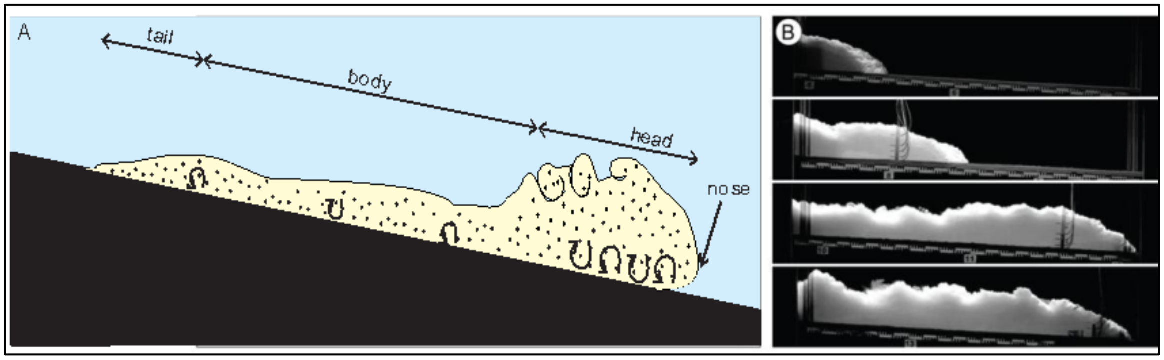

Figure 2.5: A) Illustration of a turbidity current showing the head, body, and tail regions. Note the overhanging nose at the front of the head that forms in response to frictional forces between the lower boundary of the flow and the static bed and the upper boundary of the flow and ambient fluid. Modified from Khan and Arnott, 2012. B) Time lapse photographs of a turbidity current created in a laboratory setting. From Jobe.Z, 2012. Note the similarities between figures A and B.

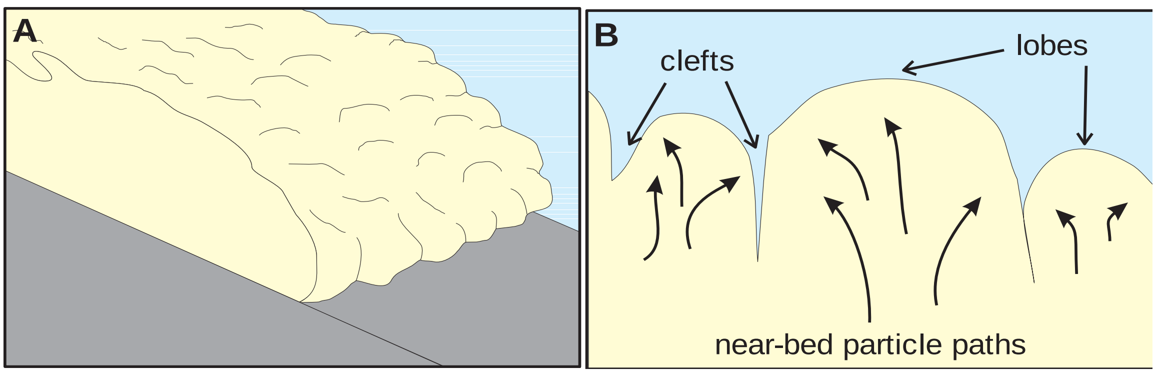

Figure 2.6: Instability at the front of a turbidity current head. A) The lobes and clefts that form at the contact between the overhanging nose and solid boundary B) A schematic view of lobes and clefts viewed from below. Illustrations from Khan and Arnott, 2012).

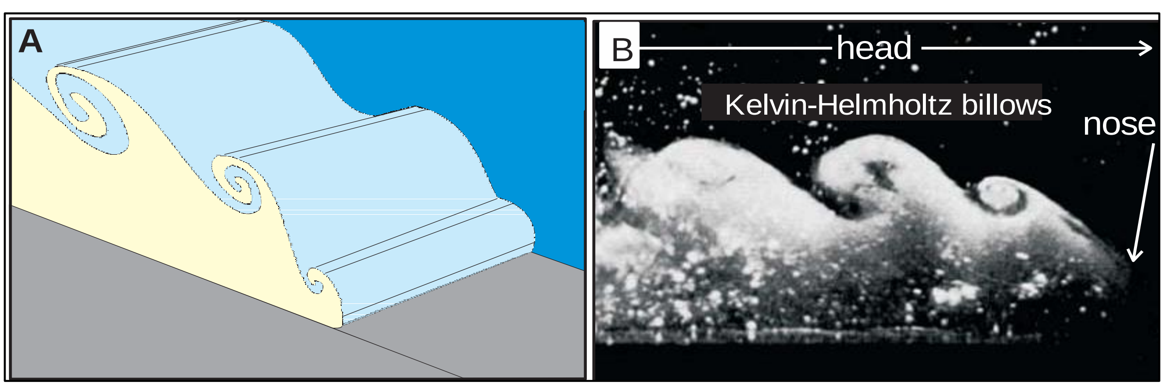

Figure 2.7: Instability that takes place between the upper boundary of the flow and the ambient fluid. A) Schematic illustrating the developing Kelvin-Helmholtz billows (From Khan and Arnott, 2012). B) Image of the head of a saline gravity current showing well developed Kelvin-Helmholtz billows (after Simpson, 1969).

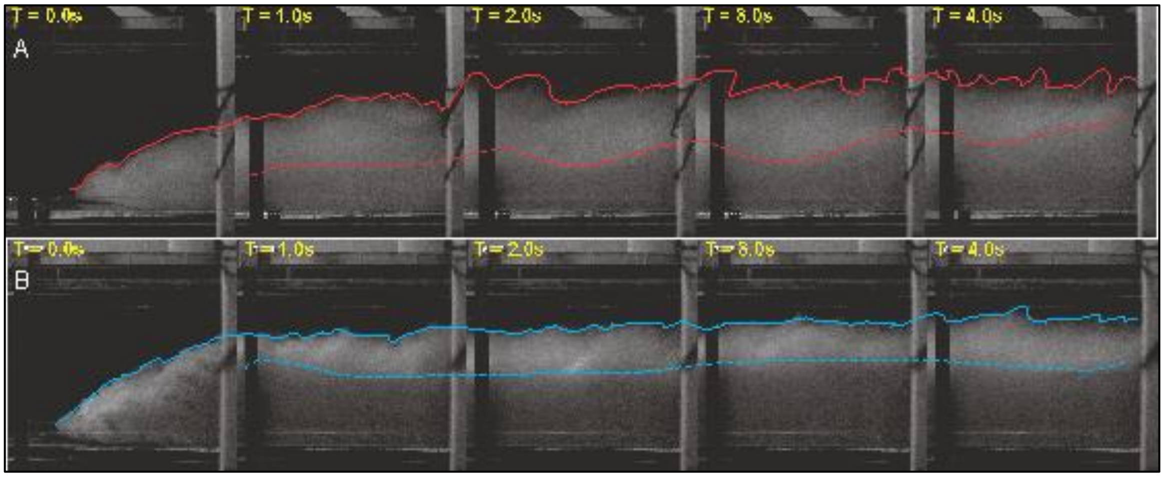

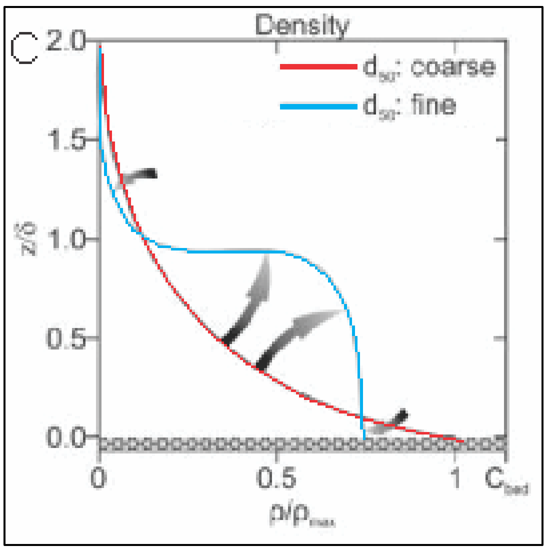

Figure 2.8: Top: High speed photographs of the downflow evolution of two flows with the same sediment concentration and flow speed but vary in grain size (From Tilston experiments, 2014). Solid lines outline the vertical extent of Kelvin-Helmholtz instabilities, A): A coarse-grained sediment gravity current (d50: 0.30mm, 22.5% by mass). Here, KH instabilities are large, highly undulatory, resulting in a higher amount of ambient fluid entrainment and thus a greater amount of mixing (depicted by the undulatory and diffuse nature of the dashed line that traces out vertical variations in sediment concentration (i.e. density)). B) A fine-grained sediment gravity current (d50: 0.15mm, 25% by mass). Here, KH instabilities are small and barely cut downwards, resulting in less ambient fluid entrainment and less mixing/dilution of the flow (depicted by the thick plug-like nature of the lower part of the flow and its sharp, planar upper surface (dashed line). C) Left: Graph depicting density structure of a coarse vs fine-grained flow. Coarse-grained flows exhibit an exponential density profile whereas fine-grained flows have a more ‘plug’-like density profile.

2.2.3 Turbidites

Turbidites are the deposits of turbidity currents (Kuenen, 1957) and deposition is generally initiated when competence and/or capacity become exceeded. This commonly occurs due to a spatial and/or temporal decrease in flow speed caused, for example, by changes in slope, transition from confined to unconfined environments, or reduction in sediment concentration. Sediment that falls from suspension moves temporarily along the bed and results in the formation of a medley of bed-load, unidirectional, sedimentary structures reflecting progressively waning flow conditions (Southard and Boguchwal, 1990; Kneller and McCaffrey, 2003). Bouma (1962) originally described the idealized succession of sedimentary structures, later termed the Bouma sequence, for deposition from a single, decelerating, non-cohesive, low-density turbidity current (1962). The Bouma sequence includes five intervals that from base to top fine upwards and are termed the T_a–T_e divisions (Figure 2.8). The T_a division consists of massive to graded, structureless, coarse to medium sand, commonly with flute and tool marks at its base. These beds are commonly interpreted to form in the upper plane flow regime (Walker, 1965); however, high sedimentation rates are thought to prevent planar lamination from developing (Walton, 1967). Arnott and Hand (1989) confirmed this assumption experimentally by showing that high suspension fallout suppresses the development of planar lamination. The T_b division typically ranges from medium- to fine-grained sand and is interpreted to represent upper-regime plane bed deposition. However, more recently Arnott (2014) argued that planar lamination is indicative of traction transport on a bed that lacks the surface defects from which angular bed forms like ripples and dunes form, and as such, planar lamination can form at any flow speed. The T_c interval is deposited in the lower flow regime and is made up of small-scale cross-laminated fine to very fine sand. Climbing ripple cross- stratification forms when sedimentation rates are high relative to bed load transport rates (Allen, 1971). The T_d interval comprises silt and interlaminated silt-mud couplets that form through both suspension and traction processes (Piper, 1978; Stow, 1979; Stow and Shanmugam, 1980). The T_e interval consists of homogeneous, structureless mud deposited completely from suspension (Kelts and Arthur, 1981).

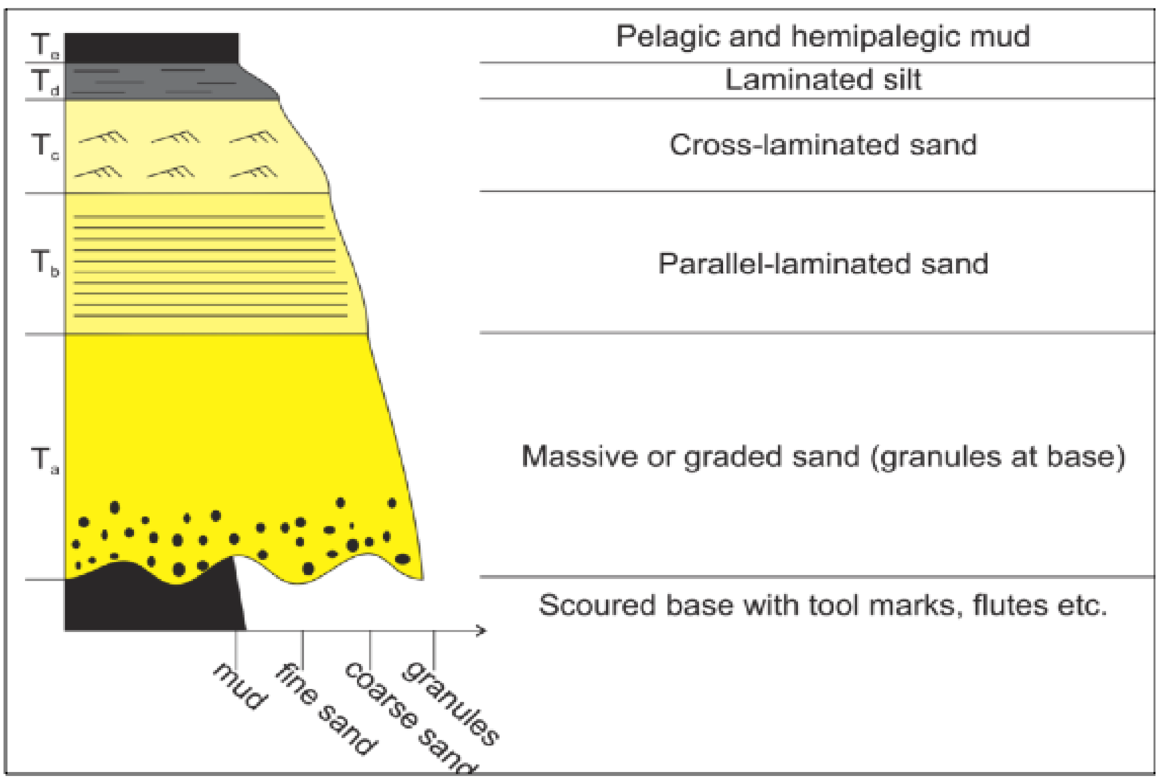

Figure 2.9: Idealized sequence of sedimentary textures and structures formed by a decelerating, dilute turbidity current (after Bouma, 1962, from Terlaky, 2014).

Bouma turbidites are interpreted to be deposited by low-density turbidity currents where volumetric sediment concentration is less than 9%. Flows with a higher sediment concentration are termed high-density turbidity currents and are thought not to deposit classic Bouma turbidites. For these strata, Lowe (1982) proposed a classification based on grain size and sediment concentration in the formative flows – R indicating gravel sediment (conglomerate) and S indicating sandy sediment (sandstone) (Figure 2.9). Deposits, whether conglomerate or sandstone consisted ideally of three units, although deposits typically consisted of more than one unit: a basal traction unit (R1/S1) consisting of upper-stage planar lamination or dune cross-stratification, an intermediate unit (R2/S2) made up of stacked inversely graded layer formed by traction carpet processes, and an upper normally graded unit (R3/S3) deposited directly from suspension (S3 being equivalent to the Bouma T_a division. Lowe (1982) also described another common sand-rich deposit observed in the deep-marine sedimentary record -- massive, poorly-sorted sandstones. These strata, like the S and R turbidites are thought to represent deposition from high-density turbidity currents, but where rates of sedimentation were higher. Under these conditions bed-surface sorting processes associated with traction sediment transport were muted, which in turn caused the aggrading deposit to appear “massive” (Arnott and Hand, 1989).

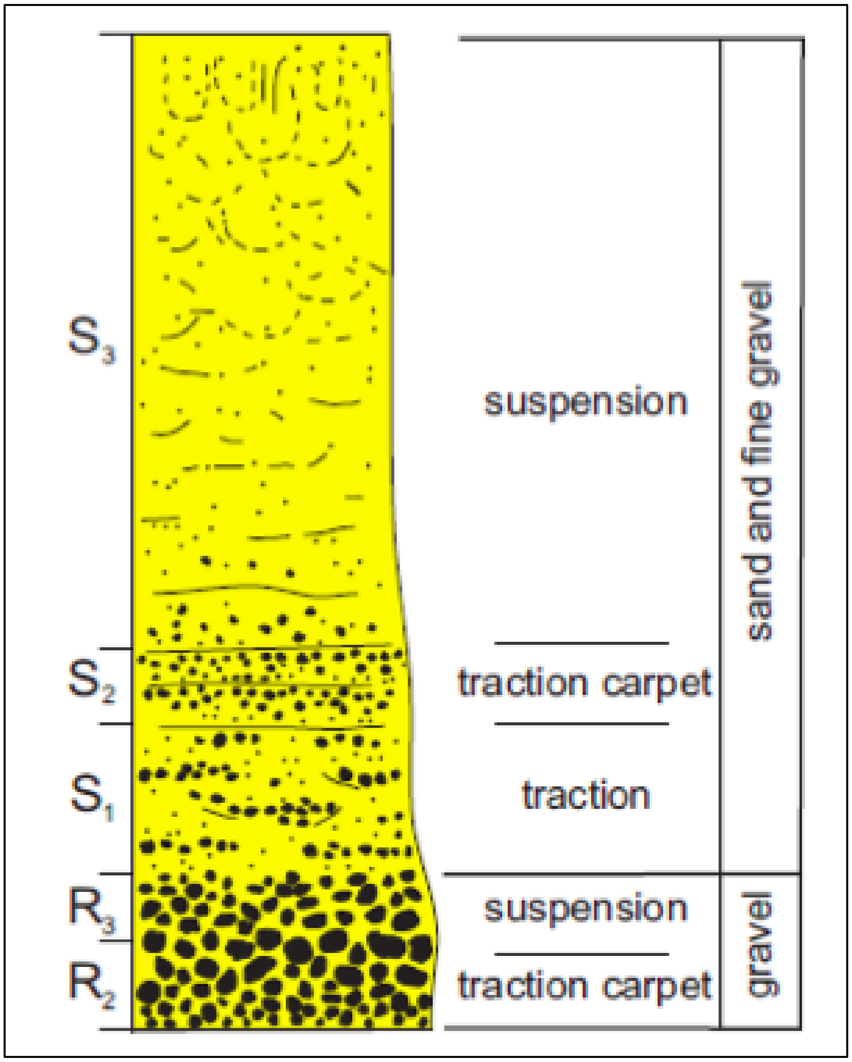

Figure 2.10: Idealized deposit of a sandy high-density turbidity current proposed by Lowe, 1982

2.3 Matrix-rich (Transitional) Flow Deposits

Recently, strata with anomalous matrix content have been increasingly observed in the deep-marine sedimentary record and have been interpreted to represent deposition from flows with complex internal rheological boundaries, or with transitional turbulent-laminar rheologies (Lowe and Guy, 2000; Haughton et al., 2003; Talling et al., 2004; Sylvester and Lowe, 2004; Kane and Ponten, 2012). Many terms for these deposits have been proposed, and include: hybrid beds, co-genetic debrite-turbidites, linked-debrites, sandy debris flows, submarine transitional flow deposits, slurry beds, etc. The characteristics and depositional mechanisms of hybrid event beds, co-genetic debrite-turbidites, slurry beds, transitional flows deposits and matrix-rich sandstones are discussed next.

2.3.1 Hybrid Event Beds (HEB's)

Hybridid event beds are characterized by distinctive layers indicative of cohesionless (turbulence-supported) or cohesive (mud-supported) flow, with no bed boundary separating the various layers (Haughton et al., 2009). Accordingly, these beds suggest deposition from flows that are transitional between submarine debris flows and turbidity currents. Over the past decade, HEBs have been described in a number of modern and ancient turbidite systems, including: Agadir Basin (Africa; Talling et al., 2007), Marnoso-arenacea Formation (Italian Apennines; Talling et al., 2012b), distal lobe of the Mississippi fan (Gulf of Mexico; Talling et al., 2010), Jurassic and Paleocene subsurface reservoir units in the North Sea (Haughton et al., 2009) and the Karoo Group (Africa; Hodgson, 2009).

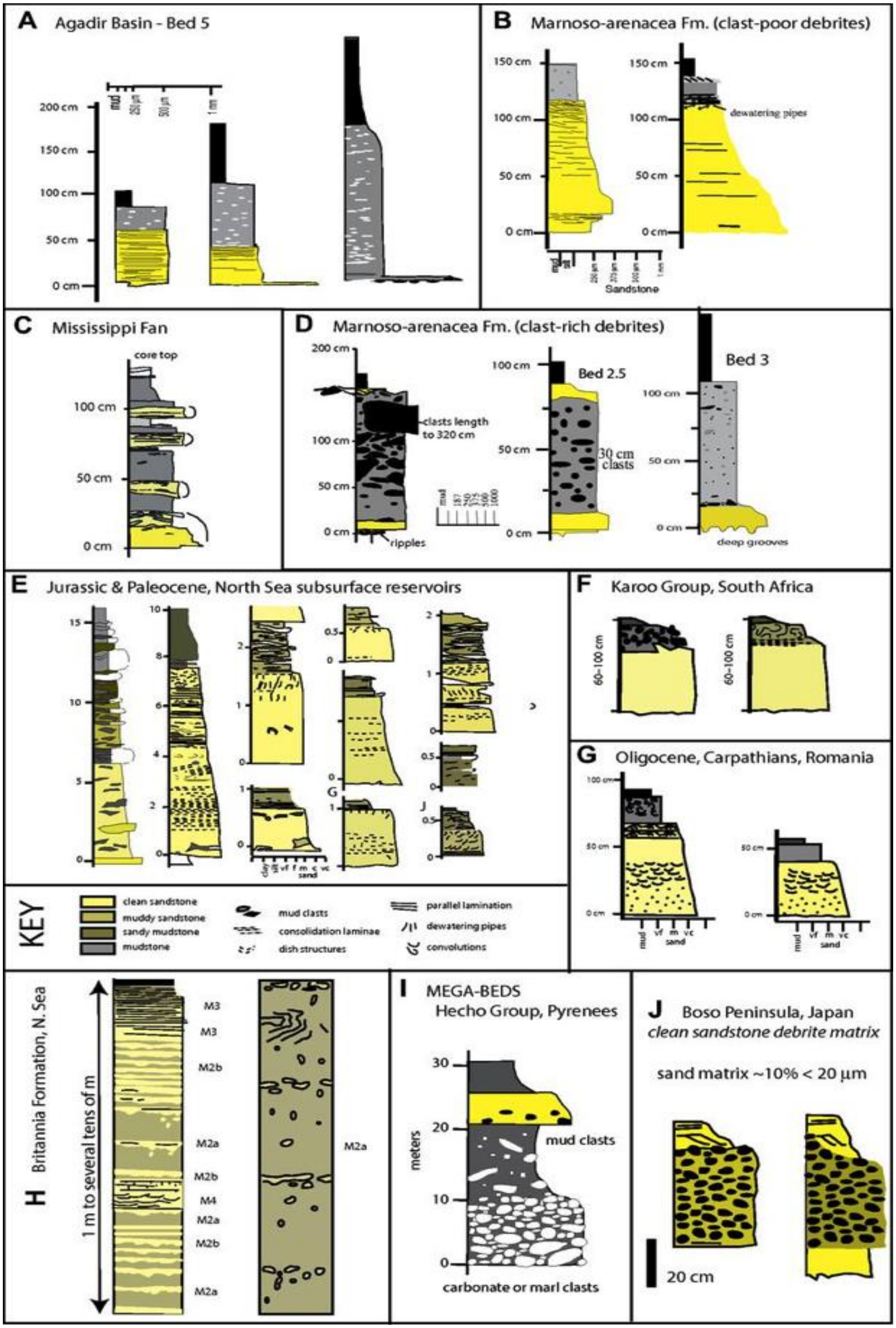

Figure 2.11: Sedimentary logs depicting varieties of hybrid event bed deposits from various locations. From Talling, 2012.

Stratigraphically upward HEBs comprise up to five divisions: (H1) basal clean, ungraded or graded, structureless sandstone; overlain by (H2) alternating bands of matrix-poor and matrix-rich sandstone; followed by (H3) matrix-rich sandstone with mudstone clasts, granules and shear fabrics (more commonly termed a 'linked-debrite'); (H4) parallel and ripple cross laminated sandstone and (H5) massive mudstone.

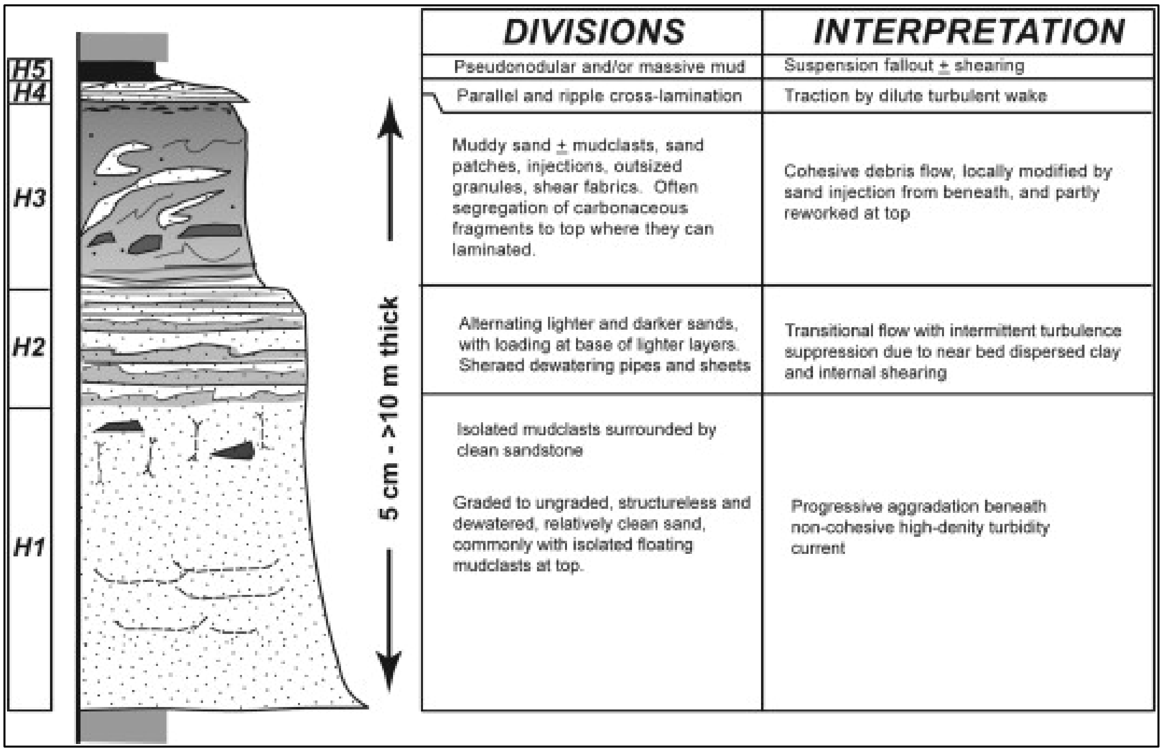

Figure 2.12: Schematic of an idealized stratigraphic log depicting all 5 (H1- H5) divisions of a hybrid event deposit. From Haughton et al., 2009.

Haughton et al. (2003; 2009) proposed that these divisions were deposited during a single flow event that transformed longitudinally from turbulent to laminar flow, suggesting that each division was associated with a specific flow state. Several mechanisms have been proposed for flow transformation based on field observations. One mechanism suggests that a debris flow was partially transformed into a forerunning turbidity current. The forerunning turbidity current moved independently of the debris flow and deposits a basal massive sandstone beds (H1 and H2). Haughton et al. (2009) proposed that the lack of tractional structures in the basal deposits was indicative of a turbidity current with a 'short' runout distance and likely overrun by the debris flow before tractional structures could form. Alternatively the flow transformation may be the result of the turbidity current "bulking-up" by mud particles and fragments being eroded from the seafloor. Flow turbulence would have disaggregated the mud clasts, and further increased the mud content in the flow and ultimately resulted in a fractionated flow. The experimental work of Baas and Best (2011) illustrates the flow transformation of hybrid event beds through five rheological stages: Turbulent flow (TF); turbulent-enhanced transitional flow (TETF); lower transitional plug flow (LTPF); upper transitional plug flow (UTPF) and quasi-laminar plug flow (QLPF) (Figure 2.12). In TF and TETF, flow velocity is sufficiently high to prevent clay/mud from exhibiting cohesive properties. This is interpreted to be the basal portion of hybrid event beds (H1 and H2). As the clay/mud concentration increases, a plug-like flow region forms and turbulence becomes suppressed. The plug forms in the upper part of the flow where shear is lowest and as clay concentration increases it expands downwards and leads to UTPF. As the plug flow continues to thicken the viscosity and yield strength of the flow eventually suppresses all turbulence and the flow evolves into a QLPF. Based on the field observations and experimental data the five stratal divisions of hybrid event beds are interpreted as the following flow transformation: (H1) represents a fully turbulent, high density turbidity current with aggradation; (H2) is a transitional (or intermediate) flow with intermittent turbulence suppression; (H3) as turbulence becomes suppressed the flow becomes laminar causing en-masse freezing of sediment; (H4) represents the trailing low-density turbulent cloud and finally, (H5) is mud suspension fallout. Hybrid event beds are commonly located along the lateral and distal edges of an overall turbulent transport system (e.g. deep-water fans and basin plane sedimentary systems; Houghton et al., 2009). Hybrid event beds share common characteristics with other matrix-rich transitional flow deposits.

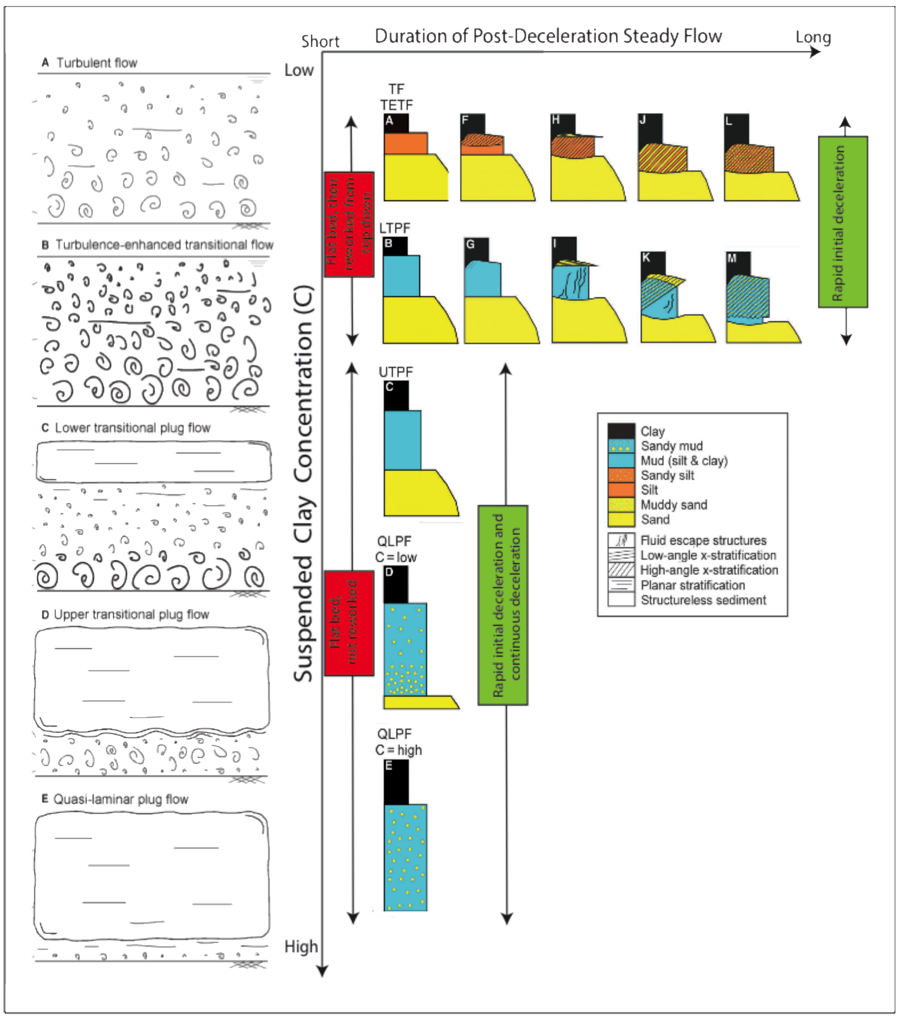

Figure 2.13: Left: Schematic representation of flow structure in a flow evolving from turbulent to quasi-laminar plug flow. Note that as the plug thickens downward, turbulence becomes damped and the flow becomes more laminar. Right: Idealized stratigraphic logs of deposits from each type of flow. The structure of the deposits varies depending on the type of flow, suspended clay (mud) concentration and the duration of steady flow (post-initial deceleration). Matrix-rich strata described in this study are interpreted to represent deposition from UTPF and/or QLPF conditions. Modified from Baas and Best (2011).

2.3.2 Cogenetic Debrite-Turbidite Deposits

Cogenetic debrite-turbidite beds are homologous with the linked debrite (H3) division of hybrid event beds discussed above. Their basic character is distinctive in that they comprise a mud-rich, ungraded sandstone interval encased between matrix-poor sandstone, siltstone or mudstone (Talling et al, 2004; Amy and Talling, 2006). The mud-rich unit exhibits characteristics of en-masse deposition such as the chaotic dispersal of clasts and the ungraded nature of the bed (implying en-masse deposition with no subsequent settling of grains) and is thus termed a debrite. Similarly, the mud-poor sandstone beds show features indicative of layer-by-layer deposition and therefore is termed a turbidite. Two end-member types of cogenetic beds are distinguished based on the presence (Type 1) or absence (Type 2) of mud clasts (Talling et al, 2004; Amy and Talling, 2006). From detailed field observations it was shown that clast size and abundance decreased systematically downflow until none remained, suggesting a genetic link between Type 1 and Type 2 strata. Both types consist of a graded or ungraded, clean, mud-poor sandstone at their base. In Type 1 beds the basal layer is thinner (<20 cm) and typically coarser than the upper, mud-rich, debrite. Outsized mud clasts, subtle parallel laminae and water-escape structures are common towards the top of the bed. The intervening mud-rich, debrite unit has a distinctive blue hue (attributed to increased mud content of approximately 15-20%) and is dominated by the presence of chaotically dispersed mud clasts. In the case of Type 2 beds the basal unit is thicker (>20cm) and the outsized clasts and subtle laminae that are common at the top of Type 1 beds are generally absent. The most distinct feature of Type 2 beds is the lack of mud clasts and higher mud content in the debrite unit (approximately 30-50%). Based on paleocurrent measurements, the positioning of hemipelagic layers, and the fact that the debrite unit is always overlain by a clean sandstone (i.e. later event) cogenetic debrite-turbidite beds are interpreted to represent deposition from a single flow that exhibited both laminar and turbulent flow states. Talling et al. (2004) proposed five possible scenarios to explain the deposition of cogenetic debrite-turbidites: 1) Turbidity current formed by dilution of initial debris flow; 2) Debris flow formed by an initial turbidity current that erodes the sea floor; 3) Turbidity current triggers secondary debris flow; 4) Debris flow formation due to deceleration of initial turbidity current; 5) Deceleration of a low-yield strength debris flow leading to settling of coarser sediment. However, based on the interpreted location of cogenetic debrite-turbidite strata the most plausible depositional model is through the erosion of a mud-rich seabed by an initially more mud-poor turbidity current. In this case, the debris flow is hypothesized to be formed as sediment and mud concentrations increase and the flow develops cohesive strength. Cogenetic debrite-turbidite beds are interpreted to be deposited on the unchannelized distal part of the basin-floor and basin-plain fans, particularly along their distal and lateral margins (Haughton, 2009).

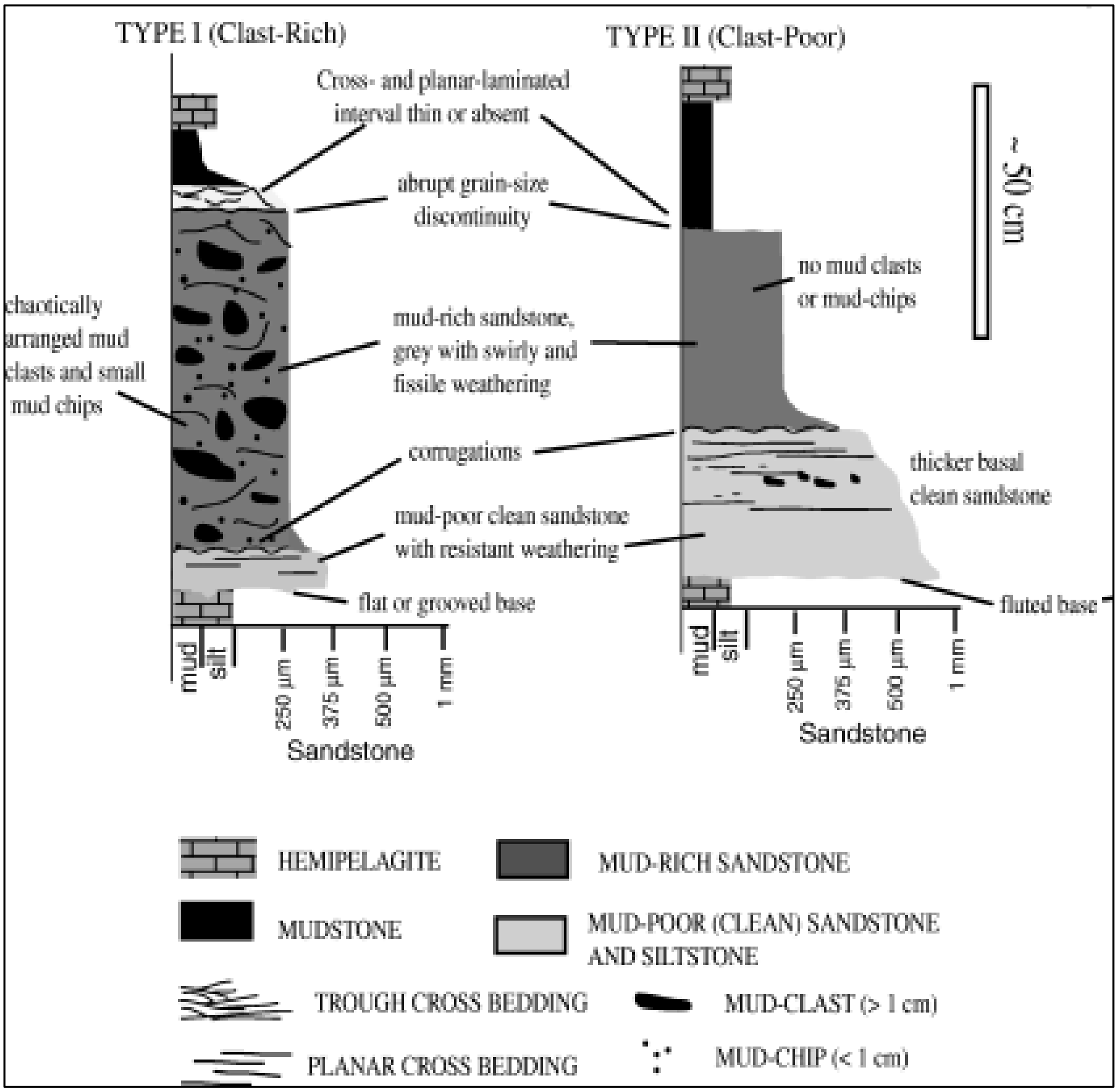

Figure 2.14: Idealized stratigraphic logs of Type I and Type II co-genetic debrite-turbidite deposits (From Talling et al, 2004)

2.3.3 Slurry Flow Deposits

Like above, slurry flow deposits are interpreted to represent deposition from turbulent, mud-rich flows that are transitional in behavior between turbidity currents and debris flows (Lowe and Guy, 2000). This discussion on slurry flow deposits will focus on two examples: Oligocene flysch of the East Carpathians, Romania (Sylvester and Lowe, 2004), and Lower Cretaceous Britannia Formation, UK North Sea (Lowe et al. 2003; Lowe and Guy, 2000). The first example describes two end-member deposits with no transitional facies suggesting that each end-member was deposited by a unique process. The second example provides a more in-depth analysis of the distinct structures and textures of slurry flow beds.

Slurry Flow Deposits from the Oligocene flysch of the East Carpathians, Romania.

Here, two end member slurry flow deposits, specifically a coarser-grained mud-rich sandstone and a finer-grained mud-rich sandstone, were identified. The first is a poorly-sorted, fine- to very fine-grained, mud-rich sandstone ranging from 10-50 cm thick. Locally, planar lamination may be common towards the top of the bed, but otherwise tractional structures are absent. Also, mudstone clasts are common within the upper part of the bed. In contrast the mud-rich deposit ranges from very fine sand to coarse silt and is typically normally graded. Planar lamination is much better developed and is described as being intermediate to microbanding and the planar lamination observed in the Tde divisions of turbidities. Notably, mudstone clasts are rare to absent.

Two depositional models were presented for the first coarser-grained type of deposit and are dependent on the initial flow conditions (Sylvester and Lowe, 2004). The first model requires high rates of suspended sediment fallout in order to hinder the fine-tailed fraction of the flow from being displaced upward. As a consequence, mud becomes increasingly concentrated in the near-bed shear layer, which then causes the near-bed layer to become cohesive (Sylvester and Lowe, 2004). An alternative model begins with a flow that initially is rich in mud. Again, as a consequence of the high fallout rate of the coarser-grains the distribution of suspended grains shifts towards finer sediment. This, in turn, results in a considerable increase in the amount of mud floccules left in suspension. The high sediment concentrations in the lower portion of the flow coupled with high sedimentation rates results in the trapping of finer sediment. This gives rise to a cohesive near-bed shear layer and the formation of a rheological interface between the lower cohesive portion and the upper turbulent portion of the flow. As a result, there is no mixing between the two portions of the flow and deposition from the turbulent portion of the flow resumes only after the cohesive layer has been depleted or has been deposited (Sylvester and Lowe, 2004). The second type (finer-grained) of slurry flow deposit is interpreted to be deposited by flows exhibiting minor fluctuations in flow properties such as variations in turbulence suppression, resulting in the deposition of alternating mud-rich and mud-poor sand strata (Sylvester and Lowe, 2004).

Slurry flow deposits from the Lower Cretaceous Britannia Formation, UK North Sea

Slurry flow deposits exhibit sedimentary structures unlike those in classical turbidites, especially extensive dewatering structures and wispy lamination (Lowe et al, 2003). Beds range in thickness from a few centimeters to 30 m and commonly contain 10-30% detrital mud matrix. In addition strata exhibit up to seven divisions, each with a unique assemblage of sedimentary structures, which in turn make up five bed types. The possible seven sedimentary structure divisions are: (M1) current structured and massive divisions; (M2) banded units (composed of megabanded (M2A), macrobanded (M2B) and mesobanded (M2C)); (M3) wispy laminated sandstone; (M4) dish-structured divisions; (M5) fine-grained, microbanded to flat-laminated units; (M6) foundered and mixed layers that were originally laminated to microbanded; and (M7) vertical water-escape structured divisions.

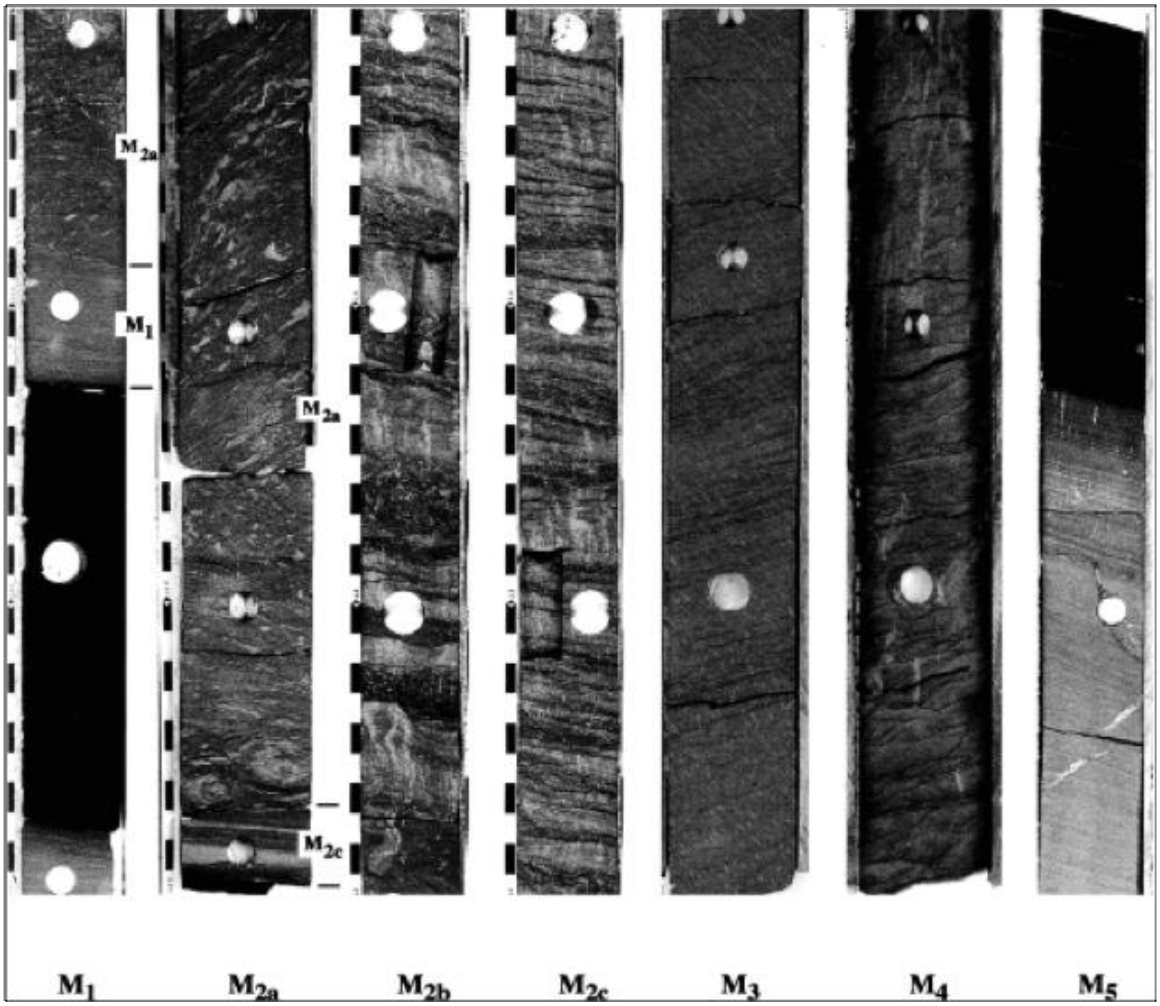

Figure 2.15: Sedimentary structure divisions M1, M2, M3, M4 and M5 of slurry- flow beds (From Lowe and Guy, 2000).

The following flow transformation is proposed for the deposition of these divisions. Deposition from fully turbulent turbidity currents deposited the M1 division. As the flow waned, both mud and sand grains settled causing an increase in the near-bed grain concentration and flow density. However, the abundant and faster settling coarse grains caused the mud grains to become trapped while coarser grains continued settling to the bed. As a result, the particle concentration and mud content in the near-bed region continually increased. Here, mud grains became disaggregated causing an increase in effective clay surface area. This eventually increased near-bed cohesion, shear resistance and viscosity leading to the suppression of turbulence in a layer immediately adjacent to the bed and it is transformed into a cohesion dominated viscous sublayer (Lowe and Guy, 2000). The banded units (M2) are interpreted to represent the formation, evolution and deposition of such cohesion-dominated sublayers. M3 divisions require a less muddy flow with faster rates of suspended sediment fall out in order to develop thin, short-lived viscous sublayers that form wispy lamination. Lowe and Guy (2000) reported that these sediment structure divisions often stacked to form an array of bed types, which were: (I) dish-structured beds; (II) dish-structured and wispy-laminated beds; (III) banded and wispy laminated and/or dish-structured beds; (IV) predominantly banded beds; and (V) thickly banded and mixed slurried beds. Bed type is dependent on a combination of mud concentration and the rate of suspended fallout (Lowe and Guy, 2003). All of the bed types have a thin M1 division at their base and a M5, M6 or M7 division at the top. Thus, the onset of deposition of all bed types is interpreted to be from fully turbulent turbidity currents.

Type I – Dish-structured beds

Commonly, this bed type exhibits a massive sandstone base (M1) that upward becomes littered with vertical escape structures (M7) and dish-structures (M4). Type I beds are interpreted to represent rapid deposition followed by extensive dewatering and mixing of bed surface layers before the deposition of overlying sediments.

Type II – Dish-structured and Wispy-Laminated Beds

Type II beds are dominated by dish-structured (M4) and wispy laminated sandstone (M3) with common vertical escape structures (M7) towards the top of beds. These beds are typically thick (>8 m) and are interpreted to represent more than one pulse or surge during a single depositional event. The introduction of the wispy-laminated sandstone within these units implies that flow rheology had changed, likely due to an increase in mud concentration. Thus, Type II beds are interpreted to have been deposited down flow of Type I units.

Type III Beds – Wispy Laminated and Banded Units

These beds are dominated by the presence of banded units, namely mesobanding capped commonly by M5 or M5, 6 divisions. Type III beds are interpreted to have been deposited by flows containing high mud content as the development of a viscous, cohesive sublayer is necessary to produce the varied suite of banded and wispy divisions throughout the bed. Typically, banded divisions within type III beds decrease in band and couplet thickness vertically suggesting that following the initial turbulent flow (and high sediment fall out rates) a thick cohesive sublayer develops. Similarly, the upward decrease in the thickness of darker bands suggests that the mud content of the flow was declining overall. However, the presence of a muddy M5, 6 suggests that mud continued to be a major component of these flows until they ended.

Type IV Beds – Mesobanded and Macrobanded Units

These beds are similar to Type III beds in that they require a high concentration of mud in order to form the mud-viscous cohesive sublayer responsible for forming the banding. However, the thick units of ‘light’ coloured, mud-poor bands (some with thicknesses greater than 1m) suggest that while the lower portion of the flow exhibited a viscous, cohesive sublayer, the upper and middle portions of the flow continued to be dominated by turbulent sediment suspension.

Type V – Thickly Banded and Mixed Slurried Beds

Type V beds are dominated by megabanded and mixed slurried divisions (M2A) that commonly grade laterally into Type IV beds. Locally, these beds may be mesobanded, microbanded (M2B, C) and/or wispy-laminated (M3) top. This lateral facies association suggests that Type V beds originated by shearing, disruption and possibly late-stage flowage of originally banded units (Type IV). The flows depositing these beds were mud dominated and characterized by cohesion-dominated near-bed layers throughout much or all of their evolution.

Overall, slurry flow deposits are interpreted to represent deposition in the distal, unconfined parts of a turbidite deposystem such as the deep-water basin plain (Lowe and Guy, 2003).

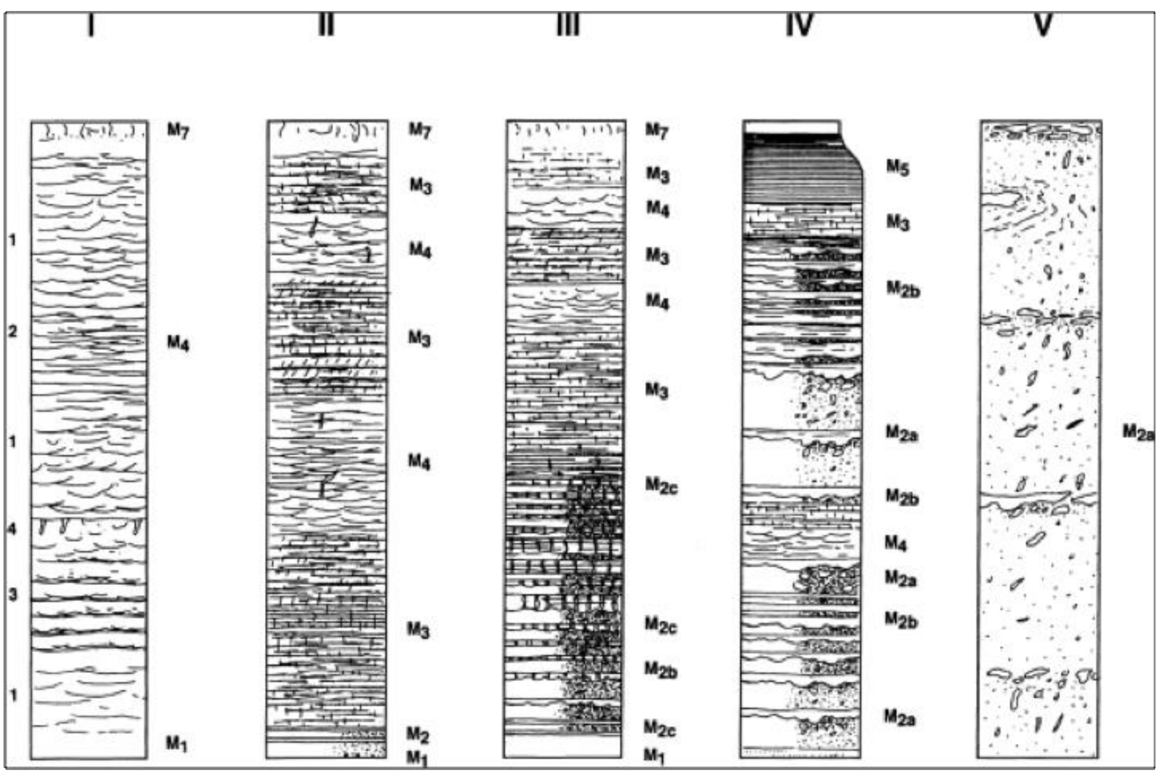

Figure 2.16: Schematic of the five basic slurry- flow bed types (from Lowe and Guy, 2000)

2.3.4 Transitional Flow Deposits

Transitional flow deposits, which are interpreted to exhibit a suite of characteristics indicative of the transition from well-mixed turbulent flow, to rheologically stratified flow and eventually, fully laminar flow and have been described from strata the Wilcox Formation, Gulf of Mexico (Kane and Ponten, 2012). Transitional flow resemble slurry flow and hybrid bed deposits in that they comprise multiple stratal divisions in addition to features like light-dark banding, dewatering structures and faint or wispy lamination. Nine bed types are described of which seven are interpreted to be transitional flow deposits between two end-member types: clean turbidites (type 0) and thin silty turbidites (type VIII).

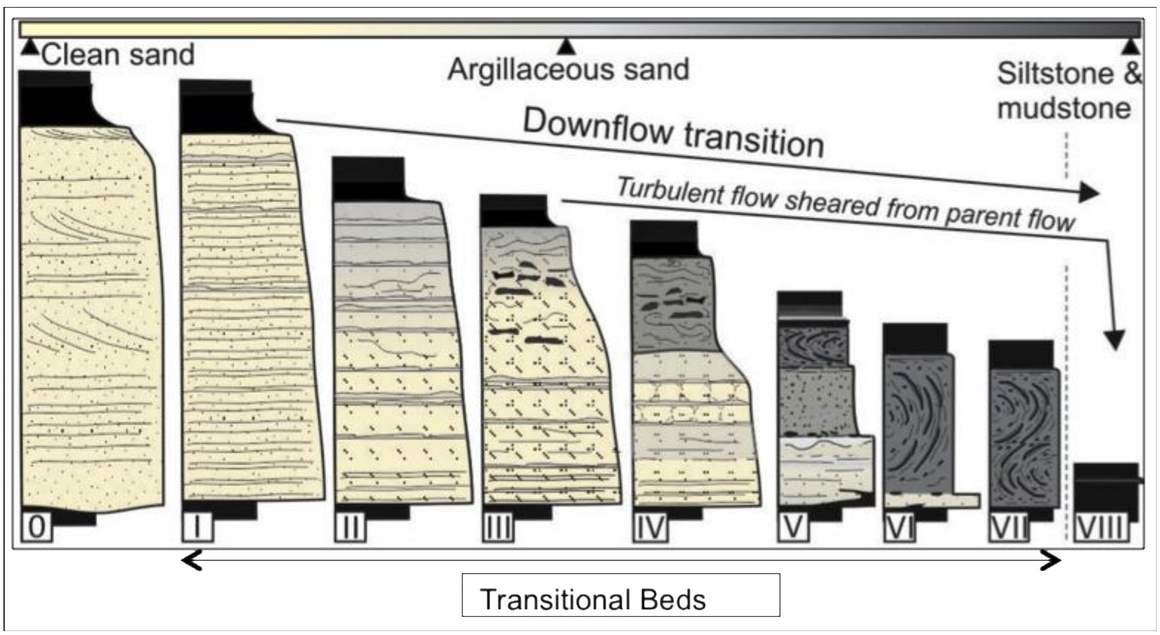

Figure 2.17: Schematic of idealized bed types 0-VIII. Types I-VII represent deposition from a transitional flow. From Kane and Ponten, 2012).

The seven transitional flow deposit bed types are as follows: Type I (TI) is composed of thick, normally graded sandstone with subtle parallel lamination and mud caps; Type two (TII) consists of graded sandstones with a vertical transition from plane-parallel lamination to massive and/or weakly laminated and/or dish-structured sand with intermittent light and dark color banding; Type III (TIII) is composed of massive sandstone overlain by finer strata (silt/mud), that commonly are banded and contain mud clasts. Type IV and Type V beds each have five divisions. Type IV (TIV) include (1) a lower, clean sandstone with a diffuse to sharp upper contact; (2) a clay/silt rich sandstone, with common dewatering pipes between bands; (3) clast-rich argillaceous sandstone; (4) very thin, relatively clean ripple or parallel-laminated siltstone; and (5) a normally graded cap. In contrast, Type V divisions are sharply bounded and composed of: (1) a thin, clean sandstone base (commonly with sheared flames and fabric); (2) an argillaceous sheared sandstone overlying a boundary marked by small rounded clasts; (3) a clast-rich sandy siltstone with a strongly deformed and/ or sheared fabric; (4) a thin (1–2 mm) relatively clean silt with uncommon ripple lamination; and (5) a normally graded cap. Type VI (TVI) consists of thin (millimeters to a few centimeters) relatively clean sandstone overlain by a thicker sandy siltstone and lastly Type VII is made up of beds that are entirely sandy siltstone or silty mudstone with organic material, often with a graded silty cap. Bed types I and II are interpreted to represent the initial, well-mixed turbulent parts of the flow that lead to the development of internal shear boundaries. Types III and IV are interpreted to be deposited from stratified flows where shear boundaries produce a divide between the basal high sediment concentration with dampened turbulence and the upper transitional to quasi-laminar flow (Kane and Ponten, 2012). As the clay/mud concentration continues to increase, disaggregation of fines and clay flocculation leads to the formation of a complete plug flow. The grading and mixed composition common in bed types VI and VII are interpreted to represent deposition from the overriding turbidity current. Eventually, all bed types are capped by silty-turbidites (Type VIII) representing deposition by a dilute turbulent cloud. Transitional flow deposits are interpreted to occur at the base of sandy lobe packages and be partial to forming during flows with long run-out distances and access to abundant mud within a passive margin system.

2.3.5 Matrix-rich Sandstones in the Windermere Supergroup

Matrix-rich sandstone beds have previously been recognized in deep-water strata of the Windermere Supergroup (Leclair and Arnott, 2003; Arnott, 2007; Rocheleau, 2012; Davis, 2011; English, 2013). Recently, Terlaky (2013) and Terlaky and Arnott (2014) described in detail matrix-rich sandstones from the Upper and Middle Kaza groups. These matrix-rich sandstones, like those in this study, are lithologically different from those discussed above and suggest a different mechanistic origin (See Chapter 4: Depositional Model and Chapter 5: Discussion).

2.4 Dynamic Recrystallization of Quartz

Although strata in the Castle Creek study area have undergone a complex history of structural and metamorphic deformation, detailed analysis of their microstructure can provide valuable insight into quantitative measurements of matrix content and identifying different transitional facies. Here, the mechanisms and regimes of dynamic quartz recrystallization are briefly discussed.

Recrystallization is a common microstructural transformation that occurs during the deformation, metamorphism and diagenesis of rocks. Simply put, it is a deformation-induced re-working of grain size, shape or orientation with little to no chemical change (Poirier and Guillopé, 1979). More specifically, dynamic recrystallization is one of the processes by which a crystalline aggregate, in this case quartz-dominated sandstone, adapts to the stress and strain imposed during deformational events (Urai, et al., 1986). Drury et al. (1990) describe two processes by which the dynamic recrystallization of quartz may occur depending on the strain rate and temperature of deformation 1) subgrain rotation and 2) grain-boundary migration. Sub-grain rotation involves geometrical softening – as temperature increases internal stresses are reduced by the migration of dislocations in the crystal lattice. These changes in crystal orientation result in the formation of new grain boundaries resulting in the formation of subgrains. Grain-boundary migration consists of grains changing (typically reducing) their free or stored energy between neighboring grains in an attempt to relieve strain and reestablish an equilibrium energy state. Commonly, this results in the migration of pre-existing grain boundaries. Stipp et al, (2002) describe three types of dynamic quartz recrystallization based on strain-rate and temperature of deformation: 1) bulging recrystallization (BLG) 2) subgrain rotation recrystallization (SGR), and 3) grain-boundary migration recrystallization (GBM). Below the key characteristics of each stage are discussed in order of increasing temperature of occurrence.

2.4.1 Bulging Recrystallization

Bulging recrystallization initiates between 250-400°C and is characterized by bulging grain boundaries and small (silt to fine-sand) recrystallized subgrains along grain boundaries and micro-fractures (Figure 2.18). Much of the original quartz grains and structure is preserved because the recrystallized grains make up only about 1-30% of the total grains. In this case, the temperature is low enough to prevent the complete separation of subgrains and thus many subgrains are described as bulging (i.e. not detached from the original grain). Commonly, bulging subgrains are formed through a combination of the two mechanisms described above (Stipp et al., 2002).

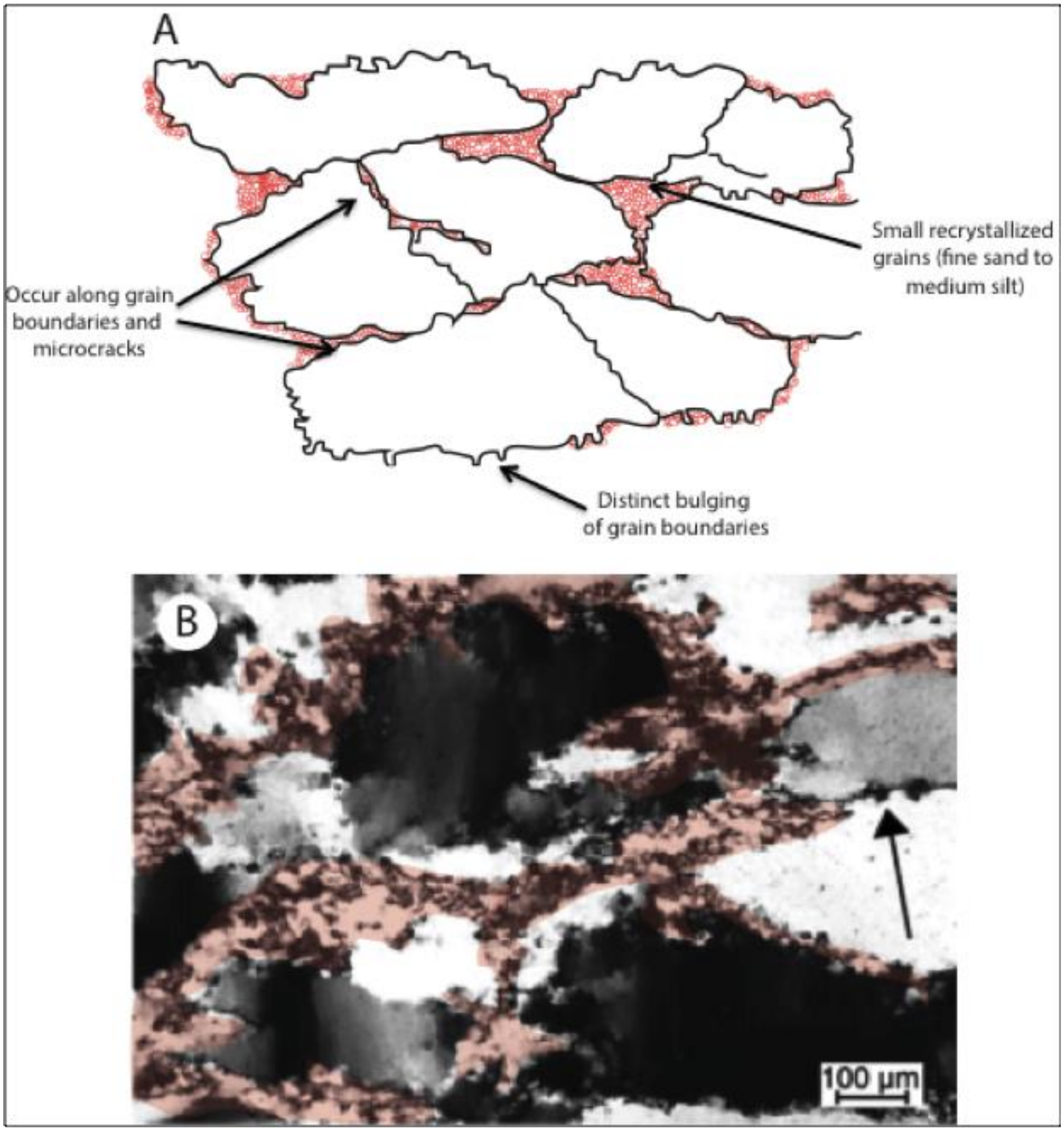

Figure 2.18: A) Schematic of bulging recrystallization. The red grains represent fine-grained subgrains. Note the bulging or undulatory shape of the original grain boundaries. B) Photomicrograph of bulging recrystallization. Fine-grained subgrains are highlighted in red are only common between grains (as depicted by the arrow). Modified from Stipp et al, 2002.

2.4.2 Subgrain Rotation Recrystallization

Subgrain rotation recrystallization occurs between 400-500°C. A key distinguishing feature of these grains is their relatively straight boundaries and lack of microscopic undulose extinction. Subgrains have similar size and orientation and form unique sweeps or ribbons within larger grains and in interstitial spaces (Figure 2.19). Subgrains range in size from medium to coarse sand and may be similar to the size of the original grains. Typically, subgrains comprise 30-90% of the grain volume and are visually quite distinct (Stipp et al, 2002). Due to the higher temperature, geometrical softening occurs and subgrains are able to rotate in order to alleviate stress, thus subgrain rotation becomes the dominant recrystallization mechanism.

2.4.3 Grain-boundary Migration Recrystallization

Grain-boundary migration recrystalization only initiates at high temperature (500-600°C). An indication of grain boundary migration is the lobate and interfingered boundaries between grains (Figure 2.20). Here, grains are much larger than those in the previous two types and typically of the order of 1-4 mm. At high temperatures, geometrical softening occurs rapidly and little to no internal grain structure remains. At this point grain boundaries expand in order to compensate for the strain on the grain and as a result the quartz becomes 100% recrystallized (Stipp et al., 2002).

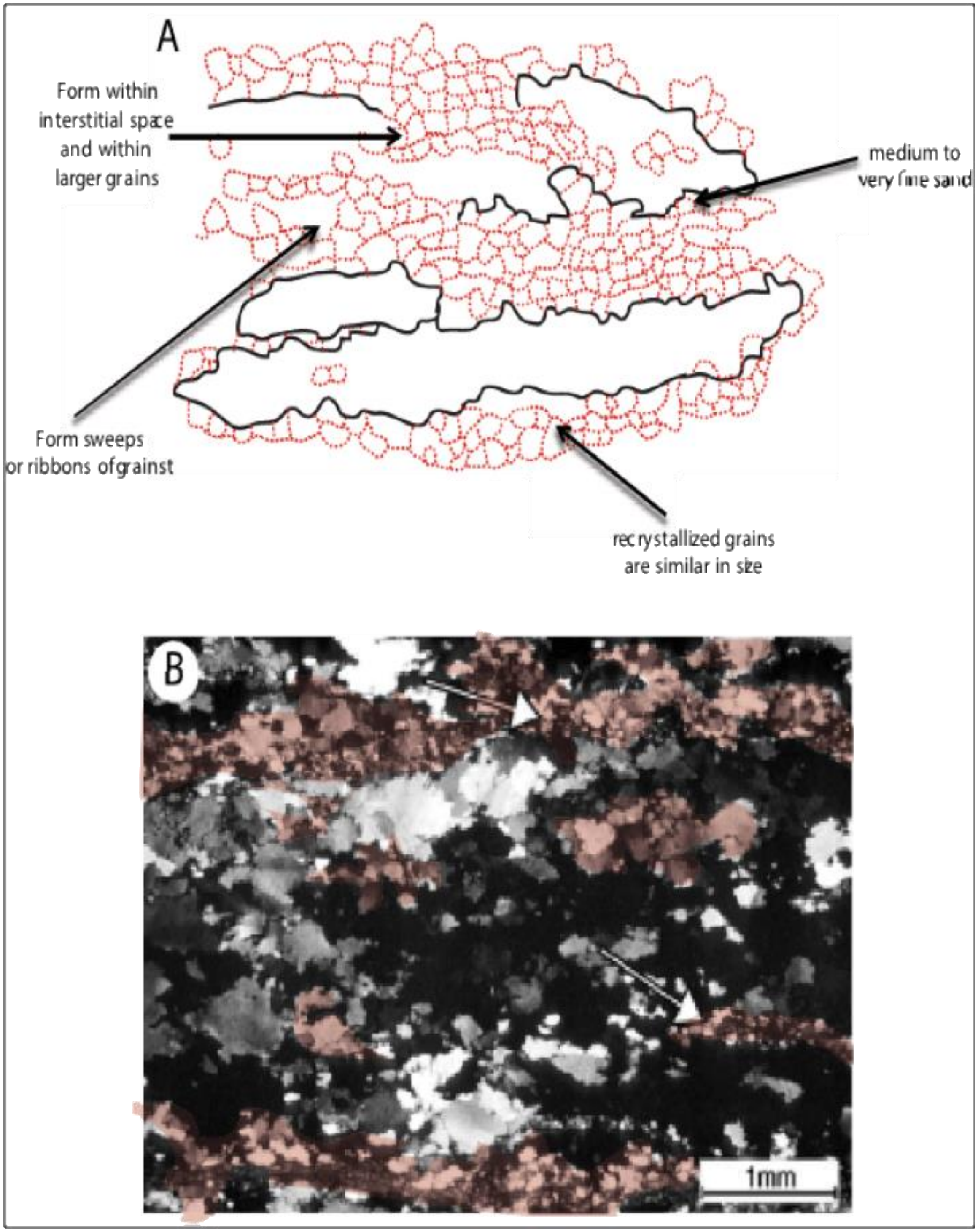

Figure 2.19: A) Schematic representation of subgrain rotation recrystallization. Subgrains are in red, original grains in black. Note the similar size of the subgrains and the remnants of original grains. B) Photomicrograph of subgrain-rotation recrystallization. Subgrains are highlighted in red. Modified from Stipp et al, 2002.

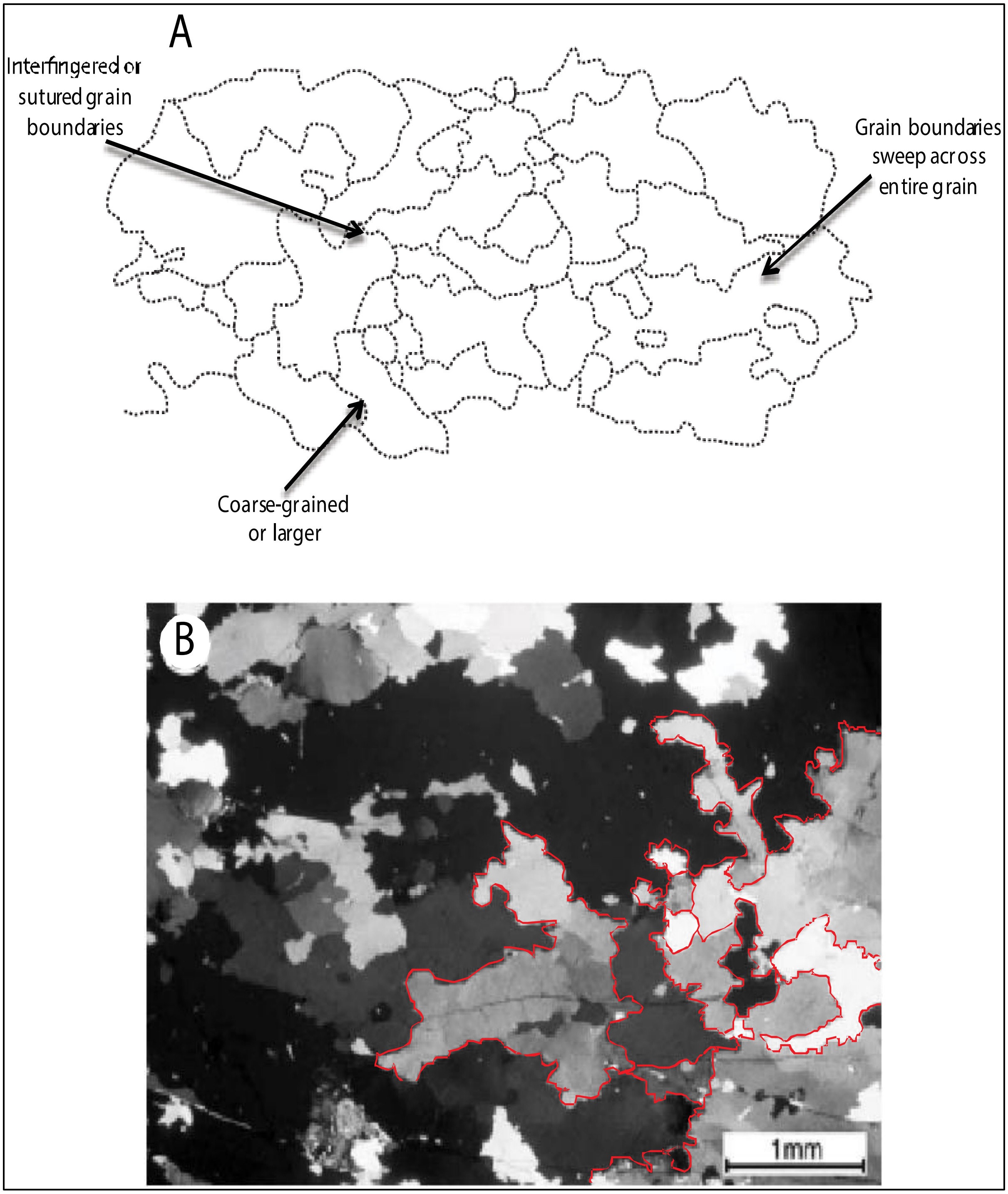

Figure 2.20: A) Schematic of grain-boundary migration recrystallization. Note the interfingered or jig-saw like nature of the grain boundaries. B) Photomicrograph of 100% recrystallized grains due to grain-boundary migration. Outlined in red is a portion of the grain boundaries to emphasize the interfingering. Modified from Stipp et al, 2002.

2.4.4 Recrystallization of Castle Creek Strata

Rocks may show more than one stage of recrystallization depending on the fluctuations in temperature during deformation as well as the original water content, matrix content and pore space. Generally, more intense recrystallization is present in rocks dominated by grain-to-grain contacts and those with low water and matrix contents. Here, there is no buffer between the grain and the quartz grains that are undergoing the internal strain of deformation (Drury et al., 1990). The rocks at the Castle Creek study area are of lower greenschist metamorphic grade (Ross and Arnott, 2007). Based on the temperature regimes of dynamic quartz recrystallization, only bulging and subgrain rotation recrystallization are expected to occur here (Figure 2.20). The interpretation and implication of the amount of quartz recrystallization in each facies is discussed in Chapter 5. It is important to note that all strata at Castle Creek have been recrystallized and the matrix discussed in the next section, excluding minor silt, is composed of muscovite and chlorite that are interpreted to represent recrystallized (detrital) clay minerals such as illite and smectite.

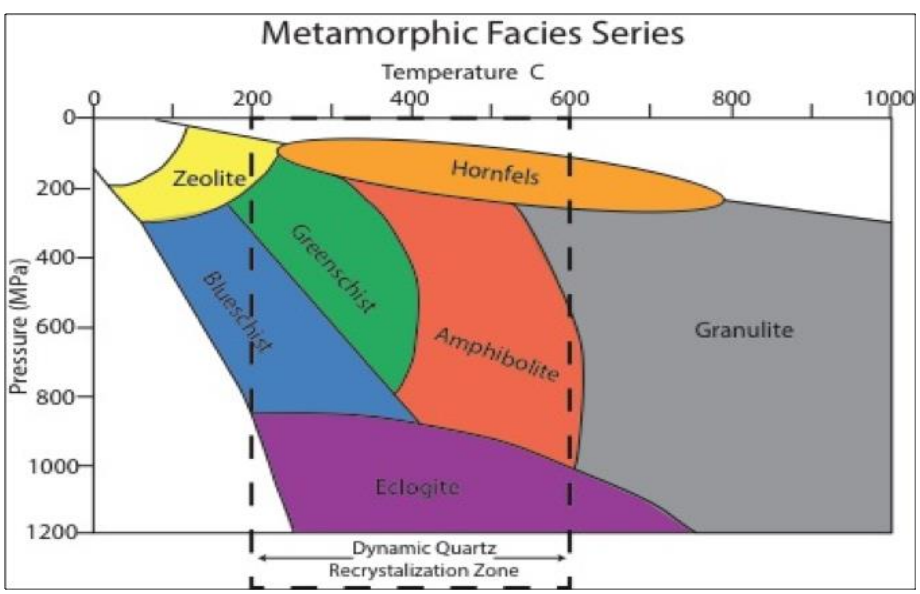

Figure: 2.21: Diagram of metamorphic facies series showing the dynamic quartz recrystallization zone. Strata at Castle Creek are lower greenschist facies and thus are expected to only exhibit bulging and subgrain rotation recrystallization.

Chapter 3: Facies Descriptions and Interpretations

3.1 Introduction of Facies

Bed-by-bed, centimeter-scale fieldwork examining strata in the Upper Kaza Group at Castle Creek identified five facies. Facies were subdivided based on unique assemblages of macro- and microscopic lithological characteristics including; bedding contacts, grain size and sorting, bed thickness, sedimentary structures, matrix percent by volume, degree of recrystallization and colour. Grain size is described based on the classification of Wentworth (1922); upper (U) and lower (L) are used as additional grain size descriptors for each subdivision. Bed thickness terminology follows McKee and Weir (1953) and Ingram (1954): lamina (<1cm); very thinly-bedded (1-3cm); thin bedded (3-10cm); medium bedded (10-30cm) and thick bedded (>30cm). In addition to field-based descriptions, detailed thin-section analysis (including grain measurements and mineralogical point-counting) was conducted to provide a more precise quantification of matrix content and the degree of dynamic quartz recrystallization. Thus, Folk's (1964) classification of sedimentary rocks based on the percentage of sand, silt and clay is used to better quantify mineralogical and textural composition. Matrix, within the context of this thesis, is defined as all interstitial chlorite; muscovite and silt (see petrographic descriptions in Appendix B and Chapter 5 discussion). Dynamic quartz recrystallization is defined by the amount of subgrain rotation or bulging of quartz grains (See Chapter 2).

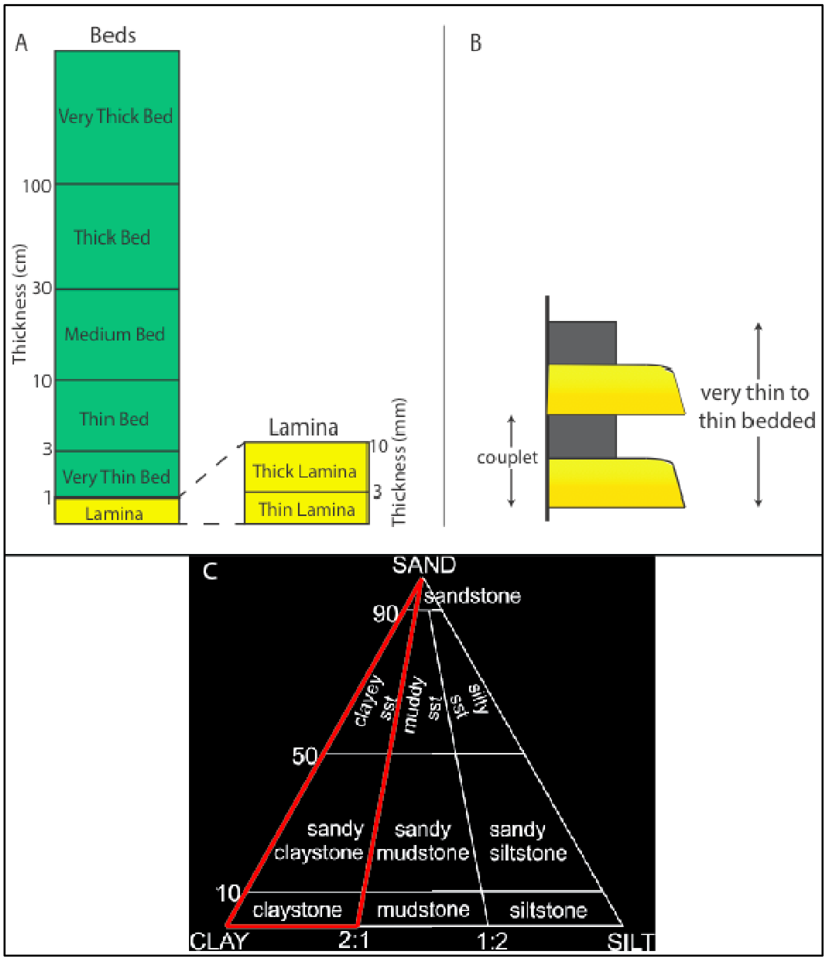

Figure 3.1: Common terminology used throughout this chapter. A) Bed thickness is described according to McKee and Weir (1953) and Ingram (1954) (Modified from Boggs, 2002). B) Schematic representation of a couplet for the purposes of this thesis. Couplets are very thin to thinly bedded and consist of a basal, sandier (fine to very fine sand) layer and a upper, muddier layer. C) Folk's (1964) classification scheme for sedimentary strata based on composition is used to better describe facies in this thesis (common descriptors used outlined in red).

Based on the abovementioned characteristics, the following five facies have been identified (Figure 3.2):

F1: Turbidites.

F2: Matrix-poor Sandstones

F3: Intermediate Clayey Sandstone

F4: Sandy Claystone

F5: Fine-grained Banded Couplets

Matrix-poor and matrix-rich facies are considered end-member facies for the purpose of this thesis, whereas clayey sandstone and banded couplets commonly represent transitional facies between the two end members. Importantly, these facies commonly grade laterally into one another over distances of 10's to 100's of meters, the physical basis of which is discussed in detail in Chapter 4.

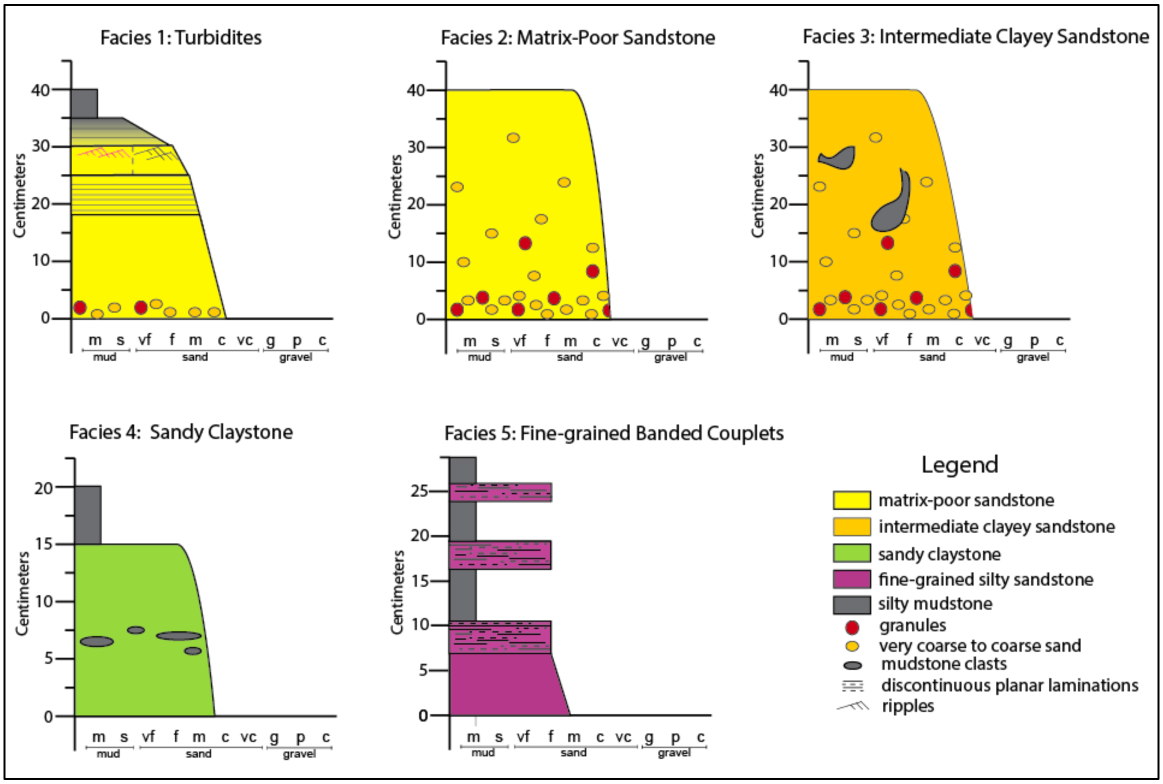

Figure 3.2: Idealized stratigraphic logs for each facies.

3.2 Facies 1: Turbidites

Turbidite display an upward sequence of sedimentary characteristics that where fully developed consist of a: structureless, graded basal unit (T_a), planar lamination (T_b), small-scale cross stratification (T_c), siltstone capped with mudstone (T_{de}). More commonly, the succession is incomplete and consists typically of upper division turbidites (T_{cde}), although a basal planar laminated unit (T_b) is common. In the Upper

Kaza turbidites occur as: 1) medium- or 2) very thin to thinly-bedded turbidites (Figure 3.3). Medium-bedded turbidites, which range from 12-30 cm thick, commonly exhibit a complete to nearly complete turbidite sequence. Strata grade from upper medium sandstone in the T_a to lower medium-upper fine sandstone in the T_b/T_c layers. The T_a layer is commonly the thickest and ranges from 15-30 cm. The T_b/T_c layers range from 10-25 cm thick with the T_c layer being consistently thinner. Cross-stratification (T_c) commonly occurs as a single, well-sorted set with a distinctive red colour attributed to the presence of ferroan calcareous cement. The T_b/T_c layers are then abruptly overlain by 5-10 cm thick unit of multiple, thin-bedded sets of T_d/T_e. A single turbidite unit may be composed of multiple turbidites and the overall unit thickness ranges from 60-130 cm thick. In contrast, very thin-to thinly-bedded turbidites grade from upper/lower fine sandstone in the T_b and T_c layers to very fine sandstone overlain by siltstone then mudstone in the T_{de} layers. Grain size only exceeds lower fine sandstone where a rare basal, coarse to medium T_a unit is present. Thin-bedded turbidites often stack to form units ranging from 10 cm to ~6 m thick. Locally, planar laminated (T_b) and ripple cross-stratified (T_c) sandstones are carbonate cemented. Very thin-bedded turbidites consist of siltstone interbedded with mudstone with uncommon diffuse and discontinuous formsets and planar lamination (units T_{de}±T_{bc}).

In the study area, the top of the measured section is marked by a 6 m thick unit of very thin-to thinly-bedded turbidites that extends across the width of the outcrop (~800 m). In addition to this occurrence, turbidites crop out locally and are most common in the northwestern part (Section 2 and Section 3) where they are interbedded with matrix-rich and transitional facies.

3.2.1 Interpretation of Turbidites

Turbidites in the study area are analogous to Bouma's classical turbidite model (1962), and are interpreted to have been deposited by decelerating dilute, low density turbidity flows (e.g. Mulder and Alexander, 2001). Although uncommon in this study, the basal ungraded T_a unit is interpreted to represent direct suspension deposition with limited bed-load transport and hence textural sorting on the bed (e.g. Arnott and Hand, 1989). As the rate of deposition decreased, longer periods of bed-load transport allowed for the development of planar lamination (T_b). Small-scale cross-stratification (T_c) is interpreted to have formed by the downflow migration of unidirectional current ripples. In some beds, ripple sets are laterally discontinuous, a condition most probably related to limited sediment availability (i.e. sediment starved). These sediments are then overlain by a cap of siltstone/mudstone (T_d) suggestive of the cessation of continuous sandy bedload transport and deposition of silt from the overlying dilute fine-grained sediment cloud. In addition, clay floccules in the muddy suspension may lead to a distinctive segregation of clay and silt particles, resulting in the rhythmic alteration of mud and silt deposition (Stow and Bowen, 1980) – this style of deposition dominates in very thin-bedded turbidites. The uppermost structureless T_e division is interpreted to represent the very finest grained suspension settling towards the end of the flow and/or post-event hemipelagic fallout (Khan and Arnott, 2010). As mentioned above, it is common for parts of the sequence to be incomplete and the lack of traction sedimentary structures (T_b and/or T_c) is likely due to suspended-load fallout rates that were sufficiently high to limit traction transport and suppress bed form development (Arnott and Hand, 1989; Arnott and Leclair, 1989).

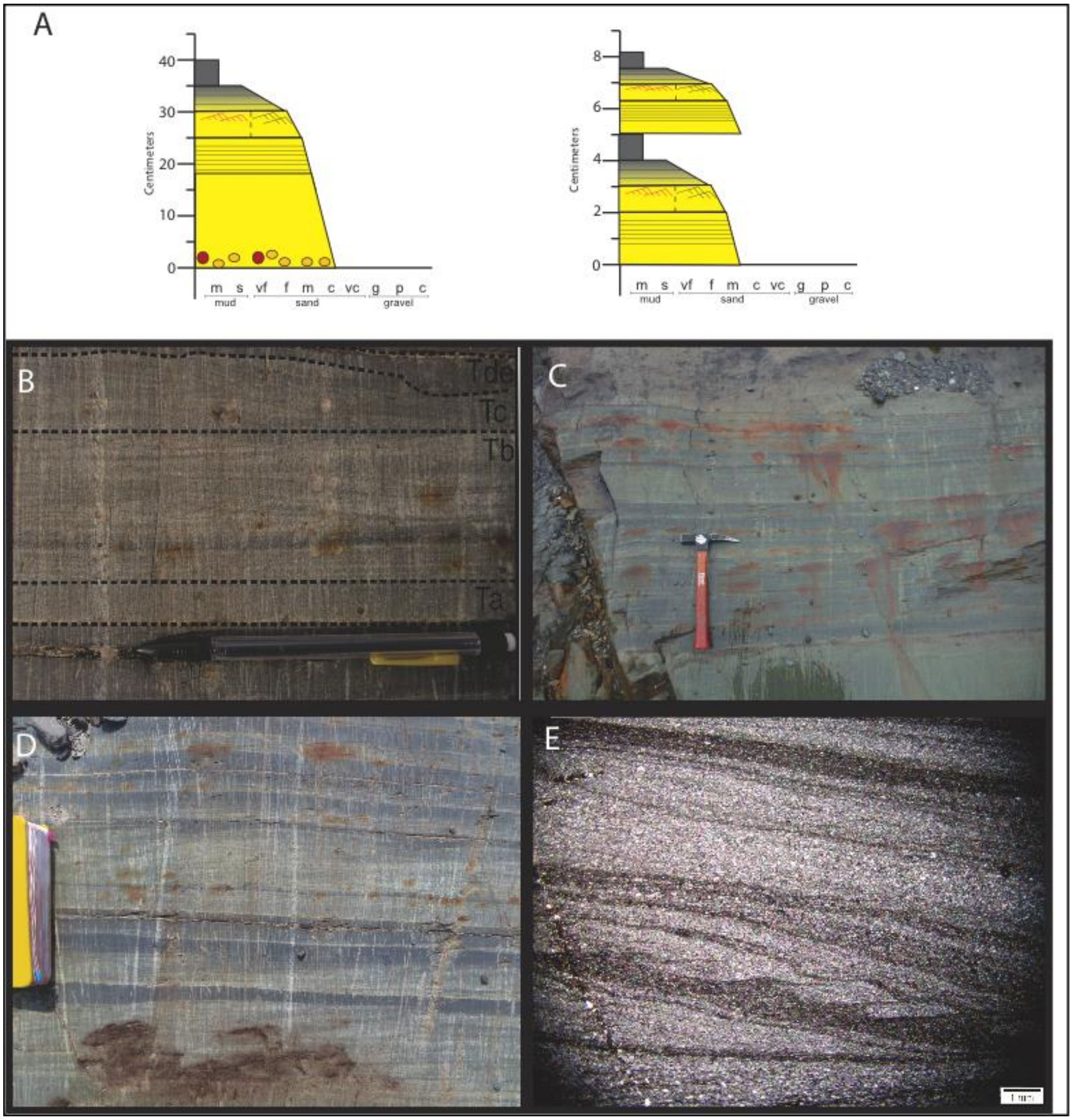

Figure 3.3: Examples of Facies 1 turbidites in the study area. A) Idealized stratigraphic logs of Facies 1. B-D) Show turbidite beds at various scales and thicknesses throughout the study area. Note that the vertical lines are glacial striations. B) Close up of very thinly-bedded turbidite sequence C) ~70 cm thick unit of mostly upper division turbidites. D) Thin-bedded T_{b-e} turbidite sequence. E) Photomicrograph of very thinly-bedded T_{c-e} turbidite sequence. Here the largest grain size is lower very fine sand.

3.3 Facies 2: Matrix-poor Sandstone

Matrix-poor sandstones are massive or coarse-tail graded, structureless, lower coarse sandstone with dispersed very coarse sand grains and granules that grades upwards to lower medium sandstone with dispersed coarse grains. Locally, an up to 7cm thick concentration of coarse grains and granules may be present at the bottom of beds. Bed thickness and bedding contacts vary widely depending on the section of the study area and can be subdivided into two types: 1) macro beds: ranging from 1 m – 3 m thick and 2) meso beds: ranging from 15 cm – 80 cm thick. Macro-beds are consistently structureless and basal contacts are undulatory and only discernable when there is a major (visual) grain size change, thus these beds are commonly amalgamated. Dewatering (pipes and dish structures) and loading structure (flames) are rare and only occur in 2% of beds. Macro-bedded matrix-poor sandstones dominate Section 1 (S1) of the outcrop. Although less common in Section 2 (S2), macro-beds are distinguished by large (up to meters long and 10's of centimeters thick), irregularly shaped, mudstone and sandy claystone clasts.

Meso-bedded, matrix-poor sandstones commonly have sharp, planar basal contacts with local scours that are 10-25 cm deep. Locally, irregularly shaped mudclasts that range from 3-15 cm thick and 0.5-2 m long are observed and tend to be dispersed within the middle or upper portions on the bed. Three sub-facies of meso-bedded matrix-poor sandstone are recognized: A) matrix-poor sandstones overlain abruptly by a 5-10 cm thick silty-mudstone cap; B) matrix-poor sandstone overlain abruptly by a well-stratified, dark grey, fine-grained, planar laminated sandy-siltstone that grades upwards to a massive silty-mudstone; C) matrix-poor sandstone overlain by centimeter-thick, single cross-stratified or planar-laminated sets that range from 5-20 cm thick that often are overlain abruptly by a few centimeter thick mudstone cap. Typically, these tractional structures consist of medium to coarse-grained sandstone and commonly are visually distinct due to their red colour attributed to the presence of a ferroan calcareous cement.

3.3.1 Petrographic Analysis of Matrix-Poor Sandstones

Based on the analysis of 45 petrographic samples, the matrix content in matrix-poor sandstones does not exceed 14% by volume and averages at ~9 %. Samples are dominated by grain-to-grain contacts and grains are generally moderately sorted and subrounded to subangular. Dynamically recrystallized quartz and recovery quartz subgrains comprise 22%-47% by volume with an average of ~ 34% by volume. Subgrain rotation makes up ~65% of the dynamic recrystallized quartz volume and commonly forms in the interstitial space and within larger quartz grains creating visually very obvious sweeps or ribbons of subgrains (Figure 3.4G). Recrystallized grains show relatively straight boundaries and generally no undulose extinction. Commonly, SGR and quartz grains may be similar in size although where subgrains are locally abundant they are typically smaller and range from upper fine to very fine sand size (Figure 3.4G). Bulging recrystallization (BLG) is manifest by the interfingering and bulging of grain boundaries (Figure 3.4G). On average BLG grains make up ~ 35% of the dynamic recrystallized quartz volume.

3.3.2 Interpretation of Matrix-Poor Sandstones

Flows that deposited strata of Facies 2 are interpreted to be deposited from concentrated density flows (Mulder and Alexander, 2001), also termed high density or high energy turbidity currents (Lowe, 1982, Sylvester and Lowe 2004), and are interpreted to be equivalent to the Ta division in a Bouma turbidite or the S3 division in a Lowe sequence. Matrix-poor beds are interpreted to have been deposited when sediment concentration exceeded flow capacity (Allen 1991) and resulted in rapid deposition and aggradation of the bed. The high rate of suspended sediment fallout limited traction transport and aided in suppressing the development of angular bed forms (Arnott and Hand 1989). More specific to this study area, the massive and amalgamated, macro-bedded, coarse grained, matrix-poor sandstones are interpreted to represent deposition within the axis of a hydraulic jump. Downflow of the jump the flow rapidly expanded causing velocity to decrease abruptly and the coarsest sediment fraction to be rapidly deposited. The coarse-tail grading that is common in these beds indicates a progressive waning of depositional energy. Matrix-poor beds overlain by mudstone caps (MPSS-2A), well-stratified fine-grained tops (MPSS-2B) or traction structures (MPSS-2C) are interpreted to have been deposited along the margins of the jump or further downflow. MPSS-2A (silty-mudstone cap) is interpreted to represent an initial episode of rapid deposition followed by a period of full bypass, followed by suspension settling of very fine-grained sediment from the tail of the flow and/or the cessation of the flow followed by later hemipelagic fallout (Khan and Arnott, 2010). In MPSS-2B the abrupt change from medium-coarse sand to a cap of upper (darker) fine-grained sand is attributed to a temporary pause in deposition, as the flow continued to decelerate and the sediment concentration decreased before it recommenced under lower rates of sedimentation and the deposition of fine-grained planar laminated sand. Cross-stratified sand is interpreted to indicate even lower near-bed sediment concentration that permitted the initiation and growth of current ripples (equivalent to the T_c division of a classical turbidite). These strata are then overlain by a cap of silty-mud deposited from the fine-grained tail end of the flow (similar to Bouma T_{de} division). Lastly, MPSS-2C is interpreted to represent conditions of low near-bed sediment concentration but made up of sediment reworked from the upper part of the underlying part of the bed. The similarity in grain size between the upper and lower parts of the bed suggests that they were likely formed during a single depositional event.

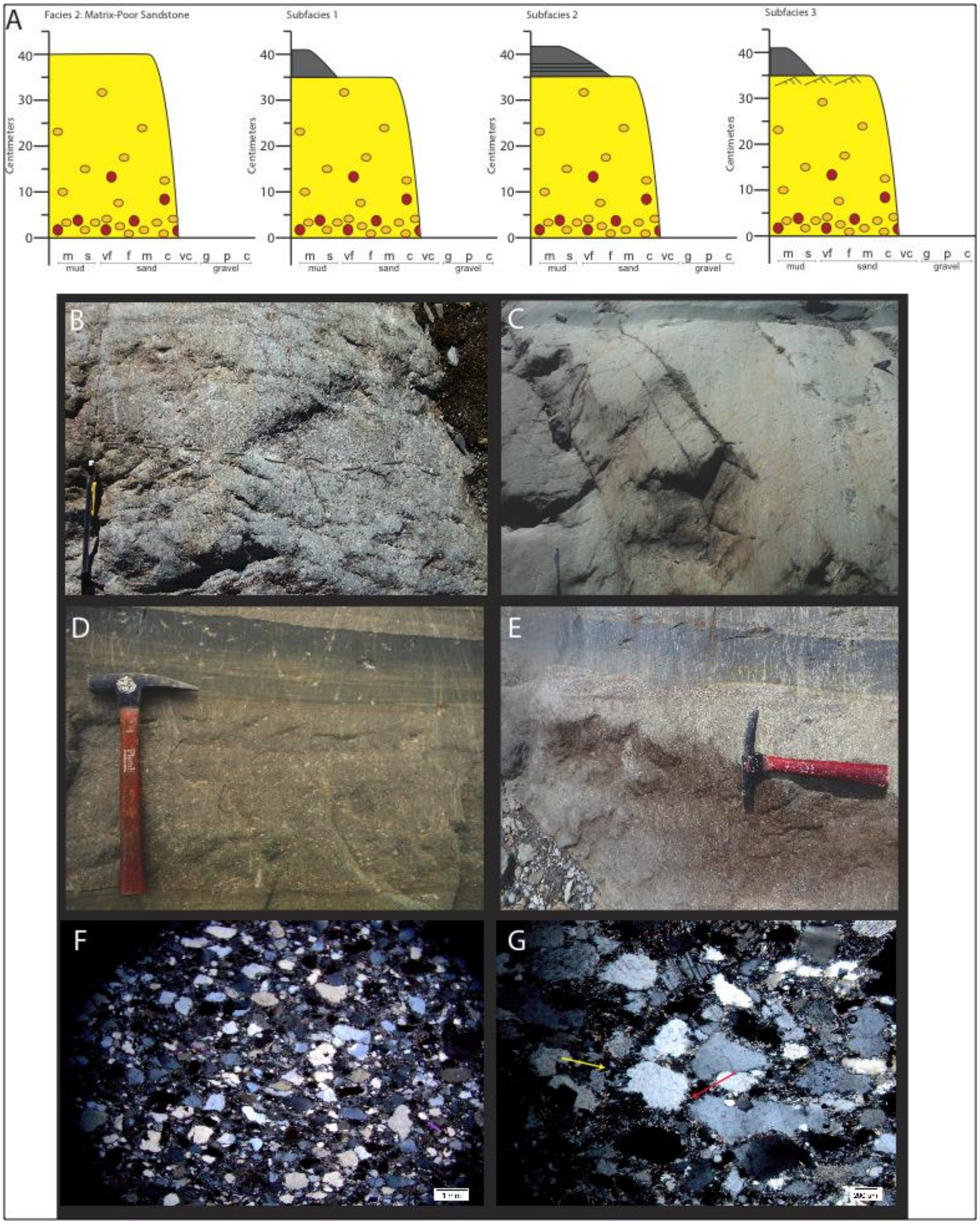

Figure 3.4: Examples of Facies 2: Matrix-poor sandstone and three subfacies. A) Idealized stratigraphic logs of Facies 2. B) Contact between two matrix-poor sandstones; note the abrupt grainsize change from lower medium with dispersed coarse grains to upper coarse with abundant very coarse grains and dispersed granules. C) Example of Subfacies 1: sandstone overlain by a mud cap. Pencil for scale in bottom left corner. D) Example of Subfacies 2: sandstone with a laminated/ripple cross-stratified fine-grained cap. E) Examples of Subfacies 3: sandstone with ripple cross-stratification at the top of the bed

(below mud cap). Commonly the ripples are carbonate cemented (as in the photo). F) Photomicrograph of a matrix-poor sandstone in cross-polarized light at 1.25x magnification. Note the absence of matrix and abundance of grain-to-grain contacts. E) Photomicrograph of matrix-poor sandstone from F in cross-polarized light at 5x magnification. Note the abundance of subgrains between larger grains (yellow arrow) and the bulging and undulatory nature of grain boundaries (red arrow).

3.4 Facies 3: Intermediate Clayey Sandstone

Clayey sandstones are categorized as an intermediate or transitional facies between classical turbidites and sandy claystones. Intermediate clayey sandstones are light brownish-grey and coarse-tail graded with a distinctive 5-10 cm thick concentration of coarse to granule size grains at the base of the bed. Towards the top, beds grade gradually to upper fine-grained sandstone with dispersed medium and lower coarse sand grains. Beds range from 60-120 cm thick but locally may be as thin as 20 cm. Bed bases are commonly flat, sharp and planar – loading and dewatering structures are not observed. In addition, irregularly shaped, large (0.5-3 m long, 0.15-1 m thick) clasts are common in the middle part of the bed. While these beds resemble matrix-poor sandstones, in the field they are distinctively thicker, greyer in colour and microscopically unique (Figure 3.5).

3.4.1 Petrographic Analysis of Intermediate Clayey Sandstones

Intermediate clayey sandstones are composed of 15-42% matrix – averaging ~ 25%. Grain-to-grain contacts, although less common compared to classic matrix-poor sandstones, make up ~45% of samples. Grains are generally subangular to subrounded, with distinct ‘jagged’ or ‘bulging’ edges and are moderately sorted. Moreover, dynamic recrystallization of quartz

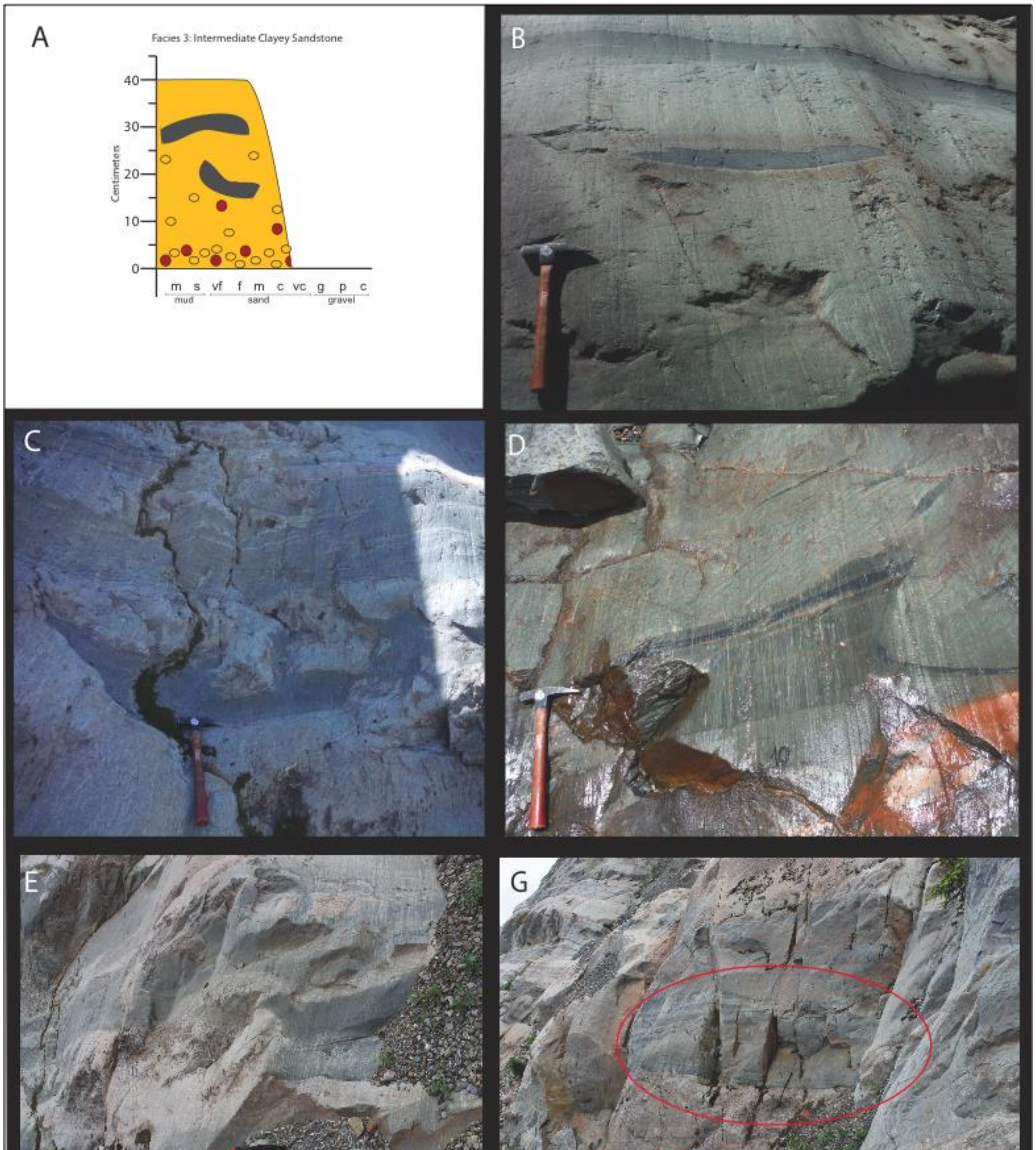

Figure 3.5: Idealized stratigraphic log of facies 3. B) Example of intermediate clayey sandstones bed. C-G) Examples of large irregularly shaped clasts within beds of facies 3. Note the lithology of the clasts includes mudstones (C) matrix-rich strata (D) and turbidites (E and G).

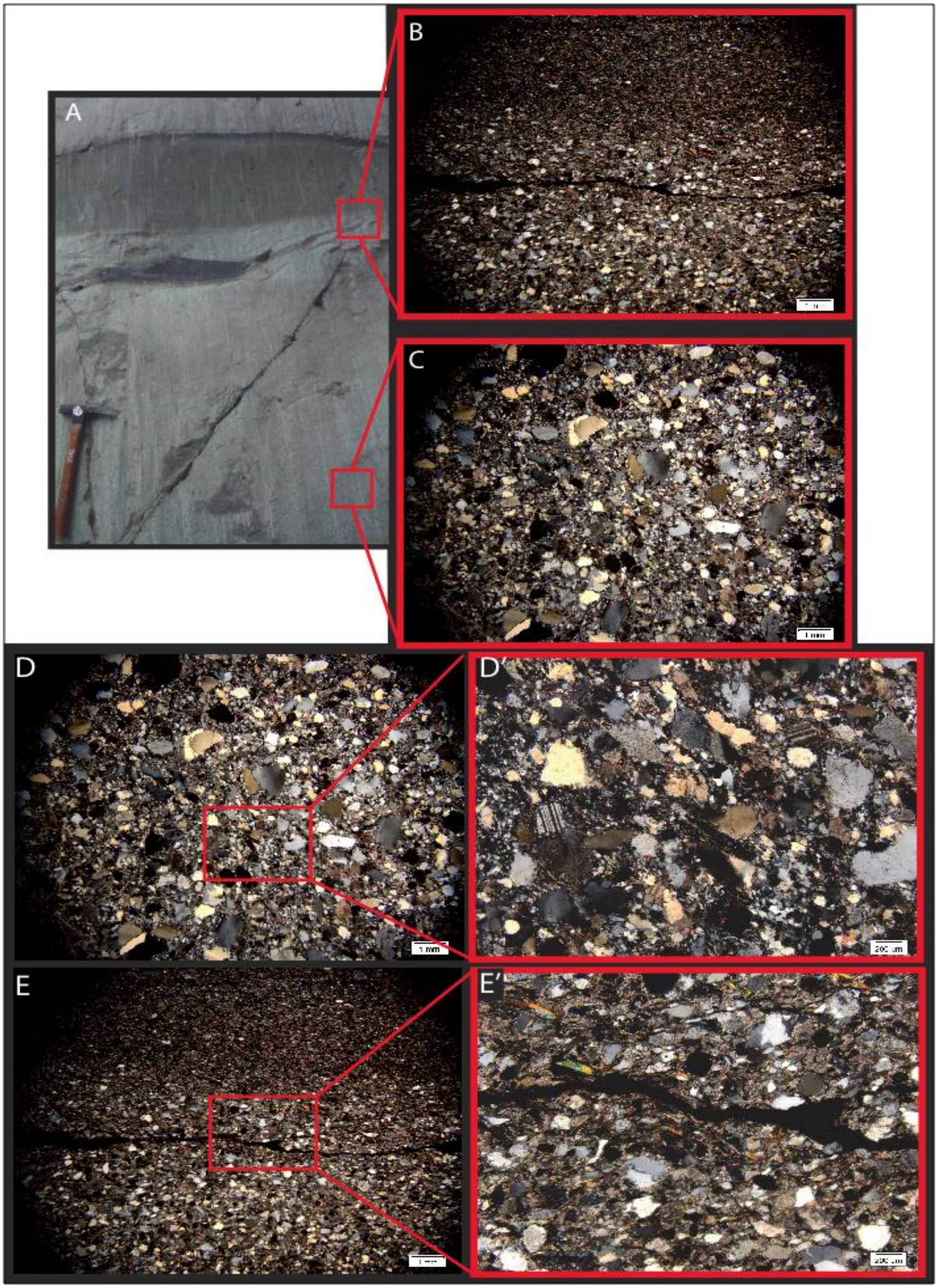

Figure 3.6: Example of the unique mineralogical composition of facies 3. A) Example of intermediate clay sandstone and the sample site of photomicrographs B and C. B) Cross-polarized photomicrograph at 1.25x magnification of the top of an intermediate clayey sandstone. Note the abundance of matrix and decrease in grain size. C) Cross-polarized

photomicrograph at 1.25x magnification of the base of an intermediate clayey sandstone. Note the difference between B and C. D-D') 5x magnification cross-polarized of the basal portion of the bed (C). Subgrains and bulging grain boundaries are abundant. In contrast, E-E' is the upper portion of the bed (B) at 5x magnification. Here, there is no grain to grain contacts, recrystallized grains and an abundance of matrix.

grains ranges from 5 - 41% (average~ 22%) and is dominated by sweeps of subgrains (SGR) (~85% by volume) and minor bulging (BLG) (~15% by volume; Figure 3.5). Differences in the characteristics of recrystallization in relation to matrix content are discussed in detail in Chapter 5. In addition, as the matrix content increases upwards in individual beds, there is a change from mostly grain-to-grain contacts with minor to rare (≤15%) matrix and abundant (recovery) subgrains at the base of the bed, to about ~ 20% matrix content, 20% subgrains and 60% framework grains in the middle of the bed and, finally, up to ~30-40% matrix and minor to rare (≤8%) subgrains in the upper part of the bed (Figure 3.6).

3.4.2 Interpretation of Intermediate Clayey Sandstones

Like Facies 2, deposition of the massive, coarse-grained base of Facies 3 beds is interpreted to represent initial high sediment fallout from collapsing high-density, turbidity currents. This, then is overlain by a coarse-tail graded unit indicating at least minor differential grain settling under more dilute flow conditions with minor turbulence (Mulder and Alexander, 2001). Furthermore, the increased matrix content in the upper half of the bed indicates an increased fine-grained (silt/mud) sediment concentration, which most likely affected flow rheology. This fine-grained sediment is interpreted to have been sourced by local seabed erosion in a hydraulic jump associated with local (channel) avulsion (See Chapter 4: Depositional Model). These lithological characteristics are suggestive of a more transitional flow rheology, specifically, quasi-laminar plug flow, rather than deposition by classic high- (or low) density sediment gravity flows. Quasi-laminar plug flows (QLPF) consist of a rigid (i.e. non-deforming), fine-grained, laminar plug-like layer moving above a weakly turbulent to laminar basal shear layer (Baas et al., 2009, 2011), as a consequence of the rapid deceleration and fallout of coarse sediment from a high-density turbidity current and accordingly an increase of suspended fine-grain (silt/clay) particle concentration. The matrix-poor basal portion of intermediate clayey sandstone beds is interpreted to be deposited from the weakly turbulent basal layer of a QLPF whereas the upper more matrix-rich portion of beds suggests hindered settling (Mulder and Alexander, 2001; Baas et al., 2009, 2011). Here, only the heavier (coarser) grains were able to settle through the fine-grained plug leading to the mixed sand-clay lithology in the upper part of the bed. Intermediate clayey sandstones of Facies 3, therefore, are interpreted to represent deposition from flows undergoing a rapidly changing rheology as a result of the decrease in flow velocity due to extensive upflow sediment fallout (i.e. the deposition of matrix-poor sandstones (F2) and an abrupt influx of mud). These strata are most common in Section 2 but are locally intercalated with matrix-poor sandstones in S1 and fine-grained banded silty mudstones and sandy claystones in S3; the implications of which are discussed later (See Chapter 4).

3.5 Facies 4: Sandy Claystones

Sandy claystones are easily identified in the field by their bluish-grey hue and smooth weathered surface -- both being attributed to the high matrix content composed of chlorite, muscovite and silt (see petrography section below (Figure 3.8). Beds range from

10-80 cm thick (average ~25 cm) and stack to form units up to 2.5 m thick. Generally, beds are structureless, massive to coarse-tail graded with a sharp, flat basal contact. Sand is typically medium, but in some cases grades upward from lower coarse/upper medium to lower medium/upper fine sand with dispersed lower coarse grains at the top of the bed. Dispersed bluish-grey to black mudstone clasts are common and locally make up to 40% of the bed volume. Clasts are commonly elongated and range from 3-45 cm long and 0.5-20 cm thick, (average 5-20 cm long and 0.5-2 cm thick) and are located within the middle to bottom half of the bed (Figure 3.7). Moreover, mudstone clasts exhibit a well-developed fabric that sub-parallels the basal contact and are typically of equidimensional throughout the bed. Commonly, beds are overlain abruptly by a 3-10 cm thick mud cap. Uncommon flame structures and rare pseudonodules are present locally, and are most common where finer-grained strata is overlain or truncated by a coarser matrix-poor sandstone unit.

Strata that exhibit this collective suite of lithological characteristics will hereafter be termed classical sandy claystones (MRSC-C) and are analogous to those described previously in the Windermere Supergroup by Terlaky and Arnott (2014). These classic matrix-rich beds make up ~ 20% of all matrix-rich strata in the study area. Additionally, a number of matrix-rich beds have been identified that comprise combinations of the abovementioned and other characteristics, and are defined individually in the following five subfacies (Figure 3.7):

Subfacies 1(MRSC-I): massive, structureless, matrix-rich beds that are similar to classic matrix-rich strata (see above) but lack mudstone clasts. Beds range from 10-60 cm thick and make up ~ 25% of all matrix-rich beds.

Subfacies 2 (MRSC-II): matrix-rich beds with traction structures near the top and comprise 15% of all sandy claystones. The top 5-8 cm of the bed (below the mud cap) is commonly lighter coloured, better-sorted, medium sand with cm-scale, single-set-thick ripple-cross stratification. A several cm thick, silt-mud cap commonly caps the ripples. Elongate mudclasts are observed locally in the middle part of some beds.

Subfacies 3 (MRSC-III): sandy claystone beds with diffuse, mm to cm scale planar lamination and make up ~15% of all matrix-rich beds. Beds range from 15-30 cm thick, are medium to upper fine-grained sandstone and commonly stack to make units 80-100 cm thick.

Subfacies 4 (MRSC-IV): sandy claystone beds with an abrupt, upward increase in matrix content. These beds consist of a thin, basal layer (~20-30% of the total bed thickness) with matrix content similar to that observed in classic matrix-rich strata (~40%). A visibly darker, massive, better-sorted, matrix-rich unit abruptly overlies the basal layer, with matrix content in excess of 50%. Beds rarely exceed 20 cm in thickness and are draped by a mudstone cap. Strata of subfacies 4 comprises only ~5% of matrix-rich strata and typically transition laterally into either classical matrix-rich beds or subfacies 1 (see above).

Subfacies 5 (MRSC-V): sandy claystone beds overlain abruptly by fine-grained, diffusely laminated sandstone unit capped by mudstone. The basal layer of the bed is 8-15 cm thick and consists of massive, matrix-rich sandstone similar to both classical matrix-rich beds and subfacies 1. A 5-10cm thick discontinuous, diffuse, mm-to-cm scale planar-laminated fine sand and silt middle layer abruptly overlies the basal layer. The uppermost layer is a few-cm-thick silt/mudstone with common dispersed fine sand grains. Beds of subfacies 5 are 25-30 cm thick and make up 20% of all matrix-rich beds in the study area. Subfacies 5 typically thins or thickens laterally over short distances (10 m or less), and commonly is associated with fine-grained banded silty mudstone (Facies 5).

It is important to note that matrix-rich strata may transition laterally into one or more subfacies and also have characteristics of one or more subfacies (e.g. the presence or absence of mudstone clasts). Sandy claystones are present in Section 1 and 2 of the study area

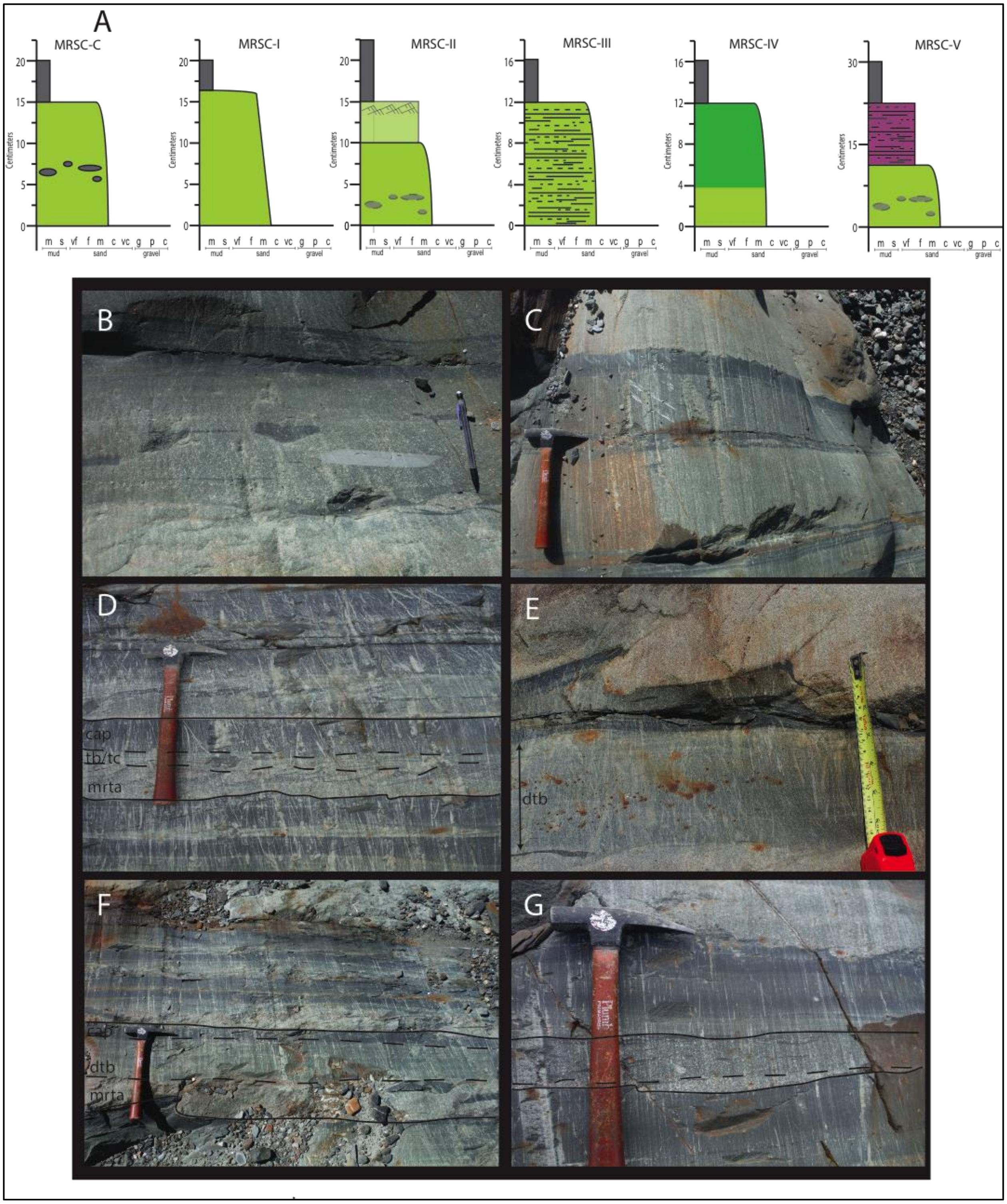

Figure 3.7: A) Idealized stratigraphic logs of classical matrix-rich beds and the five subfacies. B-G) Examples of matrix-rich beds throughout the study area. B) Classical matrix-rich bed with abundant mudclasts and a mudstone cap C) Subfacies I (MRSC I), these beds are the thickest and lack mudclasts. D) Subfacies II (MRSC II). The traction structures towards the top of the bed are outlined by the dashed lines (and labeled tb/tc). MRTA represents the basal matrix-rich, massive portion of the bed below the dashed lines.

E) Subfacies III (MRSC III): diffusely laminated matrix-rich bed (dtb represents diffusely planar laminated). F) Subfacies V (MRSC V): basal matrix-rich layer overlain abruptly by fine-grained diffusely laminated layer (represented between the dashed lines and labeled dtf). G) Subfacies IV (MRSC IV): thin, bipartite matrix-rich bed. The colour change represents an abrupt increase in matrix content.

and commonly form units up to 1.5 m thick, or are interbedded with fine-grained banded silty mudstones and turbidites. In addition, some matrix-rich beds thin and transition laterally into thin-bedded turbidites. More commonly though, matrix-rich beds and/or units either transition laterally into intermediate clayey sandstone facies or fine-grained banded beds, or are truncated over distances of several-100's of meters by matrix-poor sandstones (see chapter 4).

3.5.1 Petrography of Sandy Claystones

Sandy claystones differ from all other facies by the lack of dynamic quartz recrystallization. Instead framework grains 'float' in a matrix of chlorite-muscovite-silt (Figure 3.8). Samples from all of the subfacies indicate an average matrix content of 54% by volume. Framework grains are generally sub-angular (lesser sub-rounded), poorly sorted and range in grain size from upper coarse to upper silt (average grain size upper fine sand). The term 'floating' commonly describes classic matrix-rich beds as they tend to have the highest matrix content (between 60-75%) whereas the matrix content in the various subfacies typically ranges from 45-58%.

3.5.2 Interpretation of Sandy Claystones

Matrix-rich strata are interpreted to represent deposition along the margin of a jet flow associated with a local avulsion. Here, intense erosion of the underlying sea floor introduced a voluminous and almost instantaneous influx of fine-grained sediment into the flow. Due to their low weight and particle shape, the mostly clay and silt sediment became preferentially mobilized towards the top and margins of the flow. Initially, the flow was sufficiently turbulent to suppress the formation of clay floccules (Baas et al, 2011), which in turn, allowed the coarse grains (in this case lower coarse to medium sand grains) to quickly settle through the suspension and accumulate on a rapidly aggrading bed (Arnott and Hand, 1989; Leclair and Arnott, 2005) of intermediate clayey sandstone. However, as coarse sediment became progressively more depleted the elevated proportion of fine-grained sediment increases and eventually, as a result of increased viscosity, damped turbulence forming a quasi-laminar plug flow (QLPF). The poorly sorted nature of matrix-rich strata (coarse sand to silt and clay) suggests strong cohesive forces related to clay flocculation that inhibited mostly grain-size dependent differential deposition. Moreover, the planar nature of bed bases and scarcity of scours indicates turbulence suppression further confirming a QLTF rheology. The common, elongated mudstone clasts that are dispersed throughout matrix-rich beds are texturally and mineralogically similar to mudstone caps and thin-bedded turbidites throughout the Windermere Supergroup sedimentary pile, and therefore are interpreted to be sourced locally from erosion of previously deposited fine-grained deposits. Additionally, the preservation of their primary depositional stratification implies a short transport distance. Mudstone caps that drape matrix-rich strata are interpreted to be equivalent to T_{de} turbidite deposits and represent fine-grained suspension settling in the low-energy tail part of the current or during the interval between sedimentation events.

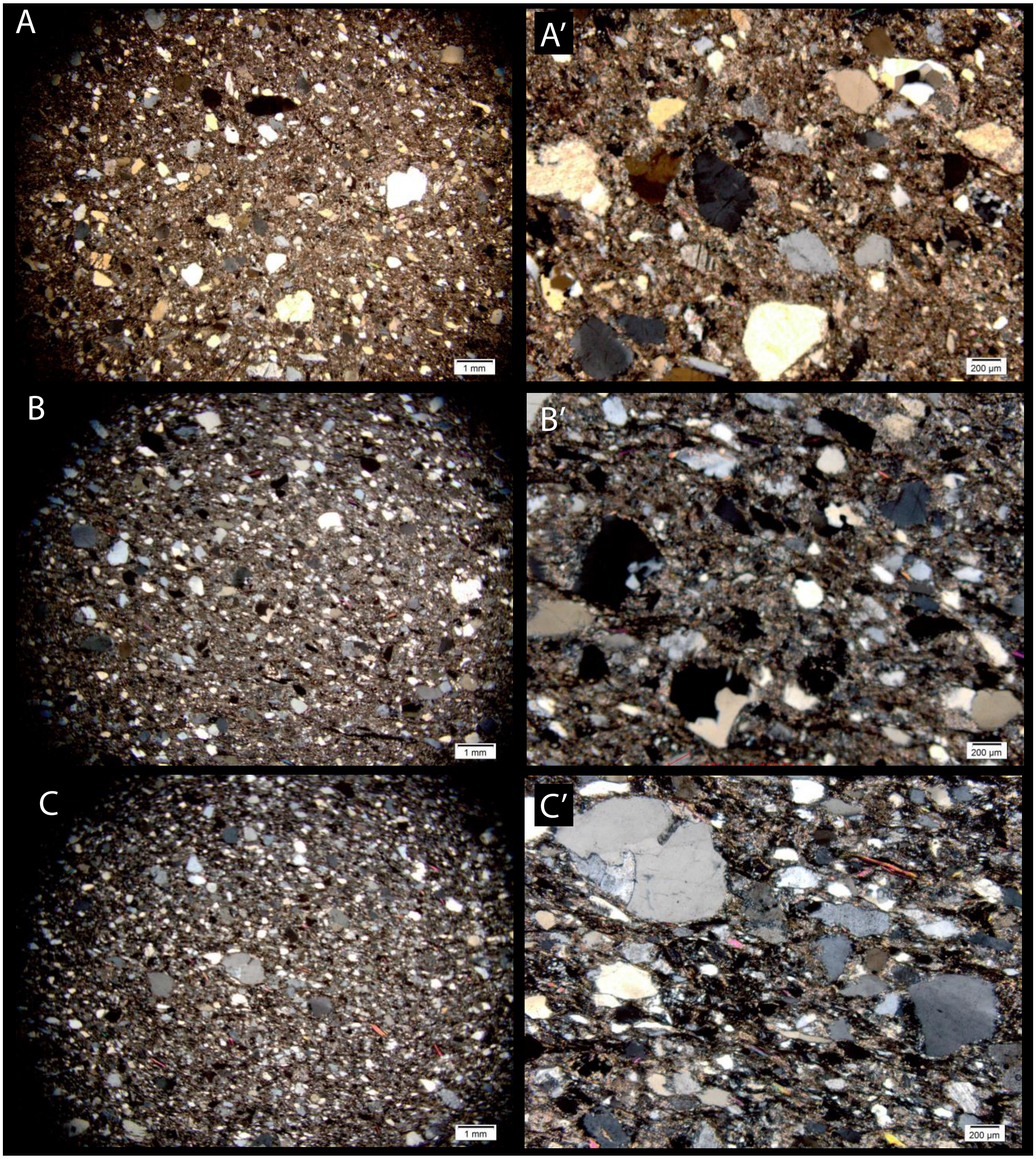

Figure 3.8: Examples of various matrix content percentages of matrix-rich beds. Note that qualitatively photomicrographs A-C resemble one another, however, detailed point counting provides quantitative evidence that matrix-content varies based on stratigraphic location within the study area. A) Cross-polarized photomicrograph at 1.25x magnification of a matrix-rich bed with 57% matrix. A') Cross-polarized photomicrograph at 5x magnification of (A). Note that grains appear to be floating in matrix. Grain boundaries are smooth and there is no occurrence of subgrains or bulging. B) Cross-polarized photomicrograph at 1.25x magnification of a matrix-rich bed with 52% matrix. B') Cross-polarized photomicrograph at 5x magnification of (B). C) Cross-polarized photomicrograph

at 1.25x magnification of a matrix rich bed with 45% matrix. C') Cross-polarized photomicrograph at 5x magnification of (C). Note the greater range in grain sizes.

Subfacies 1 (MRSC-I) is interpreted to represent deposition under conditions of high sediment fallout when the flow is still changing from upper transitional plug flow to quasi-laminar plug flow. The occurrence of low angle cross-stratification towards the top of subfacies 2 beds (MRSC II) implies that towards the end of a sedimentation event, flow speed was sufficiently low and near-bed sediment concentration exponentially distributed that ripples formed. In addition the lighter hue of this unit, indicative of lower matrix content, suggests that ripples were formed of sediment reworked from the top of the underlying matrix-rich bed (Arnott, 2012). Subfacies 3 (MRSC-III) is characterized by discontinuous, diffuse planar laminations that similarly suggest traction transport (Arnott, 2012). Moreover, the discontinuous nature of the laminations may be the result of turbulent pulses related to vertical fluid momentum transfer and consequent short-lived bursts of traction transport. The common mm-scale draping of mud over these diffuse laminations may be analogous to the wispy-laminated M3 divisions of slurry flow beds (Lowe and Guy, 2000; Lowe et al, 2003), which are interpreted to be the result of trapped clay floccules. The upward increase in matrix in Subfacies 4 (MRSC-IV) is interpreted to represent deposition from a upper transitional plug flow (UTPF) or a quasi-laminar plug flow. Lastly, the basal part of a subfacies 5 (MRSC-IV) bed is interpreted to represent deposition by a QLPF. As the fine-grained sediment concentration decreases and the plug becomes more dilute it evolves into a low concentration QLPF and a diffusely laminated unit similar to MRSC-III is deposited. The type of matrix-rich sub-facies that is deposited is likely controlled by the concentration of fine-grained sediment in the flow. The lateral change from matrix-rich strata to thin-bedded turbidites is interpreted to represent the evolution of the flow from quasi-laminar to a low energy/low-density turbidity current.

3.6 Facies 5: Fine-grained Banded Silty Mudstones

Facies 5 is made up of stacked light-dark couplets that typically decrease in thickness upwards (Figure 3.9) and are most common in Section 2, but are observed also in Section 1. Collectively the couplets form units ranging from 30-160 cm thick and consist of 2 to 7 couplets. Each couplet comprises a basal, light grey coloured, sand layer overlain abruptly by a darker, muddier layer (Figure 3.1 and 3.9). In the basal layer, grain size ranges from lower fine sand to fine silt. Coarser grains, namely fine and very fine sand are common but dispersed. The upper layer consists of silty-mudstone, with medium silt being the coarsest grain size. The basal contacts of individual layers, couplets and units of this facies are consistently flat and planar with no scouring, loading or dewatering structures. Mudclasts are also absent. Traction structures may be present depending on couplet type and are discussed below. Strata of Facies 5 typically overlie intermediate clayey sandstones (Facies 3) or sandy claystones (Facies 4) and depending on thickness form three kinds1) meso-banded: 1-10 cm thick couplet; 2) macro-banded: 10-50 cm thick couplet and; 3) mega-banded: >50 cm thick couplet. Strata are further subdivided based on the ratio of light to dark bands: 1) argillaceous: the dark, muddy band is thicker than the light band or; 2) arenaceous: the light sandier layer is thicker than the dark (Lowe and Guy, 2000). Lastly, banded couplets are categorized based on the contacts between the light and dark units. Type 1 couplets exhibit sharp, planar contacts and commonly are planar or cross-stratified; Type 2 couplets have gradational contacts and tractional structures are absent.

Based on couplet thickness, composition, structures and light to dark ratios, five types of banded silty mudstones (BSM) have been identified within the study area (Figure 3.9).

BSM 1: meso-banded, argillaceous, type 1 couplets – beds are massive and range from 3-8 cm thick, the basal light grey layer is 1-2 cm thick and the upper, dark layer is 3-5 cm thick. Couplets commonly stack to form 30-50 cm thick units composed of ~4 to 7 couplets. Generally, there is no upward change in couplet thickness. BSM 1 comprises 12% of the total banded silty mudstones in the study area.

BSM 2: meso-banded, argillaceous, type 2 couplets – a basal, light grey layer grades upwards into a darker, finer layer. Grain size in the basal layer is typically upper to lower very fine sand with upper and medium silt that eventually grades into a dark mudstone. Couplets range from 4-9 cm thick and form units 15-50 cm thick that typically overlie sandy claystone beds. Similar to BSM-1, these couplets change little in thickness upwards. BSM 2 makes up ~ 20% of total banded silty mudstones.

BSM 3: macro-banded, arenaceous, type 1 couplets – here, as the name implies, the upper, muddier dark layer is thinner than the lighter (massive) sandier layer. Couplets range from 12-30 cm thick. Strata of BSM-3 typically overlie intermediate clayey sandstones and commonly consist of 3 to 4 couplets. These beds account for 12 % of total banded silty mudstones.

BSM 4: macro-banded, arenaceous, type 1 couplets with diffuse planar lamination – the basal couplet is typically thicker than the overlying couplets in a unit. Moreover, the basal couplet is distinctive in that it comprises three layers instead of two. The lowermost layer resembles matrix-rich subfacies 1 in colour and is coarse-tail graded, upper fine sand to coarse silt that is typically 15-20 cm thick. As grain size decreases upwards to very fine sand/silt a distinctive lighter grey (middle) layer consisting of discontinuous, slightly undulatory mm-to-cm scale lamination is observed. This middle layer ranges from 3-7 cm thick and is overlain by a graded 5-10 cm thick siltstone to mudstone cap. This tripartite bed is overlain by thinner couplets making up the middle (light grey, diffusely laminated) and upper (graded silt to mud bed) layers (Figure 3.9). These strata typically overlie intermediate clayey sandstones (Facies 3) and stack to form units up to 1.10 m thick. BSM 4 makes up ~ 37% of total banded silty mudstones in the study area.

BSM 5: mega-banded, arenaceous, type 1 couplets with diffuse planar and cross-stratification; each couplet is composed of a basal ≥ 30 cm thick dark grey, fine lower to coarse silt layer composed of diffuse, discontinuous, mm to cm scale laminations. Towards the top of this basal layer a 4-6 cm thick, lighter coloured, better-sorted layer composed of discontinuous undulatory bedforms ranging in length from 10-40 mm and only a few grains high are observed (Figure 3.9). This, then, is overlain by a darker, silt to mudstone layer that ranges in thickness from 3-8 cm. Similar to BSM 4, only the middle (light grey, cross-stratified) layer and mudstone layer make-up the couplets overlying the initial mega bed. Commonly, these couplets stack to form units ~ 60-80 cm thick and rarely exceed 3 couplets. These beds predominate in the lower half of Section 2 where they sharply overlie intermediate clayey sandstones. BSM 5 makes up ~ 19% of the total banded, silty mudstones facies.

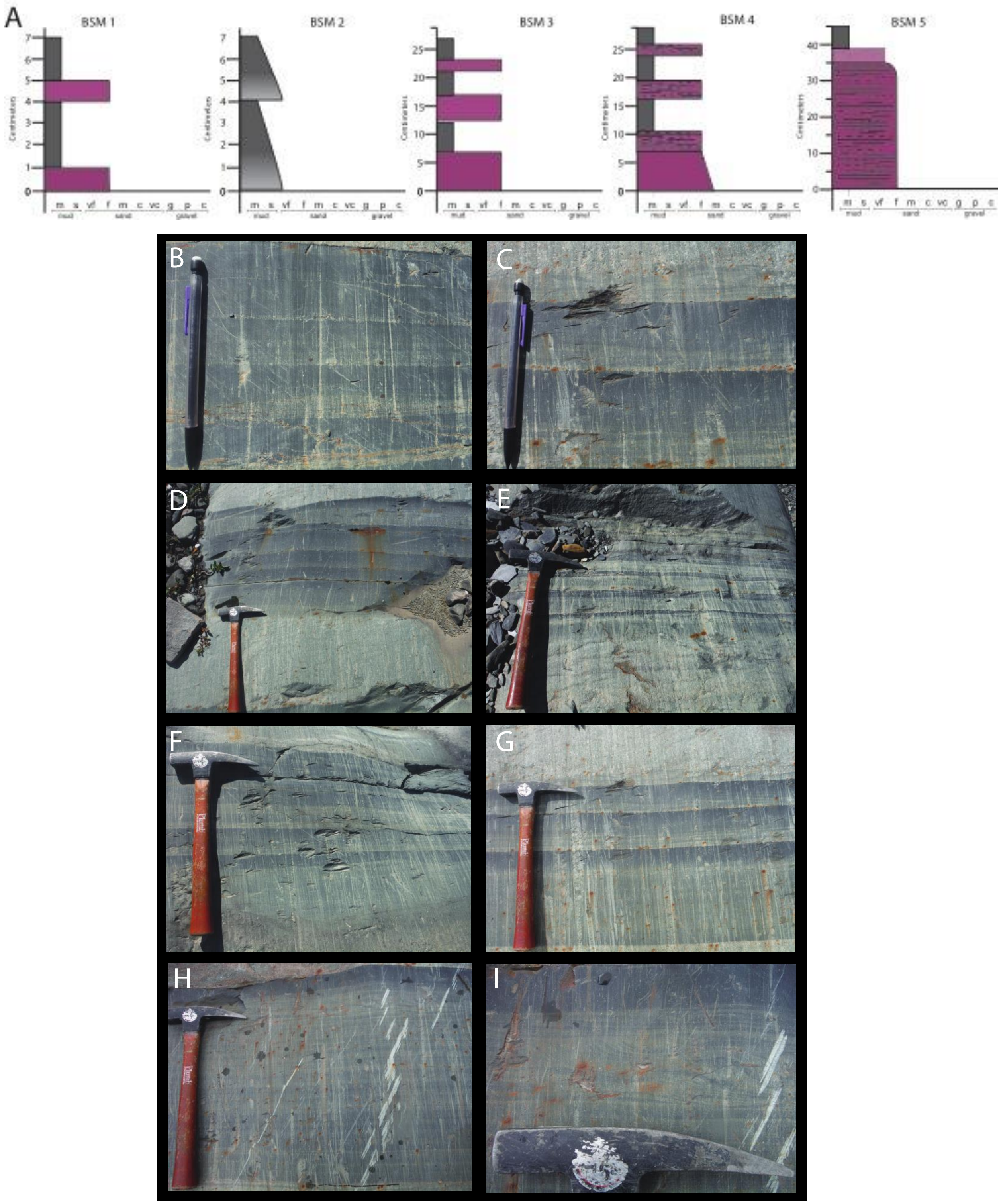

Figure 3.9 (continued on next page):

Figure 3.9 (continued): A) Idealized stratigraphic logs for the 5 kinds of banded couplets observed in the study area. B-C) Type 1: meso-banded, argillaceous, type 1 couplets. D) meso-banded, argillaceous, type 2 couplets. E) meso-banded, arenaceous, type 1 couplets. F-G) macro-banded, arenaceous, type 1 couplets with diffuse planar lamination below the boundary. H) mega-banded, arenaceous, type 1 couplets with diffuse planar and cross-stratification. I) Close up of cross-stratification at the top of the bed in (H).

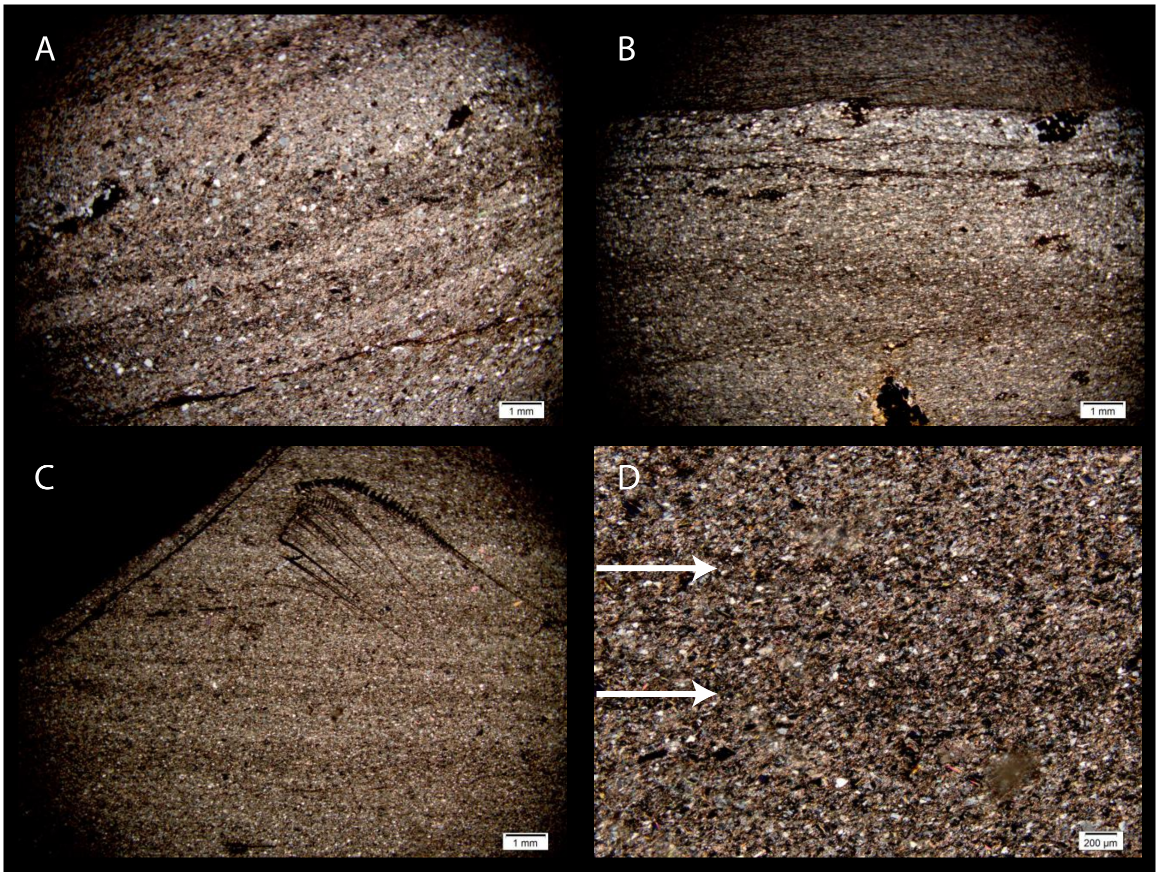

Figure 3.10: Photomicrographs of fine-grained banded couplets. A-C are taken at 1.25x magnification. A) Planar laminated part of a banded couplet. Note the discrete layers with high mud content and the dispersed coarse silt grains. B) Showing the sharp contact between the lower, sandy and upper muddy parts of a couplet. C) Diffusely laminated lower part of a banded couplet. D) Diffusely laminated bed from C at 5x magnification. Note the faint streaks of mud indicated by the white arrows.

3.6.1 Interpretation of Fine-grained Banded Silty Mudstones

The distinctive light to dark banding of silty mudstones suggests they were deposited from well-stratified flows with elevated fine-grained sediment concentration. Also, the lack of medium sand (or coarser) indicated that beds were likely deposited following the transition from turbulent to quasi-laminar flow. Furthermore, the sharp planar nature of contacts, lack of dewatering structures, the consistent lithological composition of banded units, the fining upwards trend within individual couplets and the general thinning upwards trend within a unit suggests that units made up of multiple couplets were deposited during a single rather than multiple sedimentation events. Lowe and Guy (2000) described similar banded deposits, and the following is a modified depositional sequence for banded units according to their model (Figure 3.10).

i) as flows decelerate, the coarsest grains (here, fine sand and very fine sand) settle out, increasing the particle concentration near the bed and deposited the basal, lighter band. This causes the flow to become more strongly stratified with a developing quasi-laminar plug of mud and silt particles above the near-bed layer;

ii) as the coarser grains continue to settle through the suspension, they collide with the less dense fine-grains and clay floccules causing them to disaggregate, which in turn increases the mud concentration and cohesive strength in the near-bed shear layer;

iii) eventually, the shear layer becomes so oversaturated with fine-grained sediment that grain settling ceases and en-masse freezing of the silt/mud layer occurs, depositing the upper layer of a couplet;

iv) en-masse freezing and compaction of mud and silt allows for the creation of a new, weakly turbulent shear layer and the process repeats itself until the fine and very fine sand in the upper part of the flow become exhausted, or the flow decelerates completely.

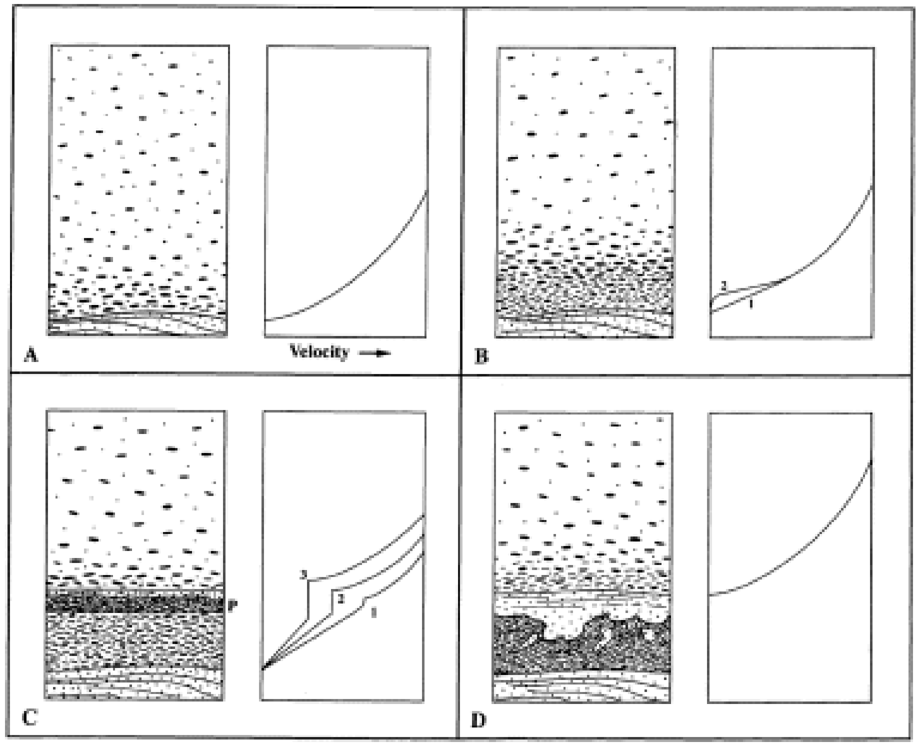

Figure 3.11: Deposition of banded beds (from Lowe and Guy (2000)). To begin, the flow is fully turbulent, and a thin active layer of bed- load sediment showing flat lamination or cross- stratification is deposited. Somewhat higher suspended- load fallout rates may result in the deposition of a thin massive bed. The lower part of the flow shows a strongly concave- upwards velocity profile characteristic of turbulent flows. (B) As the flow wanes, the settling of sand- sized mud and mineral grains increases flow stratification and sediment concentration in the lower part of the flow. Quartz and feldspar settling into the higher density near- bed zone slow but continue to settle to the bed, but lower density mud grains are retarded and ultimately retained, increasing the mud content of the basal layers. A combination of increasing sediment concentration, rising mud content and mud- particle disaggregation increases the viscosity, shear resistance and cohesive strength of the near-bed layer, eventually forming a cohesive viscous sublayer beneath the turbulent flow. The velocity profile near the bed flattens (profile 1) but is transitional at the top into the overlying flow as long as a discrete interface does not form and the layers exchange momentum as a result of turbulent diffusion. Where the viscous sublayer itself shows strong particle grading, the bed may essentially grade upwards into the flow, and the velocity profile may appear convex upwards near the bed (profile 2). (C) Increasing viscosity and strength in the viscous sublayer result in the appearance of a dynamic interface at the top of or within the upper part of the viscous sublayer. Below this interface, the cohesive strength of the viscous sublayer prevents settling of mud, quartz and feldspar grains, whereas above this interface, denser grains, mainly quartz and feldspar, are still settling towards the bed. Sediment accumulation at this interface initiates plug formation within the flow and deposition of light- band plug sediment on top of the viscous sublayer. Foundering of these early deposited light- band sediments into the underlying, still- shearing sublayer increases the particle content and strength of the upper part of the sublayer. Freezing of the sediment- charged upper part of the viscous sublayer may also contribute to plug development. Schematic velocity profiles 1–3 show velocity evolution within the flow and viscous sublayer as the plug forms and, later, as sediment accumulates on and thickens the

plug, in part by forcing compaction and freezing in the underlying shearing sublayer (profiles 2 and 3). (D) Settling mud and sand continue to accumulate on top of the plug. Brief working as bed load beneath the overlying turbulent flow forms the crudely layered sandstone of light bands. This current- deposited sandstone continues to load into the underlying mud- rich plug/viscous sublayer. Deposition on top of the plug eventually causes collapse, freezing and deposition of the entire viscous sublayer. At this point, the bed surface jumps to the top of the light band accumulating on top of the viscous sublayer at the base of the turbulent flow, and the depositional cycle begins again.

The deposition of banded couplets of Facies 5 is attributed, like those of Lowe and Guy (2000), to temporal differences in flow velocity and mud concentration. Experiments by Richardson and Meikle (1961) describe how varying concentrations of fine-grained sediment produce a variety of stratification types during suspension and deposition. Generally, at very low concentrations, there is no upwards displacement of fine-grained sediment, the flow remains mixed and differential settling occurs. As the concentration of fine-grained sediment increases flows tend to become stratified into 3 layers: 1) a basal layer consisting of only coarser grains; 2) a mixed layer composed of fine and coarse grains and 3) a upper layer consisting of only fine-grained sediment – though, the middle, mixed layer may be absent depending on the rate of fall out and sediment concentration (Richardson and Meikle, 1961).

The gradual fining upwards trend and lack of fine to very fine grains in BSM 1 suggests that couplets were deposited during the dilute, terminal stages of the plug. Furthermore the thinness of the couplets suggests a decrease in sediment fall out rates. In contrast, thick, diffusely laminated BSM 5 couplets are likely formed when there is a greater amount remaining in suspension and thus resulting in the deposition of a thicker bed. The diffuse laminations may represent traction transport and pockets of mud floccules that were unable stack greater than a few grains high before being quickly buried by settling sand grains. The undulatory, cross-stratified structures towards the tops of these beds are likely attributed to reduced rates and sediment fallout (due to a depleted supply of suspend sediment) and the general reduction in sediment concentration in the near-bed region. This, in turn, allowed by more extensive and prolonged reworking of the underlying bed by bedload transport and the development of the undulating laminations. Importantly, flow separation was almost never well developed, and as a consequence angle-of-repose ripple cross-stratification was only locally developed. The thinning upward trend common to most of the banded units is interpreted to represent the slow waning and thinning of the plume of remaining suspended sediment. The difference between argillaceous and arenaceous beds is directly related to the ratio of sand to mud within the initial flow and to the settling rates. Banded couplets require a unique set of flow circumstances in order to form. This is most evident through the specific stratigraphic occurrence of these beds and the facies typically associated with them.

Chapter 4: Facies Distribution and Depositional Model

4.1 Introduction to Lateral and Vertical Facies Trends

Walther's Law of the Correlation of Facies states that characteristic facies deposited under specific sedimentological conditions reflect a distinct depositional event and that facies lying laterally adjacent and/or vertically are (generally) genetically related (Middleton, 1973; Lopez, 2015). A number of lateral and vertical facies trends are observed within the study area, which in turn provides insight into the physical aspects of the depositional flows and their depositional history.

4.2 Lateral Facies Associations

A lateral continuum of facies changes between two end-member facies was identified in the study area. The trend between the two end-members is marked by a change from very coarse-grained, matrix-poor, amalgamated, thick sandstone (Facies 2) to much better stratified, fine-grained T_{de} thin-bedded turbidites (Facies 1; Figure 4.1) and is described in detail below.

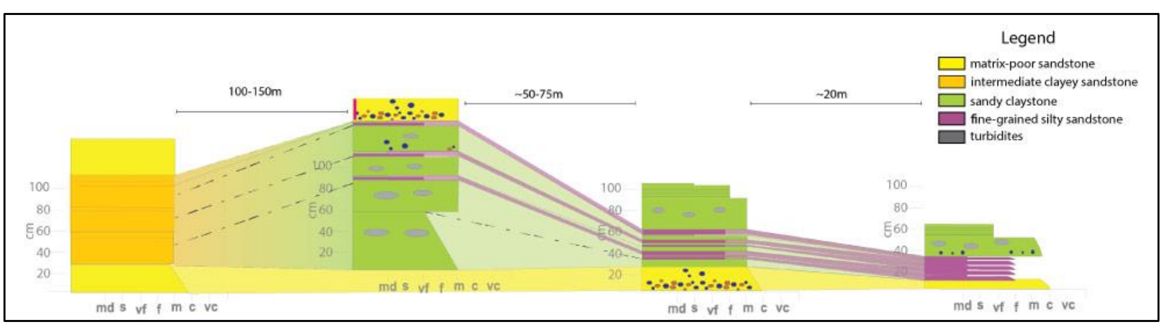

Figure 4.1: Stratigraphic correlation panel depicting the general lateral continuum from matrix-poor coarse facies to thin-bedded fine-grained facies.

4.2.1 Facies Association 1: F2: Matrix-poor Sandstone to F3: Intermediate Clayey Sandstone

This association is marked by the change from thick (> 1.5 m), granule to coarse-grained, matrix-poor (≤14% matrix content) sandstone (Facies 2) with amalgamated basal contacts to thinner (< 1.2 m), coarse-to medium-grained clayey sandstones (Facies 3) with higher matrix content (15-42% matrix content) and generally sharp, undulatory bedding contacts. F2 beds are typically massive and brownish grey in colour whereas F3 strata are coarse-tail graded with a blueier, brownish grey hue in the field. The transition from F2 to F3 is marked by the occurrence of large (>1 m x 50 cm) clasts of mudstone, T_{de} turbidites and matrix-rich strata. This lateral facies change is gradual and occurs over 100 – 250 m.

4.2.2 Facies Association 2: F3: Intermediate Clayey Sandstone to F4: Sandy Claystone

Facies Association 2 is the most drastic in the study area and is marked by major changes in bed thickness and composition (Figure 4.2). Specifically, coarse to medium grained sandstone (F3) that are 70-120 cm thick transition to beds that are 15-50 cm thick, massive to coarse-tail graded, mostly medium grained with dispersed fine grains, and matrix-rich (F4). The distinctive darker blue-grey colour of F4 is a macroscopic manifestation of increased matrix content (from 25-40% in F3 to >50-70% in F4). Basal contacts in both facies are sharp and planar. Also, F4 sandy claystones are consistently overlain by a few centimeter thick silty-mudstone cap, which is absent in F3. Traction structures (planar laminations and diffuse angular structures), which are absent in F3, are common in the upper part of F4 beds but below the mud cap. Lastly, there is a change in the shape and distribution of clasts (Figure 4.3): in F3 clasts are large (≥1 m long ± 50 cm thick) and irregularly shaped (serrated edges, blob-like) and composed of mudstone, T_{de} turbidites and matrix-rich strata (with some clasts exhibiting original stratification) and occur in the lower and middle part of the bed. Clasts within F4 are much smaller (average: 6 cm x 3 cm), similarly shaped (elongated, smooth edges) composed predominantly of mudstone and occur in the middle to upper part of the bed. The change from F3 to F4 strata occurs over a distance of 10-70 m laterally.

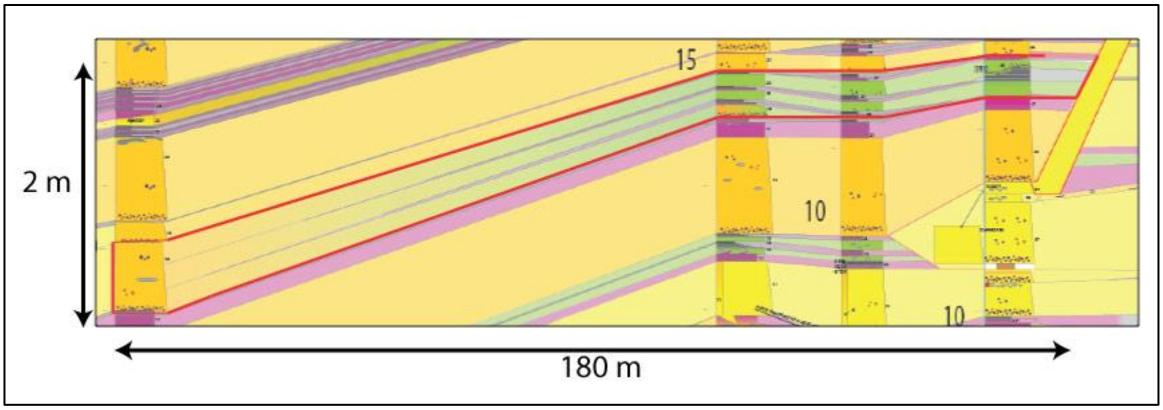

Figure 4.2: Stratigraphic correlation panel depicting the lateral facies change from intermediate clayey sandstones to sandy claystones.

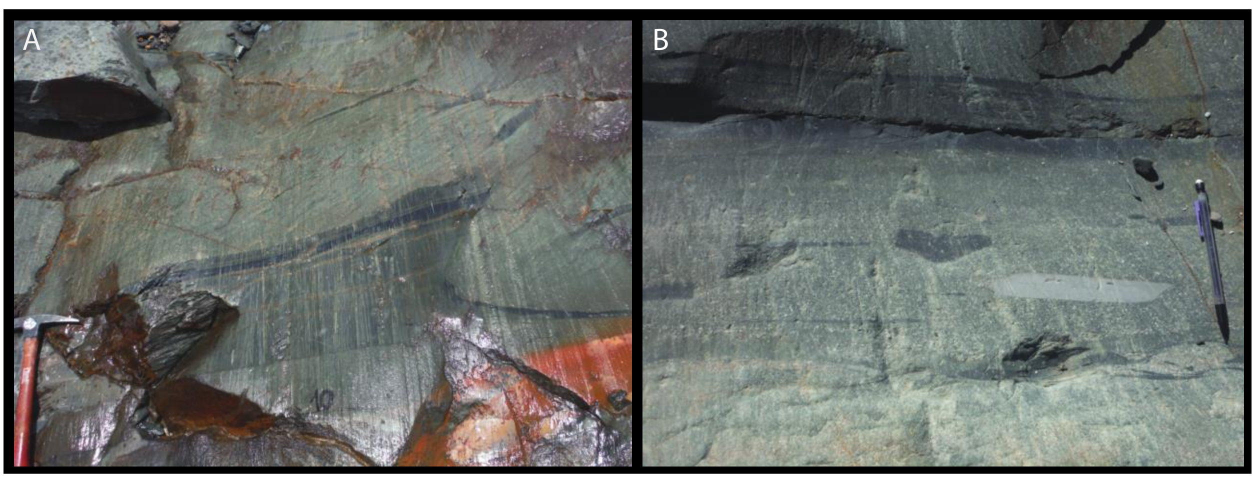

Figure 4.3: Examples of variations in clast size between intermediate clayey sandstones (A) and sandy claystones (B)

4.2.3 Facies Association 3: F4: Sandy Claystone to F5: Fine-grained Banded Couplets and/or to F1: Thin-bedded Turbidites

Strata of F4 transition laterally into strata of Facies 5 (fine-grained banded couplets) or F1 (thin-bedded turbidites; Figure 4.4). Beds typically become thinner (~5-20 cm thick) and are composed of only fine-grained sediment. Typically Subfacies V of F4 transitions into F5. Here, the matrix-rich T_a portion of F4 beds pinches out and what remains is only the thin, fine-grained, diffusely laminated part overlain by a mudstone cap (i.e. banded couplets; Figure 4.4). Where F4 transitions into F1 the matrix-rich T_a-like portion of the bed thins, but the thickness of the bed remains similar between the two facies (~10-20 cm thick). In this case, it is the thickness of the diffusely structured upper part of the bed that increases (1-3 cm in F4 and 5-8 cm in F1). The lateral facies change from F4 to either F5 or F1 occurs over a distance of less than ~15 m.

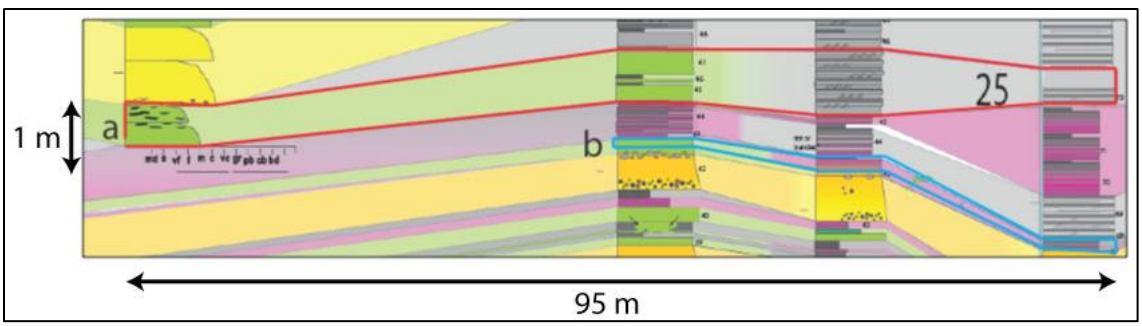

Figure 4.4: Stratigraphic correlation panel showing the lateral facies change from sandy claystones to thin-bedded turbidites (a, outlined in red) and fine-grained banded couplets (b, outlined in blue).

4.2.4 Facies Association 4: F5: Fine-grained Banded Couplets to F1: Thin-bedded Turbidites

Strata of F5 and F1 are lithological similar and as a result identifying the transition from one to the other is difficult to discern in the field. Nevertheless, notable differences include a thinning of the couplets and a slight decrease in grain size (lower fine-grained (F5) to very fine-grained/silt (F1)). In addition, the basal diffusely laminated portion of some couplets pinches out and all that remains is a thin (<2 cm thick) T_{de} turbidite. These lateral facies changes occur over a distance of 5-15 m (Figure 4.5).

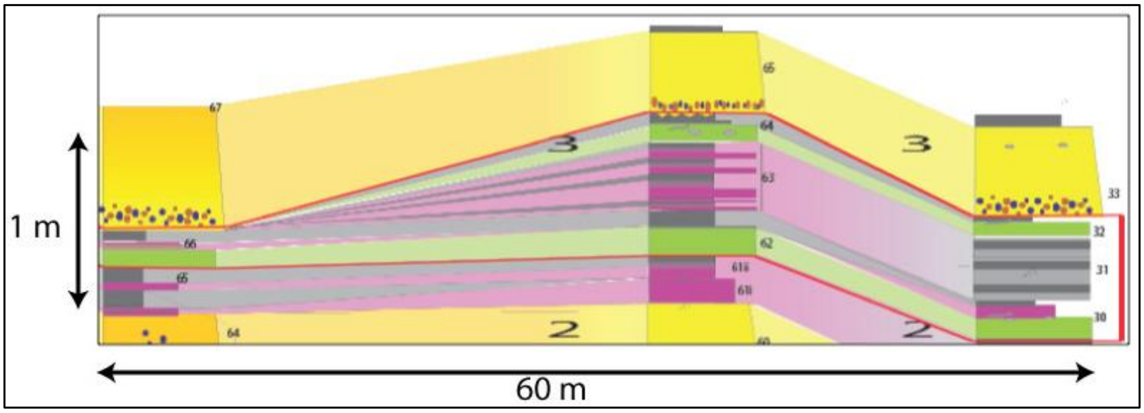

Figure: 4.5: Stratigraphic correlation showing the lateral transition from banded couplets to thin bedded turbidites.

4.3 Vertical Facies Associations

Facies 1 (turbidites) is commonly intercalated with facies 4 and 5 (sandy claystone and fine-grained banded couplets, respectively) with no noticeable upward trend. Rarely a full turbidite sequence is observed (T_{a-e}) where the T_a part of the bed sequence could be classified as F2. Thus, where a rare vertical facies association between F2 and F1 is observed, it is considered to be a full Bouma turbidite. F2 (matrix-poor sandstone) beds commonly stack to form units >5 m thick which are overlain by a mudstone layer. Similarly, it is uncommon to find a single F4 bed. Typically, 4 to 5 matrix-rich beds (F4) are stacked above one another to form a composite unit up to 1.5 m thick.

In the study area, two vertical facies associations are observed: 1) F3: intermediate clayey sandstone overlain by F5: fine-grained banded couplets and 2) F4: sandy claystone overlain by F5: fine-grained banded couplets. The vertical association between F4 and F5 likely exists due to the lateral transition from F3 into F4, thus only the vertical facies association between F3 and F5 will be discussed in detail.

Typically, a thick (80-100 cm) clayey sandstone (F3) is abruptly overlain by 2 to 7 fine-grained banded couplets (F5 Type 1-4) or a thick-bedded, diffusely laminated bed (F5 Type 5; Figure 4.7). These two-part successions then stack to form composite units that are up to 15 m thick. The abrupt change in grain size and texture, in addition to the sharp planar nature of the contacts suggest that a period of bypass occurred before the onset of F5 deposition. Thus, one F3 bed overlain by a stack of F5 couplets is interpreted to represent a single depositional event.

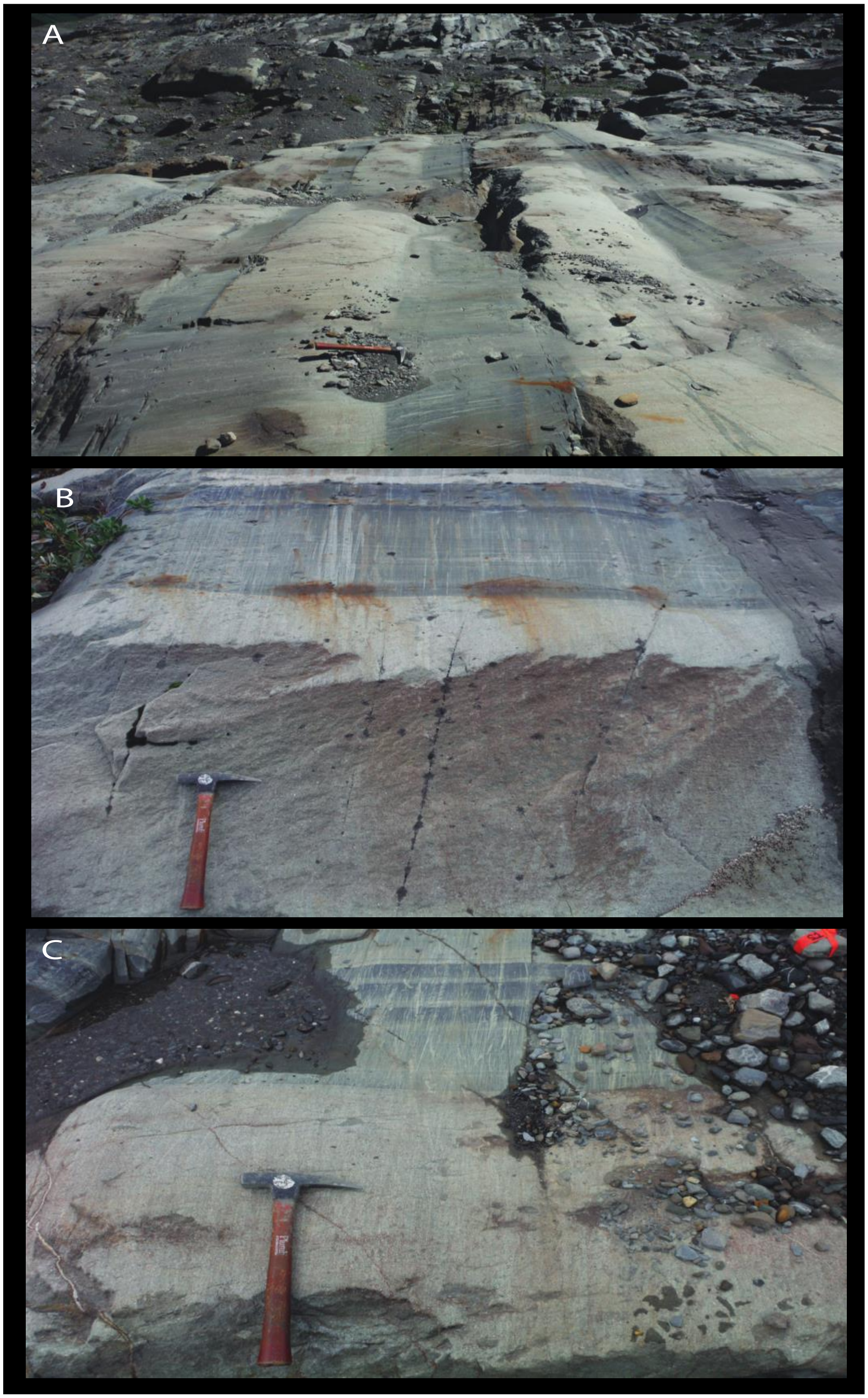

Figure 4.6: Examples of the vertical facies association between intermediate clayey sandstones and fine-grained, banded couplets throughout the study area. A) Panoramic photograph showing the abrupt, sharp and planar contacts between the two facies and the repetitive stacking. B) Example of a diffusely laminated macro bed. (BSM 5) above F3. C) Example of arenaceous, diffusely laminated banded couples (BSM 3) above F3.

4.4 Facies Distribution

Based on the vertical and lateral distribution of the five facies and their respective associations the study area has been divided into three lateral sections termed S1, S2, S3 (Figure 4.7) and five facies assemblages, respectively, P1, P2, P3, P4, P5 (Figure 4.8).

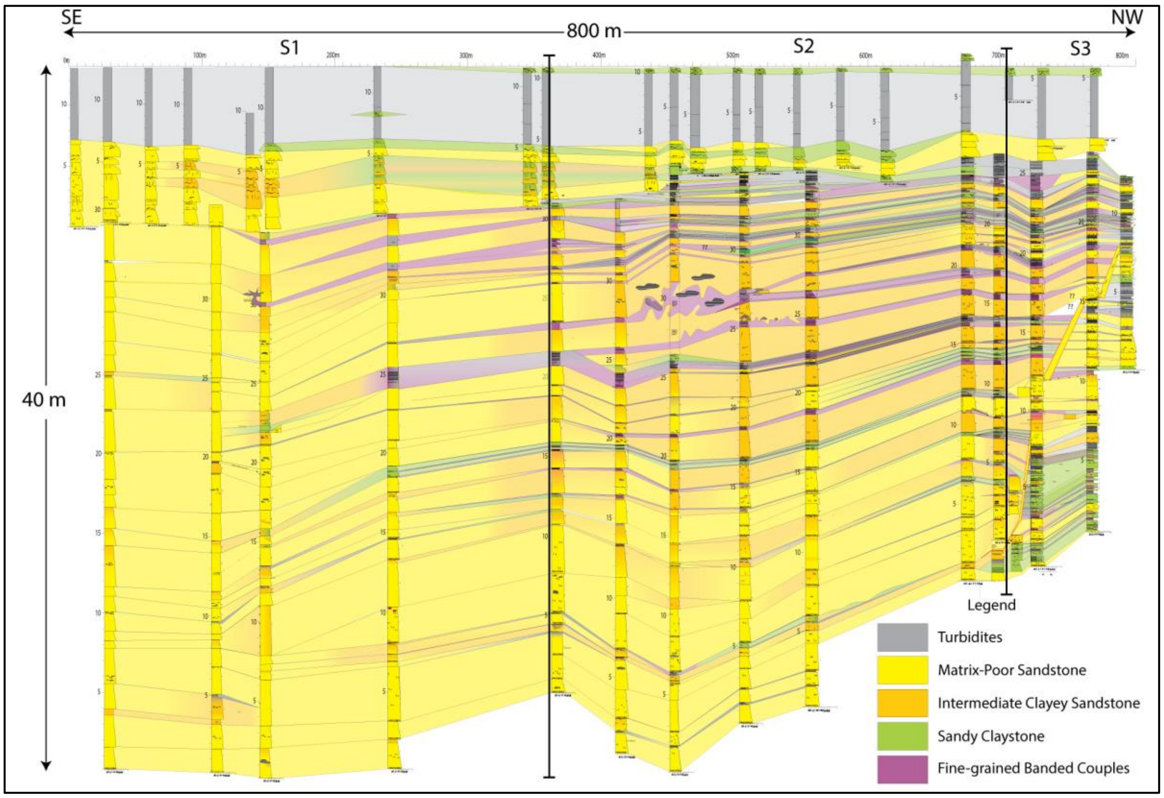

Figure 4.7: Stratigraphic correlation panel of the entire study area. Black vertical lines indicate section boundaries.

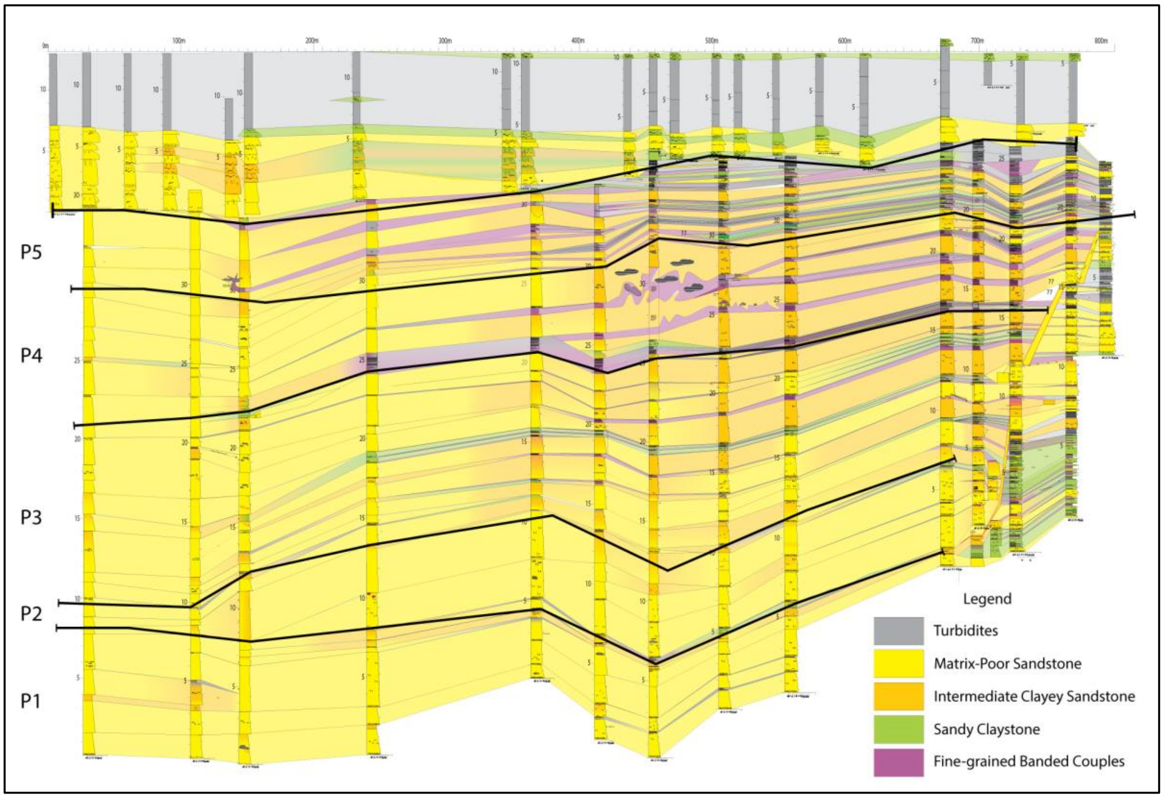

Figure 4.8: Stratigraphic correlation panel of the entire study area. Black lines indicate the boundaries of P1 to P5.

4.4.1 Lateral Sections

4.4.1-1 Section 1(S1)

Section 1 (S1) extends from the far southeast edge to about the center of the study area (a distance of ~360 m) and is dominated by amalgamated, structureless, matrix-poor, thick-bedded sandstone (F2; Figure 4.9). Strata contain no clasts or traction structures, and, because of bed amalgamation, bed contacts are difficult to discern except where a mudstone cap or abrupt change in grain size is observed. The transition from S1 to S2 occurs over ~100 m and is marked by the occurrence of abundant, irregularly-shaped clasts composed of thinly-bedded turbidites (F1), matrix-rich strata (F4) or banded couplets (F5).

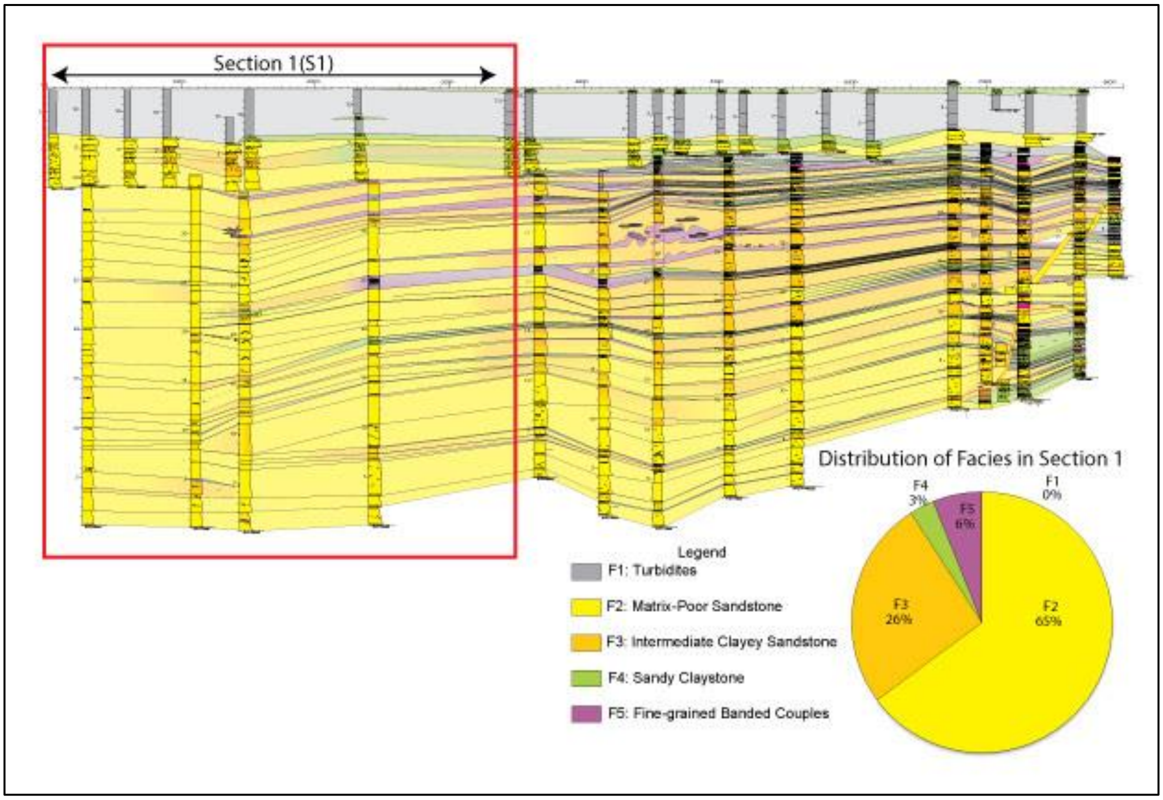

Figure 4.9: Stratigraphic location and distribution of facies in Section 1.

4.4.1-2 Section 2 (S2)

Section 2 is ~340 m wide and, in contrast to S1, bed contacts are discernible, sharp and undulatory. Strata consists mostly of meter-thick, intermediate clayey-sandstones (F3) overlain sharply by fine-grained banded couples, however towards the top of the section, matrix-rich clayey sandstones (F4) interstratified with banded couplets (F5) and thin-bedded turbidites (F1) become dominant (Figure 4.10). Distinctively strata of S2 contain abundant, large (i.e. 1 m x 50 cm, 4 m x 25 cm; 2 m x 90 cm), irregularly-shaped clasts composed of mudstone, T_{de} turbidites and/or matrix-rich strata. However, the most notable attribute of S2 is the abundance of scours, flame structures and the large number of distorted or deformed beds due to matrix-poor sandstone intrusions (likely sills or sand injections; see Kane, 2010) into well-stratified F3-F5 beds. The transition from

S2 to S3 is marked by a rapid (over a few tens of meters) and dramatic decrease in the number of large clasts, scoured contacts and the transition from intermediate clayey sandstones (F3) to sandy claystones (F4).

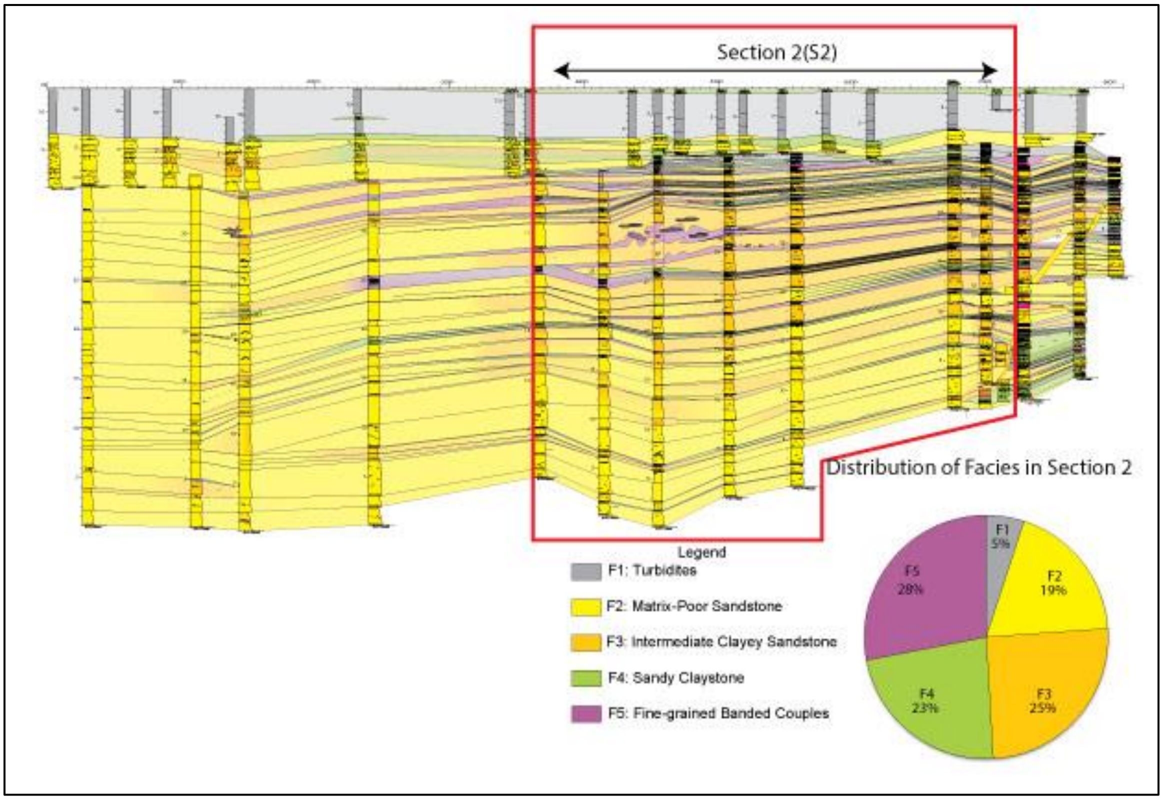

Figure 4.10: Stratigraphic location and distribution of facies in Section 2.

4.4.1-3 Section 3 (S3)

Section 3 is ~ 100 m wide and is located in the northwestern edge of the study area. This section is split into two parts due to the presence of two large scours. Because of the scours only the upper part forms a depositional continuum with strata in S2. S3 is composed of intercalated matrix-rich, fine-grained banded couplets and thin-bedded turbidites (Figure 4.11). Strata are considerably finer and thinner (≤50 cm) compared to those in S1 and S2. Bed contacts are sharp and planar with rare scours or flame structures. Furthermore, mudstone clasts are only present locally and large, irregularly shaped clasts are absent. In S3 facies change laterally from F4-F5, F4-F1 and F5-F1 over short distances (< 5m).

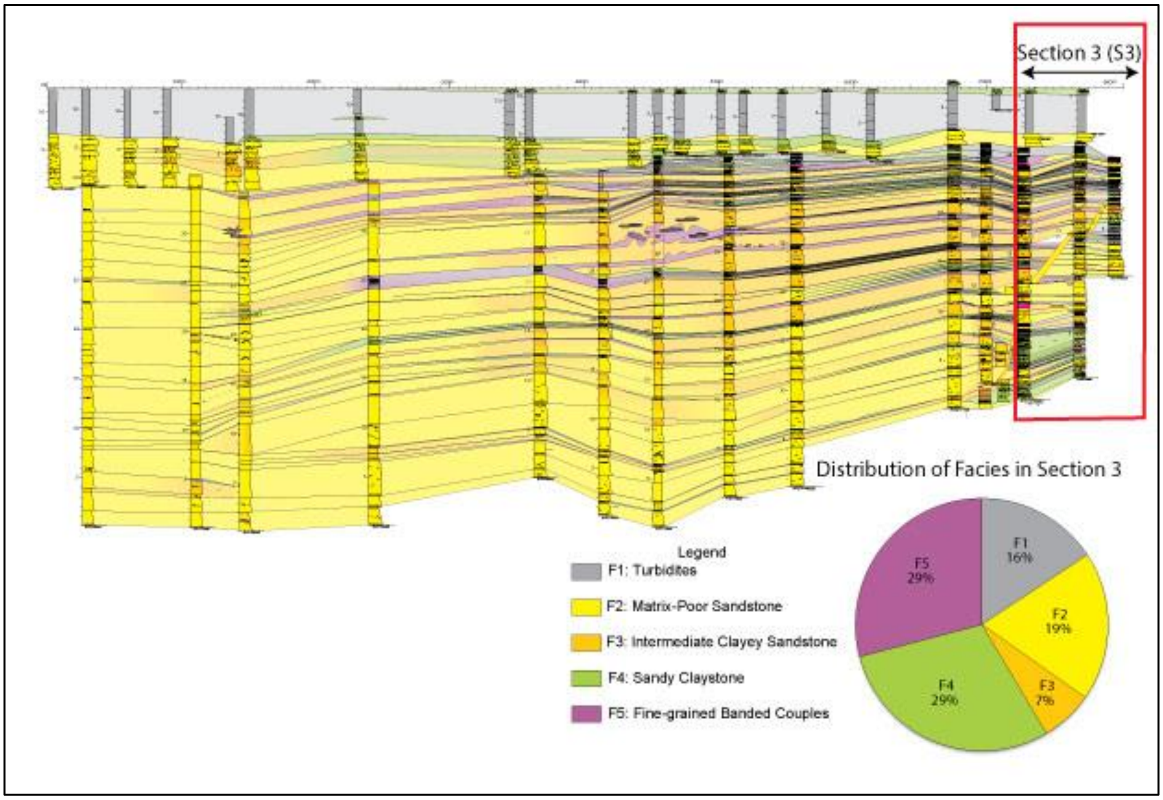

Figure 4.11: Stratigraphic location and distribution of facies in Section 3.

4.4.2 Facies Assemblages

The study area has been divided into 5 facies assemblages (referred to as packages) from the base to the top of the section (Figure 4.8). Each package is interpreted to represent a multi-event depositional continuum that collectively represents the sampling of different positions away from margin of incoming jet flows (Figure 4.11).

4.4.2-1 Package 1 and 2

Packages 1 and 2 are similar – a several-meter-thick, matrix-poor sandstone unit overlain by a few-bed-thick layer of intermediate clayey sandstones and matrix-rich mudstones. P1 is ~8 m thick and P2 is ~6 m thick (Figure 4.12). Laterally, bedding contacts in matrix-poor beds become slightly more discernable but still there is no evident laterally change in facies. Due to the homogeneity throughout these packages, P1 and P2 are interpreted as laterally extensive sheet-like sandstones deposited within and along the proximal margin of an off-channel jet flow.

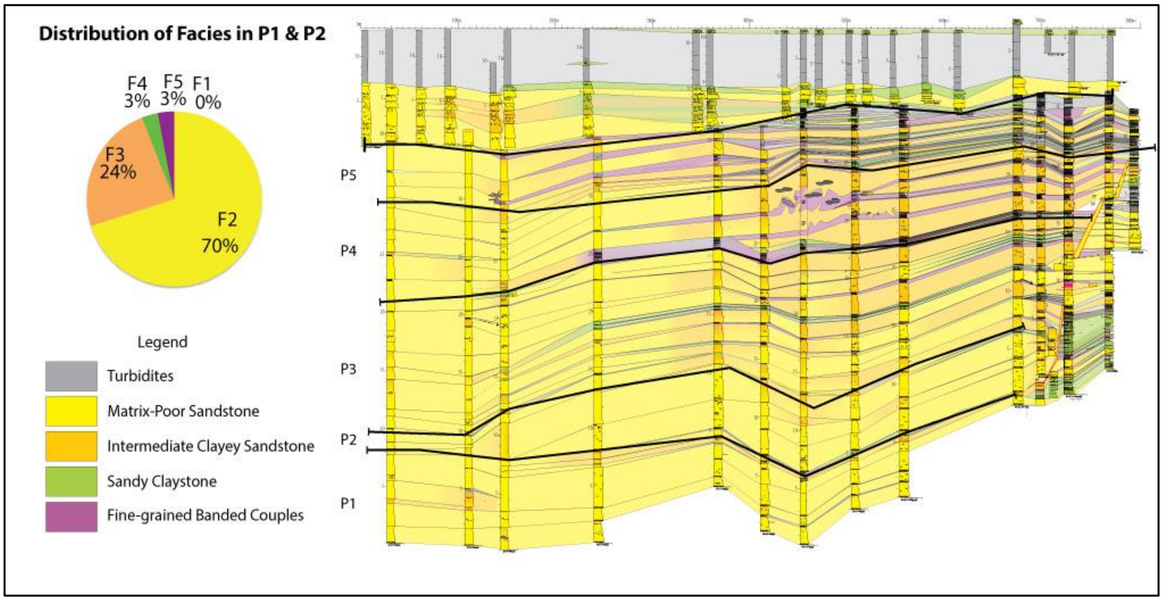

Figure 4.12: Stratigraphic location and distribution of facies in Packages 1 and 2.

4.4.2-2 Package 3

Package 3 is ~10 m thick and is composed of several vertically stacked units (~1.2 m thick) of F3-F4 and less commonly F3-F5. In contrast to P1 and P2, a clear lateral change from F2 to F3 is observed, where F2 makes up 35% of the area and F3 makes up 65% of the area (Figure 4.13). The lateral facies change from F2 to F3 suggests that P3 likely represents the transitional zone from matrix-poor to intermediate clayey-sandstones. Due to the paucity of large clasts and the low percentage of fine-grained, matrix-rich strata in P3, this package is interpreted to represent deposition further away from the margin of the jet flow.

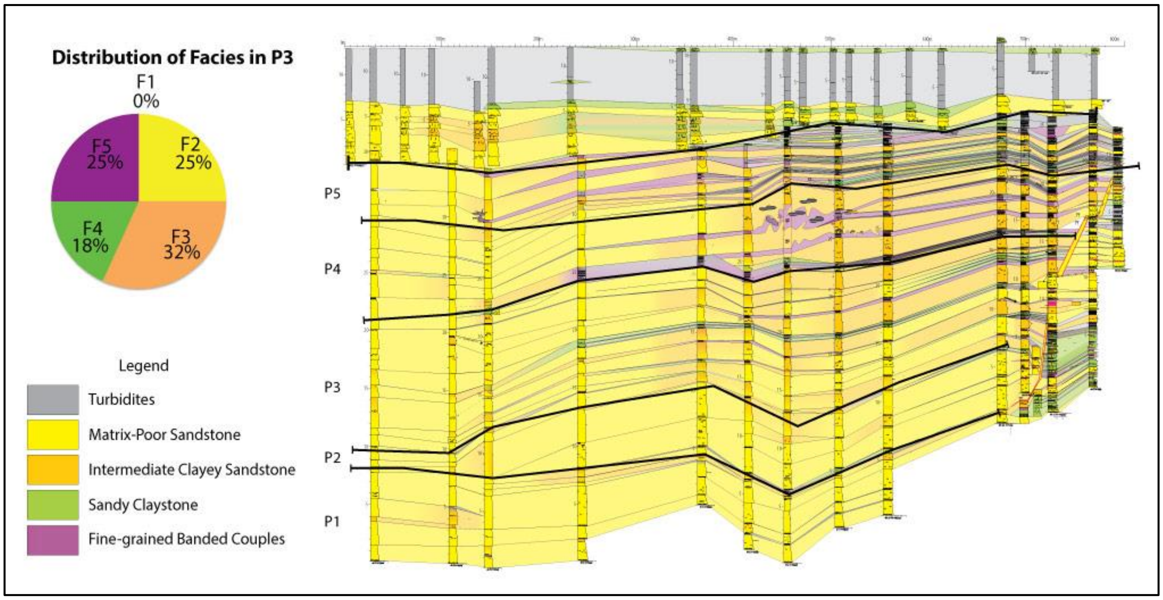

Figure 4.13: Stratigraphic location and distribution of facies in Package 3.

4.4.2-3 Package 4

This package is ~5 m thick and comprises significantly less matrix-poor sandstone than the underlying packages. P4 is composed primarily of stacked units of F3-F5. Although facies change little laterally, bedding contacts become sharper and more planar towards the northwest (Figure 4.14). This package is unique in that it contains all (three) of the clastic injection complexes in the study area and also the majority of the large, irregularly shaped clasts (dominant in Section 2). Based on the aforementioned characteristics, this package is interpreted to represent the rapid fallout of coarse-grained sand (F2 portion of the package) caused by a rapid decrease in flow speed, and accordingly, transport capacity. This resulted in the almost immediate (within several 10s of meters) deposition of intermediate clayey sandstones, which significantly also contain large rip up clasts sourced from intense avulsion-related erosion of the local mud-rich seabed.

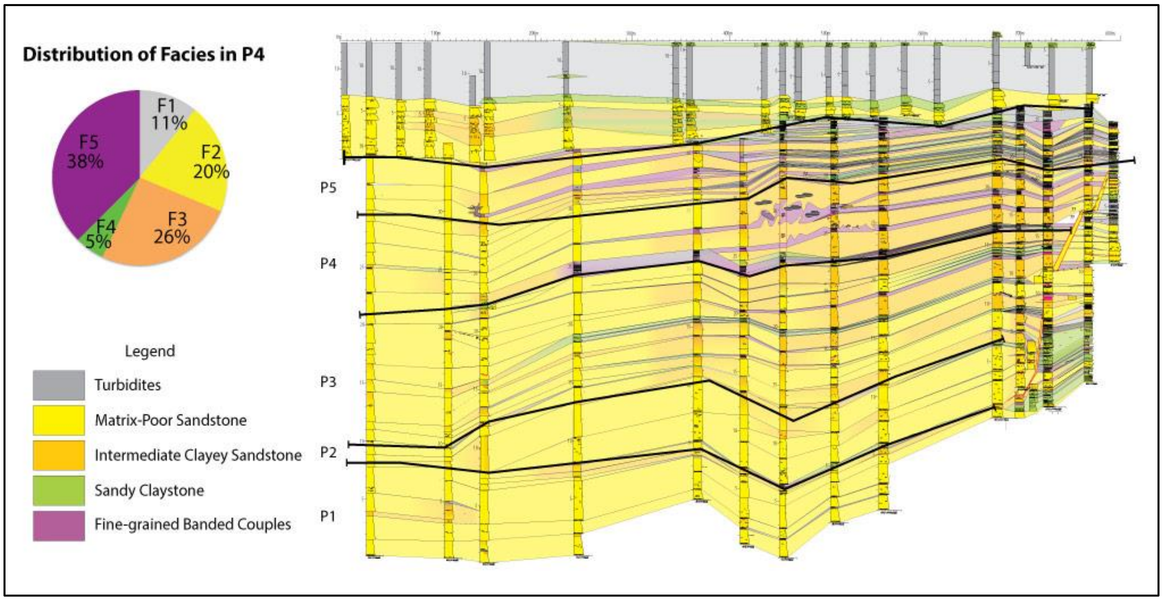

Figure 4.14: Stratigraphic location and distribution of facies in Package 4.

4.4.2-4 Package 5

Package 5 is ~5 m thick, consists of all 5 facies, and exhibits the full lateral suite of facies from matrix-poor sandstones (F2) to thin-bedded turbidites (F1; Figure 4.15), which makes P5 the idealized example of transitional flow deposits in the study area and therefore, a condensation of what is represented by a combination of packages 1 to 4. Accordingly, P5 is used as the type example in the depositional model discussed next.

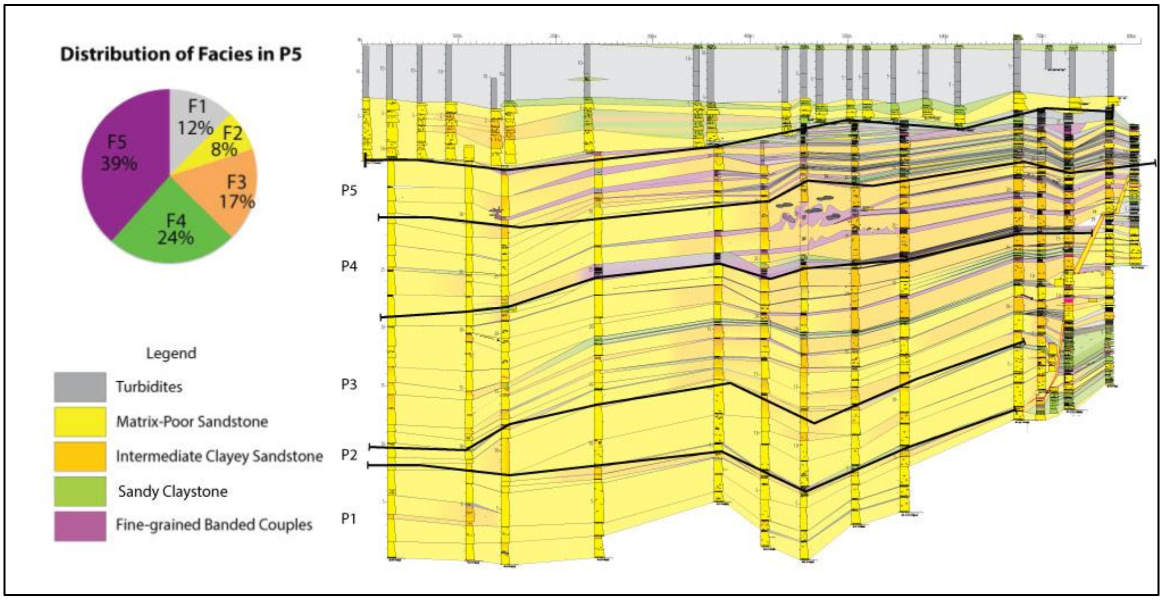

Figure 4.15: Stratigraphic location and distribution of facies in Package 5.

4.5 Depositional Model

Based on the aforementioned facies interpretations and the systematic stratigraphic arrangement of facies the following depositional model is presented to explain the depositional continuum from matrix-poor to matrix-rich strata. In part, this depositional model builds on the model presented previously by Terlaky (2014) and Terlaky and Arnott (2015).

4.5.1 Flow Initiation by Avulsion

When a channelized sediment transport conduit becomes inefficient, flow is diverted, commonly abruptly and permanently, into an adjacent, unchannelized, typically mud-rich part of the basin floor (Figure 4.16).

4.5.2 Flow Evolution

Upon exiting the parent channel, the fast-flowing supercritical flows (i.e. jet flow) expanded, which in some cases was sufficient to form a hydraulic jump. Intense turbulence production and extreme dynamic pressure fluctuations in the jet flow and/or jump deeply scoured the local seabed, and in turn quickly charged the lower part of the flow with abundant fine-grained sediment and variously-sized, irregularly shaped clasts. At the same time the continuous, but now more accelerated rate of particle settling, caused the flow to become stratified with a coarse, sand-rich basal part overlain sharply by a more mud-rich upper part.

4.5.3 Deposition

Deposition beneath the high-energy parts of the jet flow and/or jump is restricted to the minor fast-settling coarse sand grains and granules whereas most of the now more laterally- and vertically-expanded flow continued further downflow. On the margins of the jet/jump mud and sand (finer than about medium sand) were able to escape, and with increasing distance and decreasing turbulence (a consequence also of the progressive loss /deposition) of sand and proportionate increase of fine-grained sediment, and hence viscosity) clayey sandstones with intermediate amounts of matrix and containing large sand- and mudstone-rafts (F3) were deposited. Following depletion (i.e. deposition) of much of the coarse-grained sediment, the fine-grained, mud-rich upper layer of the plug flow began to deposit fine-grained banded couplets, with individual couplets interpreted to represent the alternation of suspended particle settling followed by cohesive mud (plug) emplacement (See Chapter 3 interpretation of F5). Further outward in the still expanding flow, suspended sediment consisting of grains finer than lower medium sand and common small, rounded mudclasts were able to settle through the dense sediment suspension and deposit matrix-rich strata (F4). This rapid deposition of matrix-rich beds caused energy in the flow to dissipate and become more dilute allowing for the rapid transition into fine-grained couplets (F5) or thin-bedded, upper division turbidites (F1; Figure 4.16).

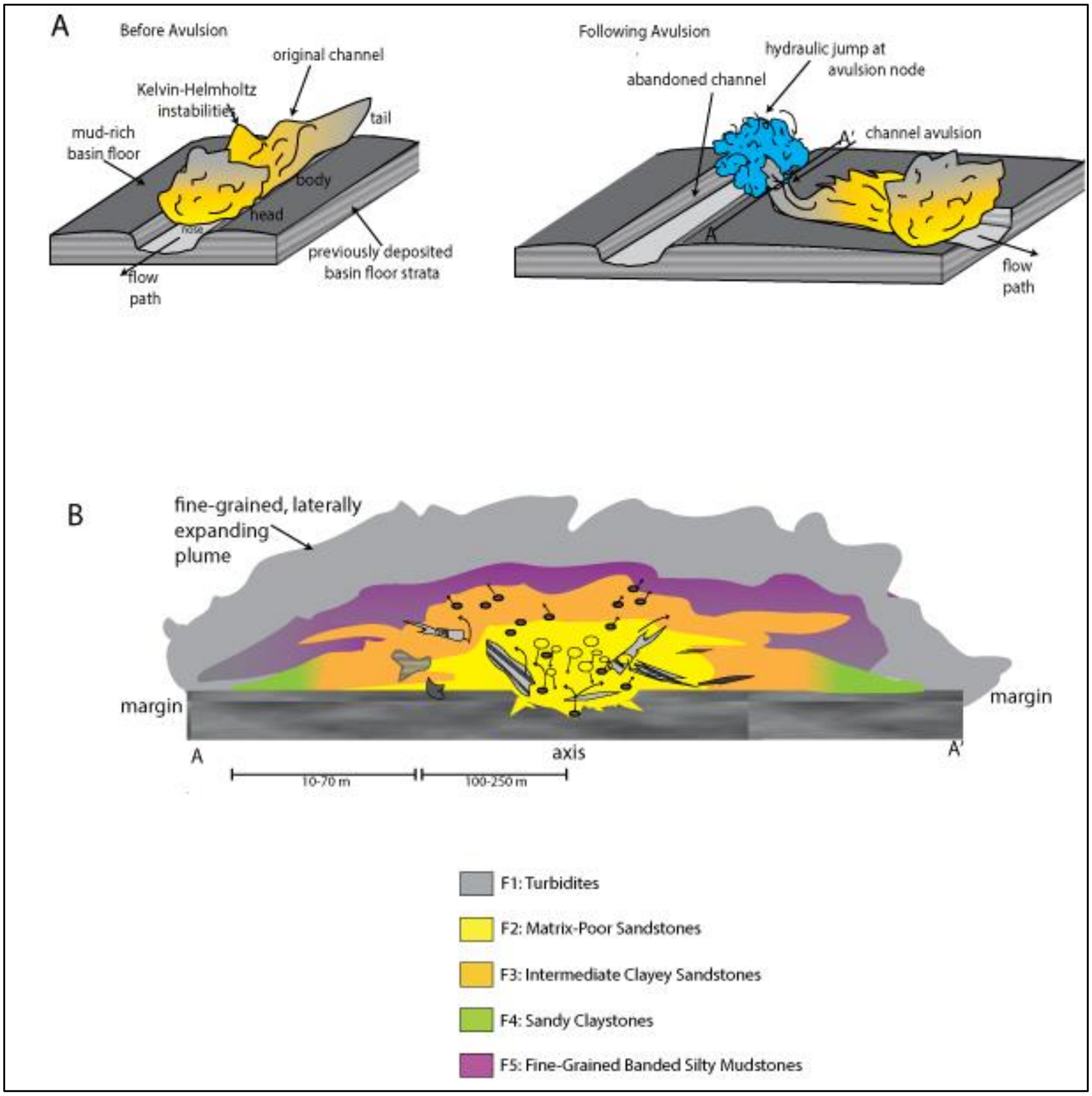

Figure 4.16: Schematic of the depositional model. A) Schematic depiction of an abrupt flow avulsion. B) Avulsion results in deep erosion of the sea-floor scour by the expanding jet (with or without an associated hydraulic jump), which then causes the abrupt introduction of large clasts and influx of fine-grained sediment into the basal part of the flow. C) (On next page) 8 m thick stratigraphic correlation panel showing detailed lateral facies transitions. Note that beds become significantly thinner and muddier towards the right side of stratigraphic correlation panel.

C

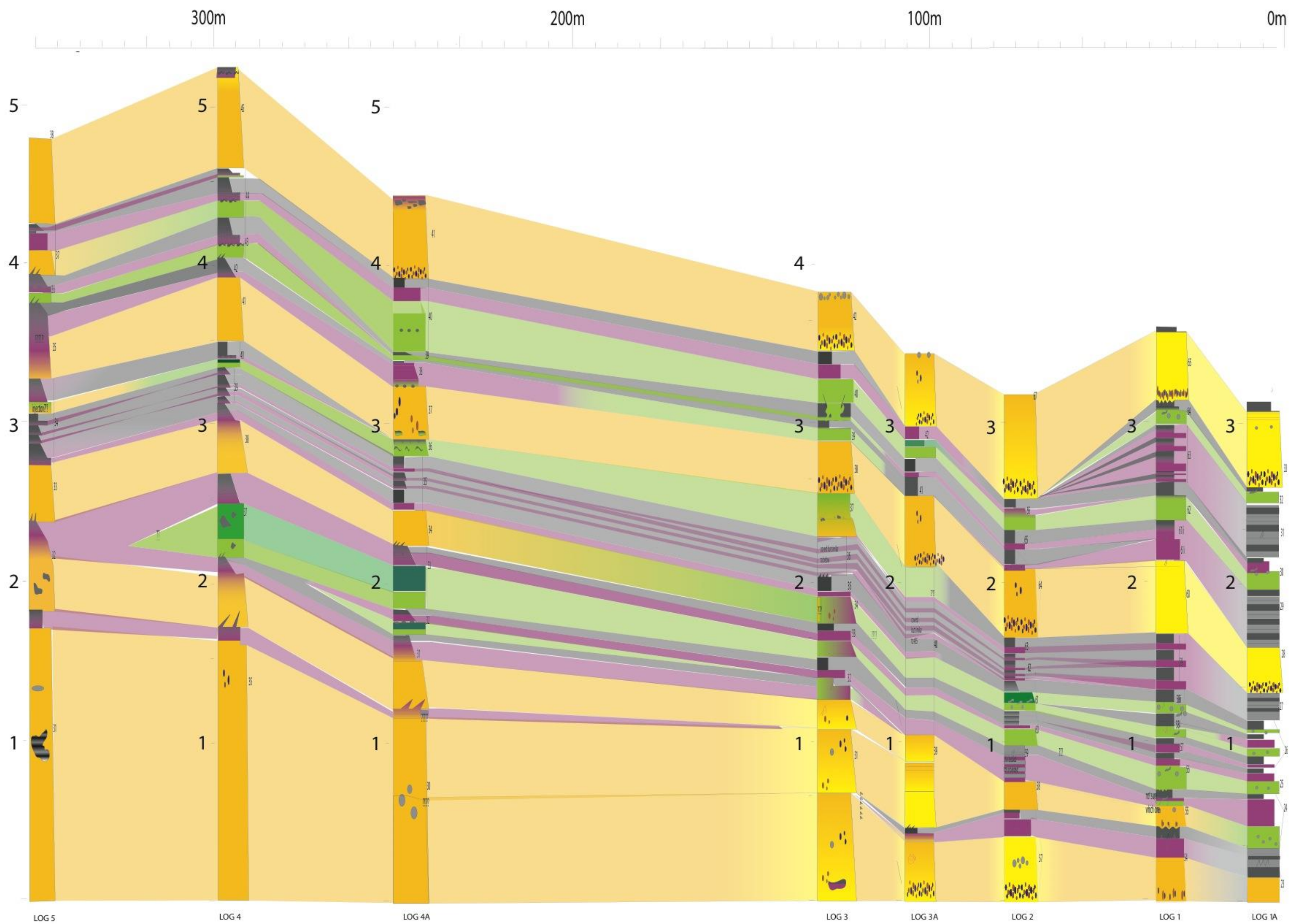

300m
200m
100m
0m
5
4
3
2
1
LOG 5
LOG 4
LOG 4A
LOG 3
LOG 3A
LOG 2
LOG 1
LOG 1A

Chapter 5: Discussion and Conclusions

5.1 Discussion

5.1.1 Implications of Petrographic Analysis

As discussed in Chapter 1, the Castle Creek outcrop has undergone at least four phases of deformation, and as a result determining the origin of the matrix in matrix-rich rocks, whether detrital or authigenic, is problematic. This study, therefore, is the first to quantitatively assess matrix content through detailed petrographic analysis (See Chapter 1.4 for methodology). Here, the results of the petrographic analysis are discussed and interpreted.

The results of detailed petrographic analyses have been summarized in a tertiary diagram (Figure 5.1; see Appendix B for raw data collected). Based on this diagram, samples are clustered into three distinct groups based on the ratio of matrix: recrystallized grains (M: R): Group 1: M:R is 1:5 and samples are described as matrix-poor sandstones (F2); Group 2: M:R is 1:1 and samples are termed as intermediate clayey sandstones; Group 3: M: R is 15:1 and samples are classified as sandy claystones. These results correspond well with qualitative, field-based observations and facies descriptions. Of note also is the inverse relationship between matrix content and recrystallized grains. This inverse relationship provides key information about the composition of the original strata prior to deformation. Subgrain formation and dynamic recrystallization are mechanisms by which detrital grains relieve deformational (tectonic) strain.

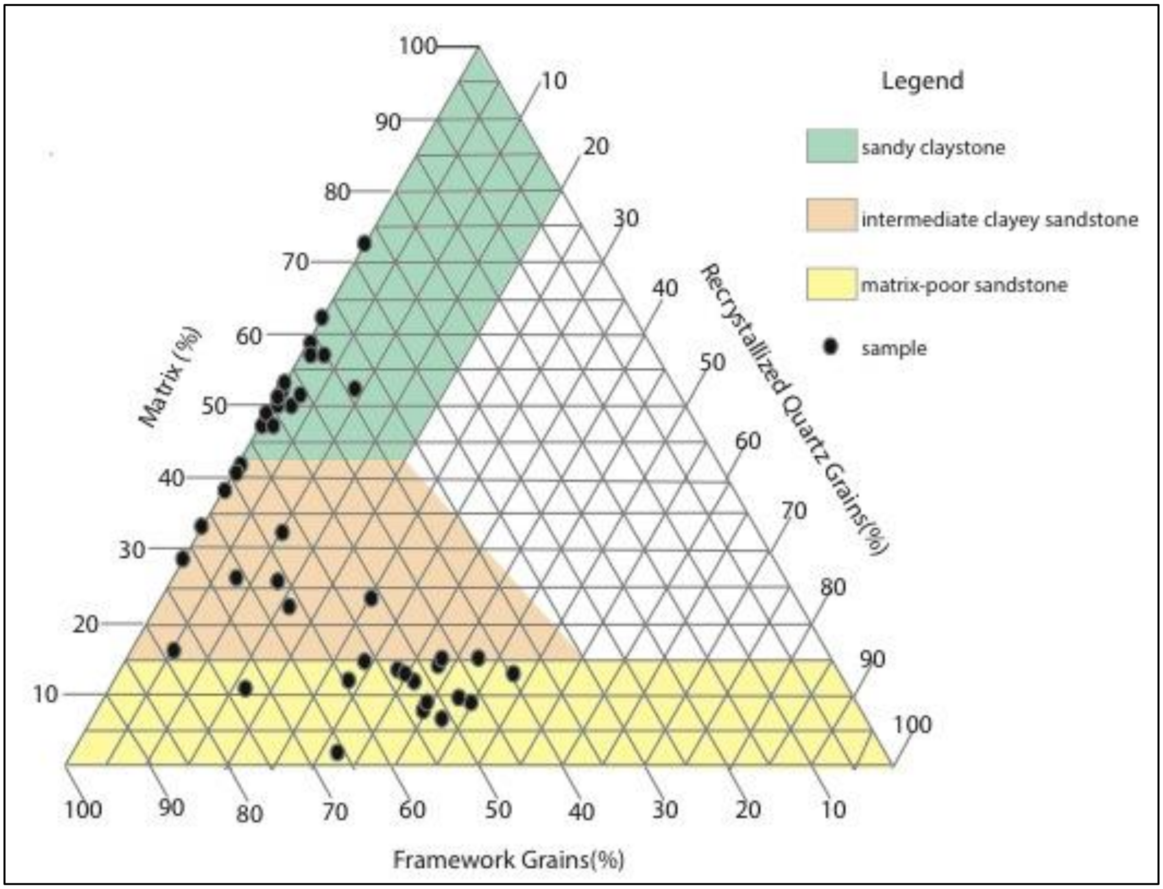

Figure 5.1: Tertiary diagram plotting the composition of 42 petrographic samples based on framework, matrix and recrystallized grain percentages. Three distinct sample clusters are evident based on M:R ratios and are highlighted by their respective facies descriptor. Note the white area on the right depicting the inverse relationship between matrix content and the amount of recrystallized grains. It is unlikely to have a sample with high matrix (> 60%) and recrystallized grain content.

Grain assemblages dominated by grain-to-grain contacts exhibit the highest degree of recrystallization. However, samples where grains are supported in a fine-grained detrital matrix exhibit significantly less recrystallization. Therefore, based on the inverse relationship between matrix content and the amount of recrystallized grains, matrix-rich strata in the study area are interpreted to have been matrix-rich at the time of deposition. Intermediate clayey sandstones illustrate this best. The base of these beds is matrix-poor and dominated by recrystallized grains whereas the top is more matrix rich with rare to no recrystallization. This suggests that the upper part of the bed had a higher detrital matrix which served to dissipate strain during deformation rather than these beds being differentially strained.

In conclusion, the detailed petrographic analysis carried out in this study provides a quantitative estimate of the amount of detrital matrix present at the time of deposition, and therein an assessment of fine-grained sediment abundance and distribution within the accumulating bed, and by extension, depositional flows.

5.1.2 Comparison of Matrix-rich Strata

Before comparing matrix-rich strata of this study with examples described elsewhere from Castle Creek and also the geological literature, a summary of key settings and observations regarding matrix-rich strata is presented first:

- massive or coarse-tail graded, medium- to fine-grained beds with 30-70% matrix, capped typically by a few to several cm thick silty mudstone;
- abundant, similarly-shaped and sized-mudstone clasts (similar in composition to surrounding mudstone beds);
- typically form 1-2 m thick units composed of stacked matrix-rich beds. Less commonly intercalated with fine-grained banded couplets (F4) and/or fine-grained turbidites (F1);
- sandy claystone units typically occur adjacent to units of intermediate clayey sandstones or matrix-poor sandstones – the lateral transition occurring over several 10s to 100s m;
- matrix-rich beds transition laterally over several 10s of meters to fine-grained banded couplets or upper division thin-bedded turbidites;

- interpreted to be deposited along the margins of a jet flow associated with a channel avulsion
- study area interpreted to be proximal basin floor.

5.1.2-1 Compared to Other Matrix-rich strata in the Windermere

While classic matrix-rich beds (MRSC-C) described here are similar to those described previously in the Castle Creek study area by English (2013); Terlaky (2014); Angus (in progress), they are far less common in this study area and, furthermore, stacked units are generally thinner (1-2 m maximum compared to several meters thick in these other studies). Other key differences include the abundance of Subfacies V (MRSC V: sandy claystone beds overlain abruptly by fine-grained, diffusely laminated sandstone unit capped by mudstone), and most notably, the paucity of bipartite matrix-rich beds (Angus, 2016). Furthermore, in this study intermediate clayey sandstones and Subfacies I (MRSC-I: massive, structureless, matrix-rich that lack mudclasts) are more common. The abundance of these facies and subfacies compared to earlier studies at Castle Creek is interpreted to be the result of variations in flow rheology and degree of confinement; it is proposed that the flows that deposited strata within this study area were likely sandier.

5.1.2-2 In Comparison to Other Transitional Flow Deposits

Similar to “slurry deposits” (Lowe and Guy, 2000; Lowe et al, 2003), “linked debrites” (Haughton et al. 2003; Amy and Talling 2006; Haughton et al. 2009), “cogenetic debrite-turbidite beds” (Talling et al, 2004), “hybrid event beds” (Hodgson, 2009; Pyles and Jennette, 2009) and “transitional flow deposits” (Kane and Pontén, 2012), matrix-rich strata in this study are interpreted to represent deposition from a changing or transitory flow. Furthermore, strata described in these studies include a thick-bedded basal T_a unit at the base of the bed, which then is overlain by a thinner matrix-rich or fine-grained bed that at least superficially resembles intermediate clayey sandstone, in turn overlain by fine-grained banded couplets (vertical facies association 1). Similarly, fine-grained banded couplets are comparable to slurry bed types III and IV due to the occurrence of wispy lamination and light/dark banding.

However a number of important lithological and depositional differences are noted. Most notably, unlike other matrix-rich deposits, strata described here lack a matrix-poor T_a beneath the matrix-rich part of the bed. Unlike the H3 (debrite) division in HEB's, and the clast-rich division in type 1 linked debrites, no debrite or debrite-associated facies is observed within the study area. The large, irregularly-shaped clasts common in S2 of the study area (and in F3) are dispersed in a "matrix" of sandstone rather than mudstone, and as a result are interpreted to have been sourced locally, and owing to their size, deposited immediately adjacent to the axis of the jet flow/jump. In addition to the clasts, the fine-grained sediment needed to form matrix-rich strata in this study is interpreted to have been sourced from erosion of the local mud-rich seafloor for the following reasons: 1) clasts are fragments of common basin floor deposits such as thin-bedded, upper division turbidites, matrix-rich beds and fine-grained banded couplets; 2) although generally uncommon, matrix-rich strata tend to form multi-bed packages rarely interstratified with other lithologies. This suggests that there is a unique set of conditions needed for the deposition of matrix-rich beds, which is different from those that deposit classical turbidites – specifically, flows with a higher near-bed fine-grained sediment concentration.

Intense scouring of the seafloor in the upflow end of an avulsion introduces a prodigious amount of fine-grained sediment into the lower part of an otherwise sand-rich flow. Avulsions, although more common in highly depositional areas like basin floor fans, are nevertheless sporadic and spatially random, explaining the irregular distribution of matrix-rich deposits in the Windermere Supergroup sedimentary pile. The paleogeographic occurrence of matrix-rich beds in the WSG differs also from matrix-rich beds described elsewhere. Linked debrite beds are typically observed “in the lateral and or distal edges of systems otherwise dominated by turbulent flow processes” (Haughton et al., 2009). Pyles and Jennette (2009) reported hybrid beds in basin-margin strata and Hodgson (2009) and Kane and Pontén (2012) similarly observed hybrid event beds and transitional flow deposits to be concentrated near the edges of lobes. Furthermore, Talling et al. (2012) report that low-strength cohesive debrites “are consistently absent in the more proximal parts of systems”. In contrast, this study area, based primarily on the previous work of Meyer (2004), Rocheleau (2012) and Terlaky (2014) is interpreted to be located in the proximal basin floor. Lastly, most reports of matrix-rich beds (or matrix-rich parts of beds) have proposed them to be deposited from flows undergoing a longitudinal change to a more cohesive behavior; whereas matrix-rich beds in the WSG are interpreted here to be deposited from flows that evolved toward more dilute and fully turbulent conditions at their lateral and/or distal run-out limit.

5.2 Conclusions

The objective of this thesis was to carefully describe and quantify the changes in a lateral transect from matrix-poor to matrix-rich strata in basin-floor deposits of the

Upper Kaza Group at the Castle Creek study area. Here the lateral succession of facies is: matrix-poor, amalgamated sandstones to better stratified intermediate clayey sandstones to sandy claystones and finally to either fine-grained banded couplets or thin-bedded, upper division turbidites. This succession of facies and their systematic spatial distribution is interpreted to represent a depositional continuum downflow and lateral to a site of channel avulsion. Immediately downflow of the avulsion node the high-energy efflux jet (and a hydraulic jump if sufficiently expanded) deeply scoured the underlying mud-rich seafloor. This scouring almost instantaneously charged the flow with fine-grained sediment, and accordingly changed the rheology of the flow, at the very least in the important near-bed region. Coarse sediment, owing to its higher settling velocity, remained in the axial part of the flow whereas finer sediment became partitioned towards the margins of the jet. It is here, towards the margins of the jet, that the distinctive lateral facies change from intermediate clayey sandstones to sandy claystones and then to either fine-grained banded couplets or thin-bedded, upper division turbidites occurs.

Detailed petrographic analysis provided a quantitative assessment of matrix-rich content in these strata and illustrated that the matrix is detrital, which was later modified by Mesozoic tectonic and metamorphic processes. It is recommended that all future studies at Castle Creek perform this analysis in order to provide a quantitative assessment of matrix content in all strata, matrix-rich or -poor. Moreover, future work should focus on examining the relationship between intermediate clayey sandstones (F3) and fine-grained banded couplets (F5), in particular to better elucidate the depositional conditions of banded couplets.

In the past 5 to 10 years matrix-rich strata have become increasingly recognized as a major component in the deep-marine sedimentary record. However, the origin and lithological variations of these enigmatic strata have been incompletely documented, and hence remain poorly understood. As they are generally considered to have poor reservoir qualities, understanding the genesis and stratigraphic distribution of matrix-rich strata is of paramount importance to the petroleum industry. Studies like this continue to add to the ever-growing literature on deep-marine sedimentary systems, and ultimately help to one day bridge the gap between large-scale 2D and 3D seismic data and small-scale, high resolution drill core observations.

References

Aalto, K.R., 1971, Glacial marine sedimentation and stratigraphy of the Toby conglomerate (upper Proterozoic), southeastern British Columbia, northwestern Idaho and northeastern Washington: Canadian Journal of Earth Sciences - Revue Canadienne des Sciences de la Terre, v. 8, p. 753–787.

Allen, J.R.L., 1991, The Bouma division A and the possible duration of turbidity currents: Journal of Sedimentary Petrology, v. 61, no. 2, p. 291-295.

Amy, L., and Talling, P.J., 2006, Anatomy of turbidite and debrite sandstones based on long distance (120 x 35 km) bed correlation, Marnoso-arenacea Formation, Northern Apennines, Italy: Sedimentology, v. 53, p. 161-212.

Arnott, R.W.C., 2007a, Stratal architecture and origin of lateral accretion deposits (LADs) and conterminuous inner-bank levee deposits in a base-of-slope sinuous channel, lower Isaac Formation (Neoproterozoic), East-Central British Columbia, Canada: Marine and Petroleum Geology, v. 24, p. 515-528.

Arnott, R.W.C., 2007b, Stratigraphic architecture and depositional processes of a proximal crevasse splay and genetically related, sinuous channel fill, Isaac Formation, British Columbia, Canada: *in* T. H. Nilsen, R. D. Shew, G. S. Steffens, and J. R. J. Studlick, eds., Atlas of deep-water outcrops: AAPG Studies in Geology 56.

Arnott, R.W.C., 2012, Turbidites, and the case of the missing dunes: Journal of Sedimentary Research, v. 82, p. 1-6.

Arnott, R. W., and F. J. Hein, 1986, Submarine canyon fills of the Hector Formation, Lake Louise, Alberta: Late Precambrian syn-rift deposits of the proto-Pacific miogeocline: Bulletin of Canadian Petroleum Geology, v. 34, p. 395–407.

Arnott, R.W.C., and Hand, B.M., 1989, Bedforms, primary structures and grain fabric in the presence of suspended sediment rain: Journal of Sedimentary Petrology, v. 59, no. 6, p. 1062-1069.

Arnott, R. W., and G. M. Ross, 2007, Overview: outcrop analysis of an ancient, passive margin, turbidite system: Windermere Supergroup, British Columbia, Canada, in T. H. Nilsen, R. D. Shew, G. S. Steffens, and J. R. J. Studlik, eds., Atlas of deep-water outcrops: AAPG Studies in Geology 56, p. 81–84.

Arnott, R.W.C., Wallace, K., and Laurin, J., 2011, Stratal architecture and temporal evolution of a passive margin mass-transport deposit, Neoproterozoic Isaac Formation, Cariboo Mountains, British Columbia, Canada, In: Mass-transport deposits in deepwater settings

(Eds. Shipp, R.C., Weimer, P., Posamentier, H.W.), SEPM Special Publication no. 96, 532 pp.

Baas, J.H., and Best, J.L., 2002, Turbulence modulation in clay-rich sediment-laden flows and some implications for sediment deposition: Journal of Sedimentary Research, v. 72, p. 336-340.

Baas, J.H. and Best, J.L. 2008, The dynamics of turbulent, transitional and laminar clay-laden flow over a fixed current ripple: Sedimentology, v. 55, p. 635–666.

Baas, J.H., Best, J.L., Peakall, J., and Wang, M., 2009, A phase diagram for turbulent, transitional and laminar clay suspension flows: Journal of Sedimentary Research, v. 79, p. 162–183,

Baas, J.H., Best, J.L., Peakall, J., 2011, Depositional processes, bedform development and hybrid bed formation in rapidly decelerated cohesive (mud-sand) sediment flows: Sedimentology, v. 58, p. 1953-1987.

Bagnold, R.A., 1954, Experiments on a gravity-free dispersion of large solid spheres in a Newtonian fluid under shear: Proceedings of the Royal Society of London, v. 225, p. 49-63.

Bagnold, R.A., 1962, Auto-suspension of transported sediment: turbidity currents: Proceedings of the Royal Society of London, v. 265, p. 315-319.

Barker, S.P., Haughton, P.D.W., McCaffrey, W.D., Archer, S.G., and Hakes, B., 2008, Development of rheological heterogeneity in clay-rich high-density turbidity currents: Aptian Britannia Sandstone Member, U.K., continental shelf: Journal of Sedimentary Research, v. 78, p. 45–68.

Barnes, N. E., and W. R. Normark, 1985, Diagnostic parameters for comparing modern submarine fans and ancient turbidite systems, in A. H. Bouma, W. R. Normark, and N. E.

Best, J.L., Kirkbride, A.D., and Peakall, J., 2001, Mean flow and turbulence structure of sediment-laden gravity currents: new insights using ultrasonic Doppler velocity profiling. In: Particulate Gravity Currents (Ids. W.D. McCaffrey, B.C. Kneller and J. Peakall), IAS Spec Publ., 31, p.159-172.

Bouma, A.H., 1962, Sedimentology of some Flysch deposits: A graphic approach to facies interpretation: Elsevier, 168 pp.

Bouma, A.H., 2000, Fine-grained, mud-rich turbidite systems: model and comparison with coarse-grained, sand-rich systems, in A. H. Bouma, and C. G. Stone, eds., Finegrained turbidite systems: AAPG Memoir 72/SEPM Special Publication No. 68, p. 9– 20.

Buckley, S., E. Schwarz, V. Terlaky, J. Howell, and R.W.C. Arnott, 2010, Combining aerial photogrammetry and terrestrial lidar for reservoir analog modeling: Photogrammetric Engineering and Remote Sensing, v. 76, p. 953–963.

Campbell, R.B., Mountjoy, E.W., and Young, F.G,. 1973, Geology of McBride map-area, British Columbia: Geological Survey of Canada, Paper 72–35, 104 p.

Cantero, M.I., Cantelli, A., Pirmez, C., Balachandar, S., Mohring, D., Hickson, T.A., Yeh, T., Naruse, H., Parker, G., 2012, Emplacement of massive trubidites linked to extinction of turbulence in turbidity currents: Nature Geoscience, v. 5, p. 42-45.

Charlesworth, H. A. K., J. L. Weiner, A. J. Akehurst, H. U. Bielenstein, C. R. Evans, R. E. Griffiths, D. B. Remington, M. R. Stauffer, and J. Steiner, 1967, Precambrian geology of the Jasper region, Alberta: Research Council of Alberta, Bulletin, v. 23, p. 74.

Coleman, J., and D. B. Prior, 1982, Deltaic environments, in P. A. Scholle, and D. Spearing, eds., Sandstone depositional environments, v. 139–178: AAPG Memoirs 31.

Colpron, M., Logan, J.M., and Mortensen, J.K., 2002, U-Pb zircon age constraint for late Neoproterozoic rifting and initiation of the lower Paleozoic passive margin of western Laurentia: Canadian Journal of Earth Sciences = Revue Canadienne des Sciences de la Terre, v. 39, p. 133–143.

Davis, L., 2010, Architecture of deep-marine interchannel deposits: Isaac Formation, Windermere Supergroup (Neoproterozoic), southern Canadian cordillera. M. Sc. Thesis, University of Ottawa.

Devlin, W. J., H. K. Brueckner, and G. C. Bond, 1988, New isotopic data and a preliminary age for volcanics near the base of the Windermere Supergroup, northeastern Washington, U.S.A: Canadian Journal of Earth Sciences = Revue Canadienne des Sciences de la Terre, v. 25, p. 1906–1911.

Drury, M.R. and J.L., Urai, 1990. Deformation-related recrystallization processes. *Tectonophysics*, *172*(3), pp.235-253.

English, M and R.W.C., Arnott, 2013. Lateral Facies Changes in Matrix - rich Sandstones, Upper Kaza Group, Windermere Supergroup, Cariboo Mountains, British Columbia, Canada

Fanning, C. M., and P. K. Link, 2004, U-Pb SHRIMP ages of Neoproterozoic (Sturtian) glaciogenic Pocatello Formation, southeastern Idaho: Geology, v. 32, p. 881–884.

Ferguson, C. F., 1994, Structural geology and stratigraphy of the northern Cariboo Mountains between Isaac Lake and Fraser River, British Columbia, Ph.D. thesis, University of Calgary, Calgary, 331 p.

Ferri, F., T. Hoy, and R. M. Friedman, 1999, Description, U-Pb age and tectonic setting of the Quesnel Lake Gneiss, east-central British Columbia: British Columbia Geological Survey Branch, Geological Fieldwork, Paper 1999–1, p. 69–80.

Flint, S.S., Hodgson, D.M., Sprague, A.R., Brunt, R.L., Van der Merwe, W.C., Figueiredo, J., Prelat, A., Box, D., Di Celma, C., and Kavanagh, J.P., 2011. Depositional architecture and sequence stratigraphy of the Karoo basin floor to shelf edge succession, Laingsburg depocentre, South Africa: Marine and Petroleum Geology, v. 28, p. 658-674.

Frenz, M., Wynn, R.B., Georgiopoulou, A., Bender, V.B., Hough, G., Masson, D.G., Talling, P.J., and Cronin, B.T., 2008, Unravelling turbidite basin fill complexity: a case study from the Late Quaternary turbidite fill of the Agadir Basin, offshore Atlantic Morocco: International Journal of Earth Sciences, v. 98, p. 721-733.

Gabrielse, H., and R. B. Campbell, 1991, Upper Proterozoic assemblages, in H. Gabrielse, and C. J. Yorath, eds., Geology of the Cordilleran orogen in Canada: Geological Society of America, Geology of North America, v. G-2, p. 125–150.

Gammon, P. R., R. W. C. Arnott, and G. M. Ross, 2007, Architectural relationship between channels, levees, and debris flows: Isaac Channel 6, Castle Creek South, lower Isaac Formation, Windermere Supergroup, British Columbia, Canada, in T. H. Nilsen, R. D. Shew, G. S. Steffens, and J. R. J. Studlik, eds., Atlas of deep-water outcrops AAPG Studies in Geology 56, p. 102–105.

Gerasimoff, M. D., 1988, The Hobson Lake pluton, Cariboo Mountains, British Columbia, and its significance to mesozoic and early Cenozoic Cordilleran tectonics: Master thesis, Queen's University, Kingston.

Google Earth, 2015, Castle Creek exposure locations. 10U 690462.73mE and 5876480.73mN. ©Cnes/Spot 2015, ©Province of British Columbia 2012, ©Google 2012. http://www.earth.google.com [September 25 2015]

Guibaudo, G., 1992, Subaqueous sediment gravity flow deposits: practical criteria for their field description and classification: Sedimentology, v. 39, p. 423-454.

Guillope, M. and Poirier, J.P., 1979. Dynamic recrystallization during creep of single-crystalline halite: An experimental study. *Journal of Geophysical Research: Solid Earth*, *84*(B10), pp.5557-5567.

Gutenberg, B. A., 1939, Tsunamis and earthquakes: Sismological Society of America Bulletin, v. 29, p. 517–526.

Hall, J.W., and Ewing, D., 2007, Three-dimensional turbulent wall jets issuing from moderate-aspect-ratio rectangular channels: AIAA Journal, v. 45, no. 6, p. 1177-1186
.

Haughton, P.D.W., Barker, S.P., McCaffrey, W.D., 2003, ‘Linked’ debrites in sand-rich turbidite systems – origin and significance: Sedimentology, v. 50, p. 459-482.

Haughton, P.D.W., Davis, C., McCaffrey, W., Barker, S., 2009, Hybrid sediment gravity flow deposits – Classification, origin and significance: Marine and Petroleum Geology, v. 26, p. 1900-1918.

Heezen, B. C., 1956, Corrientes de turbidez del Rio Magdelena: Sociedad Geografica de Columbia Bulletin, v. 51–52, p. 135–143.

Heezen, B.C., and Ewing, M., 1952, Turbidity currents and submarine slumps and the 1929 Grand Banks earthquake: American Journal of Science, v. 250, p. 849–873.

Hein, F. J., and M. E. McMechan, 1994, Proterozoic- Lower Cambrian strata of the Western Canada Sedimentary Basin, in G. D. Mossop and I. Shetsen, eds., Geological Atlas of the Western Canada Sedimentary Basin: Canadian Society of Petroleum Geologists and Alberta Geological Survey, Calgary, Alberta, p. 57–68.

Henkel, D. J., 1970, The role of waves in causing submarine landslides: Geotechnique, v. 20, p. 75–80.

Hiscott, R.N., 1994, Loss of capacity, not competence, as the fundamental process governing turbidity currents: Journal of Sedimentary Research, v. 64, p. 209-214.

Hodgson, D.M., 2009, Distribution and origin of hybrid beds in sand-rich submarine fans of the Tanqua depocentre, Karoo Basin, South Africa: Marine and Petroleum Geology, v. 26, p. 1940-1956.

Hodgson, D.M., Flint, S.S., Hodgetts, D., Drinkwater, N.J., Johannessen, E.J., and Luthi, S.M., 2006, Stratigraphic evolution of fine-grained submarine fan systems, Tanqua depocenter, Karoo Basin South Africa. Journal of Sedimentary Research, v. 76, p. 19-39.

Hogg, A.J., Huppert, H.E., and Dade, W.B., 1997, Erosion by planar turbulent wall jets: Journal of Fluid Mechanics, v. 338, p. 317-340.

Hsu, S.K., Kuo, J., Lo, C.L., Tsai, C.H., Doo, W.B., Ku, C.Y., and Sibuet, J.C., 2008, Turbidity currents, submarine landslides and the 2006 Pingtung Earthquake off SW Taiwan: Terr. Atmos. Ocean Sci., v. 19, p. 767-772.

Hubbard, S.M., Romans, B.W., Graham, S.A., 2008. Deep-water foreland basin deposits of the Cerro Toro Formation, Magallanes Basin, Chile: architectural elements of a sinuous basin axial channel belt: Sedimentology, v. 55, p. 1333-1359.

Jegou, I., Savoye, B., Pirmez, C., and Droz, L., 2008, Channel–mouth lobe complex of the recent Amazon Fan: the missing piece: Marine Geology, v. 252, p. 62–77.

Kane, I.A., Pontén, A.S.M., 2012, Submarine transitional flow deposits in the Paleogene Gulf of Mexico: Geology, v. 40, no. 12, p. 1119-1122.

Kane, I.A., 2010. Development and flow structures of sand injectites: The Hind Sandstone Member injectite complex, Carboniferous, UK. *Marine and Petroleum Geology*, *27*(6), pp.1200-1215.

Karlstrom, K. E., Ahall, K.-I., Harlan, S. S., Williams, M. L., McLelland, J. and Geissman, J. W., 2001, Long-lived (1.8–1.0 Ga) convergent orogen in southern Laurentia, its extensions to Australia and Baltica, and implications for refining Rodinia: Precambrian Research, v. 111, p. 5–30.

Kendall, B. S., Creasar, R.A., Ross, G.M., and Selby, D.S., 2004, Constraints on the timing of Marinoan “Snowball Earth” glaciation by 187Re–187Os dating of a Neoproterozoic, post-glacial black shale in western Canada: Earth and Planetary Science Letters, v. 222, p. 729–740.

Khan, Z.A., and Arnott, R.W.C., 2011, Stratal attributes and evolution of asymmetric inner- and outer-bend levee deposits associated with an ancient deep-water channel-levee complex within the Isaac Formation, southern Canada: Marine and Petroleum Geology, v. 28, p. 824-842.

Khripounoff, A., Vangriesheim, A., Babonneau, N., Crassous, P., Dennielou, B., and Savoye, B., 2003, Direct observation of intense turbidity current activity in the Zaire submarine valley at 4000 m water depth: Marine Geology, v. 194, p. 151–158.

Kneller, B., and Branney, M.J., 1995, Sustained high-density turbidity currents and deposition of thick massive sands: Sedimentology, v. 42, p. 607-616.

Kostic, S., Sequeiros, O., Spinewine, B., Parker, G., 2010, Cyclic steps: A phenomenon of supercritical shallow flow from the high mountains to the bottom of the ocean: Journal of Hydro-environmental Research, v. 3, p. 167-172.

Laurin, J., K. Wallace, R. W. C. Arnott, and E. Schwarz, 2007, Stratigraphic anatomy and depositional history of a mass-transport complex, Isaac Formation, Windermere Supergroup, British Columbia, Canada, in T. H. Nilsen, R. D. Shew, G. S. Steffens, and J. R. J. Studlik, eds., Atlas of deep-water outcrops: AAPG Studies in Geology 56, p. 119–122.

Leclair, S.F., and Arnott, R.W.C., 2003, Coarse-tail graded, structureless strata: indicators of an internal hydraulic jump: *in* Roberts, H.H., Rosen, N.C., Filion, R.H., and Anderson, J.B., eds., Shelf Margin Deltas and Linked Down Slope Petroleum Systems: Global Significance and Future Exploration Potential: SEPM, Gulf Coast Section, Houston, p. 817–836.

Leclair, S.F., and Arnott, R.W.C., 2005, Parallel lamination formed by high-density turbidity currents: Journal of Sedimentary Research, v. 75, p. 1–5.

Li, Z.X., Evans, D.A. and Halverson, G.P., 2013. Neoproterozoic glaciations in a revised global palaeogeography from the breakup of Rodinia to the assembly of Gondwanaland. *Sedimentary Geology*, *294*, pp.219-232.

Link, P.K., 1993, Middle and late Proterozoic stratified rocks in the western U.S. Cordillera, Colorado Plateau, and Basin and Range Province, *in* J.C. Reed, Jr. M.E. Bickford, R.S. Houston, P.K. Link, D.W. Rankin, P.K. Sims, and W.R. Van Schmus, eds., Precambrian: Conterminous U.S., The Geology of North America: Geological Society of America Decade of North American Geology Series, v. c-3, p. 474-690.

Lowe, D.R., 1975, Water escape structures in coarse-grained sediments: Sedimentology, v. 22, p. 157-204.

Lowe, D.R., 1979, Sediment gravity flows: their classification and some problems of application to natural flows and deposits: Soc. Econ. Paleontologists Mineralogists Spec. Pub. 27, p. 75-82.

Lowe, D.R., 1982, Sediment gravity flows: II. Depositional models with special reference to the deposits of high-density turbidity currents: Journal of Sedimentary Petrology, v. 52, p. 279-297.

Lowe,D.R., Guy, M., 2000, Slurry-flow deposits in the Britannia Formation (Lower Cretaceous), North Sea: a new perspective on the turbidity current and debris flow problem: Sedimentology, v. 47, p. 31-70.

Lowe, D.R., Guy, M., Palfrey, A., 2003, Facies of slurry-flow deposits, Britannia Formation (Lower Cretaceous), North Sea: implications for flow evolution and deposit geometry: Sedimentology, v. 50, p. 45-80.

Lund, K., Aleinikoff, J.N., Evans, K.V., and Fanning, C.M., 2003, SHRIMP U-Pb geochronology of Neoproterozoic Windermere Supergroup, central Idaho: Implications for rifting of western Laurentia and synchroneity of Sturtian glacial deposits: Geological Society of America Bulletin, v. 115, p. 349–372.

Maier, K.L., Fildani, A., Paull, C.K., Graham, S.A., McHargue, T.R., Caress, D.W., and McGann, M., 2011, The elusive character of discontinuous deep-water channels: New insights from Lucia Chica channel system, offshore California: Geology, v. 39, p. 327-330.

McDonough, M. R., 1989, Stratigraphy and structure of the Late Proterozoic Miette Group, northern Selwyn Range, Rocky Mountains, British Columbia, Ph.D. thesis, University of Calgary, Calgary, 290 p.

McKee, E.D., and Weir, G.W., 1953, Terminology for stratification and cross-stratification in sedimentary rocks: Geological Society of America Bulletin, v. 64, p. 381-390.

Menard, H. W., 1955, Deep-sea channels, topography, and sedimentation: AAPG Bulletin, v. 39, p. 236–255.

Meyer, L., 2004, Internal architecture of an ancient deep-water, passive margin, basin-floor fan system, Upper Kaza Group, Windermere Supergroup, Castle Creek, British Columbia: M.Sc. thesis, University of Calgary, Calgary, 175 p

Miall, A.D., 1985, Architectural-element analysis: A new method of facies analysis applied to fluvial deposits: Earth-Science Reviews, v. 22, p. 261–308.

Middleton, G.V., and Hampton, M.A., 1973, Sediment gravity flows: mechanics of flow and deposition. In: Turbidity and Deep Water Sedimentation (Eds G.V. Middleton and A.H. Bouma), SEPM, Pacific Section, Short Course Lecture Notes, 1-38.

Middleton, G.V., Hampton, M.A., 1976, Subaqueous sediment transport and deposition by sediment gravity flows: In: Marine Sediment Transport and Environmental Management (Eds D.J. Stanley and D.J.P. Swift), p. 197-218, Wiley, New York.

Mulder, T., and Alexander, J., 2001, The physical character of subaqueous density flows and their deposits: Sedimentology, v. 48, no. 2, p. 269-299.

Mulder, T., and Etienne, S., 2010, Lobes in deep-sea turbidite systmems: State of the art: Sedimentary Geology, v. 229, p. 75-80.

Murphy, D. C., 1987a, Suprastructure/infrastructure transition, east-central Cariboo Mountains, British Columbia; geometry, kinematics and tectonic implications: Journal of Structural Geology, v. 9, p. 13–29.

Murphy, D. C., 1987b, Kaza Group, eastern Wells Gray Park, British Columbia: Geological Survey of Canada Paper 87–1A, p. 735–742.

Murphy, D. C., and C. J. Rees, 1983, Structural transition and stratigraphy in the Cariboo Mountains, British Columbia: Geological Survey of Canada Paper 83–1A, p. 245–252.

Mussa-Caleca, M., 2008, Architecture and depositional history of a Neoproterozoic deepwater slope channel complex in a passive margin setting: Isaac Formation, Windermere Supergroup, southern Canadian Cordillera: M.Sc. thesis, University of Ottawa, Ottawa, 128 p..

Mutti, E., and W. R. Normark, 1987, Comparing examples of modern and ancient turbidite systems: problems and concepts, in J. R. Leggett, and G. G. Zuffa, eds., Marine Clastic Sedimentology: Concepts and Case Studies: London, Graham and Trotman, p. 1–37.

Navarro, L., 2006, Depositional architecture and evolution of deep-water base-of-slope and slope channel complexes in a passive margin setting: Isaac Formation, Windermere Supergroup (Neoproterozoic) southern Canadian Cordillera: M.Sc. thesis, University of Ottawa, Ottawa, 272 p.

Navarro, L., Khan Z., and Arnott, R.W.C., 2007, Architecture of a deep-water channel levee complex: Channel 3, Castle Creek South, Isaac Formation, Windermere Supergroup, Bristish Columbia, Canada, in T. H. Nilsen, R. D. Shew, G. S. Steffens, and J. R. J. Studlik, eds., Atlas of deep-water outcrops: AAPG Studies in Geology 56, p. 93–96.

Parrish, R., and R. L. Armstrong, 1983, U-pb zircon age and tectonic significance of gneisses in structural culminations of the Omineca crystalline belt, British Columbia; the Geological Society of America,

Parsons, J.D., Schweller, W.J., Stelting, C.W., Southard, J.B., Lyons, W.J., and Grotzinger, J.P., 2002, A preliminary experimental study of turbidite fan deposits: Journal of Sedimentary Research, v. 72, no. 5, p. 619-628.

Piper, D.J.W., Cochonat, P., and Morrison, M.L., 1999a. The sequence of events around the epicenter of the 1929 Grand Banks earth- quake: initiation of debris flows and turbidity current inferred from sidescan sonar: Sedimentology, v. 46, p.79–97.

Piper, D.J.W., Hiscott, R.N., and Normark, W.R., 1999b, Outcrop- scale acoustic facies analysis and latest Quaternary development of Hueneme and Dume submarine fans, offshore California: Sedimentology, v. 46, p. 47-78.

Piper, D.J.W., Normark, W.R., 2001, Sandy fans – from Amazon to Huemene and beyond: American Association of Petroleum Geologists Bulletin, v. 85, no. 8, p. 1407-1438.

Pickering, K.T., Hiscott, R.N. and Hein, F.J., 1989, Deep Marine Environments: Clastic Sedimentation and Tectonics. Unwin Hyman, London, 416 pp.

Price, R. A., 2000, The southern Canadian Rockies: evolution of a foreland thrust and fold belt: GeoCanada 2000, Field Trip Guidebook 13, 244 p.

Posamentier, H.W., and Kolla, V., 2003, Seismic geomorphology and stratigraphy of depositional elements in deep-water settings: Journal of Sedimentary Research, v. 73, no. 3, p. 367-388.

Posamentier, H.W., and Walker, R.G., 2007. Deep water turbidites and submarine fans. In Posamentier, H.W., and Walker, R.G., eds., Facies Models Revisited, SEPM Special Publication No. 84, p. 399-520.

Posamentier, H.W., Erskine, R.D., and Mitchum, R.M., JR., 1991, Models for submarine fan deposition within a sequence stratigraphic framework, *in* Weimer, P., and Link, M.H., eds., Seismic Facies and Sedimentary Processes of Submarine Fans and Turbidite Systems: New York, Springer-Verlag, p. 127–136.

Posamentier, H.W., Jervey, M.T., and Vail, P.R., 1988, Eustatic controls on clastic deposition I—conceptual framework, *in* Wilgus, C.K., Hastings, B.S., Kendall, C.G.St.C., Posamentier, H.W., Ross, C.A., and Van Wagoner, J.C., eds., Sea Level Changes: An Integrated Approach: SEPM, Special Publication 42, p. 109–124.

Postma, G., Nemec, W., and Kleinspehn, K.L., 1988, Large floating clasts in turbidites: a mechanism for their emplacement: Sedimentary Geology, v. 58, p. 47-61.

Powers, D.W., and Easterling, R.G., 1982, Improved methodology for using embedded Markov chains to describe cyclical sediments: Journal of Sedimentary Petrology, v. 52, p. 913-923.

Prélat, A., Hodgson, D.M., and Flint, S.S., 2009, Evolution, architecture and hierarchy of distributary deep-water deposits: a high-resolution outcrop investigation from the Permian Karoo Basin, South Africa: Sedimentology, v. 56, p. 2132-2154.

Prélat, A., Covault, J.A., Hodgson, D.M., Fildani, A., and Flint, S.S., 2010, Intrinsic controls on the range of volumes, morphologies, and dimensions of submarine lobes: Sedimentary Geology, v. 232, p. 66-76.

Privett, K., 2008, Architecture and depositional history of a Neoproterozoic depositional lobe in a passive margin setting, Lower Kaza Group, Windermere Supergroup, southern Canadian Cordillera, 68 p. + CD. B. Sc. Honours Thesis, University of Ottawa.

Pyles, D.R., 2007, Architectural elements in a ponded submarine fan, Carboniferous Ross Sandstone, western Ireland. *In*: Nilsen, T.H., Shew, R.D., Steffens, G.S., Studlick, J.R.J. (Eds.), Atlas of Deepwater Outcrops. American Association of Petroleum Geologists Studies in Geology, v. 56, p. 19.

Pyles, D.R., 2008, Multiscale stratigraphic analysis of a structurally confined submarine fan: Carboniferous Ross Sandstone, Ireland: AAPG Bulletin, v. 92, p. 557–587.

Pyles, D.R., and Jennette, D.C., 2009, Geometry and architectural associations of co-genetic debrite–turbidite beds in basin-margin strata, Carboniferous Ross Sandstone (Ireland): Applications to reservoirs located on the margins of structurally confined submarine fans: Marine and Petroleum Geology, v. 62, p. 1974-1996.

Pyles, D.R., Syvitski, J.P.M., and Slatt, R.M., 2011, Defining the concept of stratigraphic grade and applying it to stratal (reservoir) architecture and evolution of the slope-to-basin profile: An outcrop perspective: Marine and Petroleum Geology, v. 28, p. 675-697.

Reading, H. G., and M. Richards, 1994, Turbidite systems in deep-water basin margins classified by grain size and feeder system: AAPG Bulletin, v. 78, p. 792–822.

Reesor, J. E., 1973, Geology of the Lardeau map-area, east-half, British Columbia: Geological Survey of Canada Memoir 369, 129 p.

Reid, L.F., 2003, Stratigraphy, structure, petrology, geochronology and geochemistry of the Hobson Lake area (Cariboo Mountains, British Columbia) in relation to the tectonic evolution of the southern Canadian Cordillera: Doctoral thesis, University of Calgary, Calgary, 221 p.

Reid, L.F., P.S. Simony, and G.M. Ross, 2002, Dextral strike-slip faulting in the Cariboo Mountains, British Columbia: a natural example of wrench tectonics in relation to Cordilleran tectonics: Canadian Journal of Earth Sciences = Revue Canadienne des Sciences de la Terre, v. 39, p. 953–970.

Rocheleau, J., 2011, Depositional architecture of a near-slope turbidite succession: Upper Kaza Group, Windermerer Supergroup, Castle Creek, British Columbia, Canada: Masters thesis, University of Ottawa, Ottawa, 94 p.

Ross, G.M., 2001, The Neoproterozoic Windermere Supergroup: An on-land continental margin turbidite system: Geological Survey of Canada Open File 3932, 2 sheets.

Ross, G.M., and D.C. Murphy, 1988, Transgressive stratigraphy, anoxia, and regional correlations within the late Precambrian Windermere grit of the southern Canadian Cordillera: Geology, v. 16, p. 139–143.

Ross, G.M., and S.A. Bowring, 1990, Detrital zircon geochronology of the Windermere Supergroup and the tectonic assembly of the southern Canadian Cordillera: Journal of Geology, v. 98, p. 879–893.

Ross, G.M., and R.R. Parrish, 1991, Detrital zircon geochronology of metasedimentary rocks in the southern Omineca Belt, Canadian Cordillera: Canadian Journal of Earth Sciences = Revue Canadienne des Sciences de la Terre, v. 28, p. 1254–1270.

Ross, G.M., and Ferguson, C.A., 2003, Geology and structure cross-sections, Eddy, British Columbia; Geological Survey of Canada, “A” Series Map, 1967A, scale 1:50,000, 1 sheet.

Ross, G.M., and Arnott, R.W.C., 2007, Regional Geology of the Windermere Supergroup, southern Canadian cordillera and Stratigraphic Setting of the Castle Creek Study Area, in T. H. Nilsen, R. D. Shew, G. S. Steffens, and J. R. J. Studlick, eds., Atlas of Deep- Water Outcrops: AAPG Studies in Geology 56.

Ross, G.M., McMechan, M.E., and Hein, F.J., 1989, Proterozoic history: birth of the miogeocline, in B. D. Ricketts, ed., The western Canada sedimentary basin: Canadian Society of Petroleum Geologists, p. 79–104.

Ross, G.M., Bloch, J.D., Krouse, H.R., 1995, Neoproterozoic strata of the southern Canadian Cordillera and the isotopic evolution of seawater sulfate: Precambrian Research, v. 73, p. 71-99.

Rothwell, R.G., Thomson, J., and Kahler, G., 1998, Low-sealevel emplacement of a very lare Late Pleistocene ‘megaturbidite’ in the western Mediterranean Sea: Nature, v. 392, p. 377-380.

Schwarz, E., and R. W. C. Arnott, 2007a, Anatomy and evolution of a slope channelcomplex set (Neoproterozoic Isaac Formation, Windermere Supergroup, southern Canadian Cordillera): implications for reservoir characterization: Journal of Sedimentary Research, v. 77, p. 89–109.

Schwarz, E., and Arnott, R.W.C., 2007b, Anatomy and evolution of a slope channelcomplex set (Neoproterozoic Isaac Formation, Windermere Supergroup, southern Canadian Cordillera): implications for reservoir characterization: Journal of Sedimentary Research, v. 77, p. 89–109

Sedláček, R., Blum, W., Kratochvil, J., and Forest, S. (2002). Subgrain formation during deformation: physical origin and consequences. Metallurgical and Materials Transactions A, 33(2), 319-327.

Shanmugam, G., 2006, Deep-water processes and facies models: Implications for sandstone petroleum reservoirs: New York, Elsevier, 476 p.

Shanmugam, G., and R. J. Moiola, 1988, Submarine fans: characteristics, models, classification, and reservoir potential: Earth-Science Reviews, v. 24, p. 383–428.

Sinclair, H.D., and Tomasso, M., 2002, Depositional evolution of confined turbidite basins: Journal of Sedimentary Research, v. 72, p. 451-456.

Smith, M.D., 2009, Stratigraphic and geochemical evolution of the Old Fort Point Fm., southern Canadian Cordillera: the deep-marine perspective of Ediacaran post-glacial environmental change. Ph. D. Thesis, University of Ottawa.

Smith, M.D., Arnaud, E., Arnott, R.W.C., and Ross, G.M., 2012, The record of Neoproterozoic glaciations in the Windermere Supergroup, southern Canadian Cordillera, In: The Geological Record of Neoproterozoic Glaciations (eds. Arnaud, E., Halverson, G.P., Shields-Zhou, G.), Geological Society Memoir no. 36., 752 pp.

Stipp, M., StuÈnitz, H., Heilbronner, R., and Schmid, S. M. (2002). The eastern Tonale fault zone: a ‘natural laboratory’for crystal plastic deformation of quartz over a temperature range from 250 to 700 C. Journal of Structural Geology, 24(12), 1861-1884

Stow, D.A.V., and Johansson, M., 2000, Deep-water massive sands: nature, origin and hydrocarbon implications: Marine and Petroleum Geology, v. 17, p. 145-174.

Stow, D.A.V., and M. Mayall, 2000, Deep-water sedimentary systems: new models for the 21st century: Marine and Petroleum Geology, v. 17, p. 125–135.

Sumner, E., Amy, L., and Talling, P.J., 2008, Deposit structure and processes of sand deposition from a decelerating sediment suspension: Journal of Sedimentary Research, v. 78, p. 529 - 547.

Sumner, E.J., Talling, P.J., and Amy, L.A., 2009, Deposits of flows transitional between turbidity current and debris flow: Geology, v. 37, p. 991–994.

Sylvester, Z., Lowe, D.R., 2004, Textural trends in turbidites and slurry beds from the Oligocene flysch of the East Carpathians, Romania: Sedimentology, v. 51, p. 945-972.

Talling, P.J., 2013, Hybrid submarine flows comprising turbidity current and cohesive debris flow: Deposits, theoretical and experimental analyses, and generalized models: Geosphere, v. 9, p. 460-488

Talling, P.J., Amy, L.A., Wynn, R.B., Peakall, J., and Robinson, M., 2004, Beds comprising debrite sandwiched within cogenetic turbidite: origin and widespread occurrence in distal depositional environments, Sedimentology, v. 51, p163-194.

Talling, P.J., Wynn, R.B., Masson, D.G., Frenz, M., Cronin, B.T., Schiebel, R., Akhmetzhanov, A.M., Dallmeier-Tiessen, S., Benetti, S., Weaver, P.P.E., Georgiopoilou, A., Zuhlsdorff, C., and Amy, L.A., 2007, Onset of submarine debris flow deposition far from original giant landslide: Nature, v. 450, p. 541-544.

Talling, P.J., Masson, D.G., Sumner, E.J., and Malgesini, G., 2012, Subaqueous sediment density flows: Depositional processes and deposit types: Sedimentology, v. 59, p. 1937-2003.

Terlaky, V., 2014. Sedimentology, Stratigraphy, Architecture and Origin of Deep-water, Basin-floor Deposits: Middle and Upper Kaza Group, Windermere Supergroup, BC, Canada.

Terlaky, V. and Arnott, R.W.C., 2014. Matrix- rich and associated matrix- poor sandstones: Avulsion splays in slope and basin- floor strata. *Sedimentology*,*61*(5), pp.1175-1197.

Terlaky, V. and Arnott, R.W.C., Matrix-Rich Sandstones: Indicators Of Local Sedimentation Activation In Slope And Basin-Floor Strata.

Tilston, M., Arnott, R.W.C., Rennie, C.D. and Long, B., 2015. The influence of grain size on the velocity and sediment concentration profiles and depositional record of turbidity currents. *Geology*, *43*(9), pp.839-842.

Walker, R.G., 1978, Deep-water sandstone facies and ancient submarine fans: models for exploration for stratigraphic traps: AAPG Bulletin, v. 62, p. 932–966.

Urai, J. L., Means, W. D., and Lister, G. S. (1986). Dynamic Recrystallization of Minerals. Mineral and Rock Deformation: Laboratory Studies: The Paterson Volume, 161-199.

Vernon, R. H. (2004). Chapter 5: Microstructures of deformed rocks in A practical guide to rock microstructure. Cambridge University Press, 295-345.

Appendix A: Stratigraphic Correlation Panels

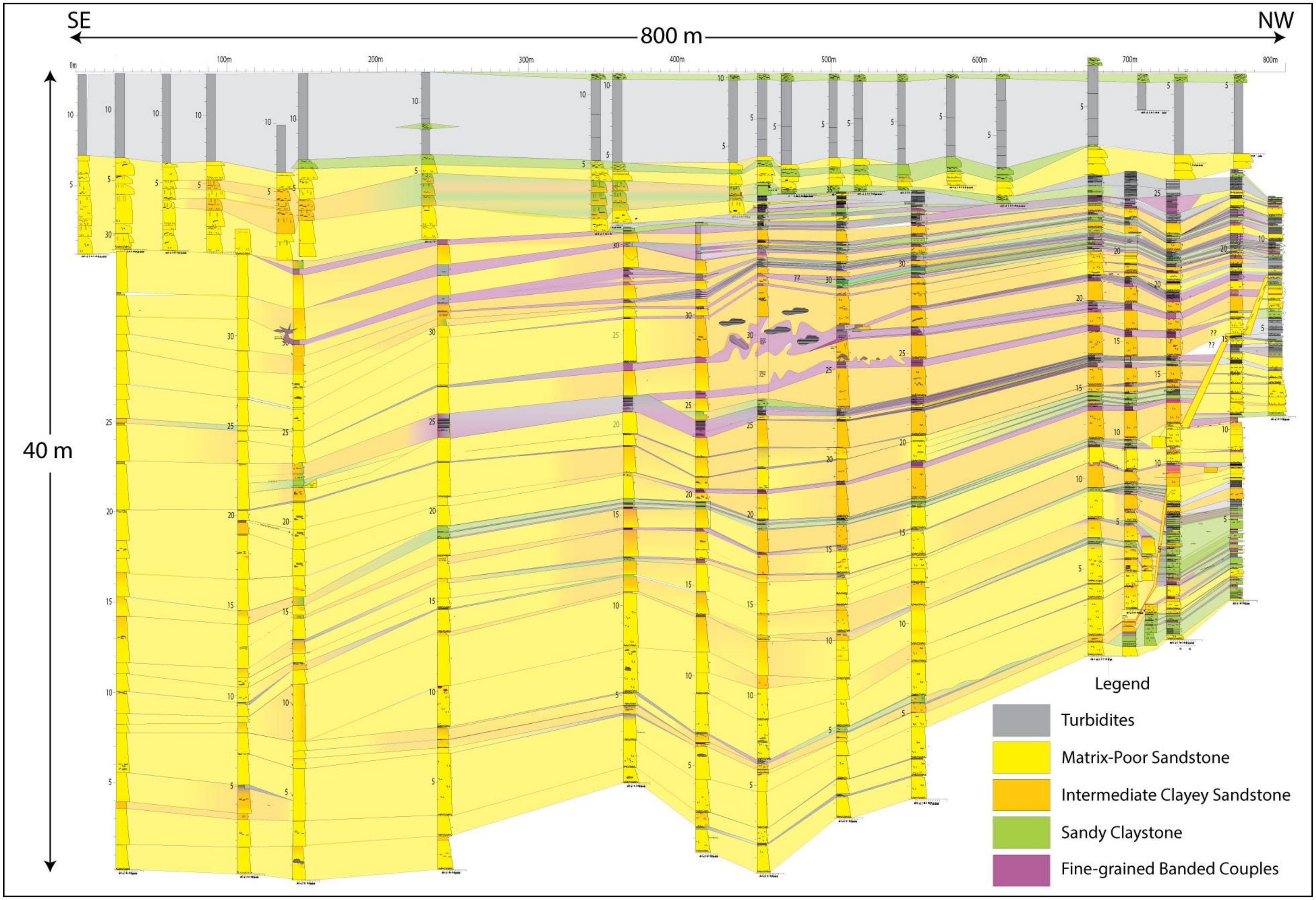

Correlation 1: Stratigraphic correlation panel of the entire study area. The upper 10 m is a section that was studied by English (2013) and the top of the thick unit of thin-bedded turbidites at the top of this section is used as the stratigraphic datum

Appendix B: Data from Petrographic Analysis

This flow chart could be used as an aid while point-counting by addressing each question in the grey boxes for each sample.

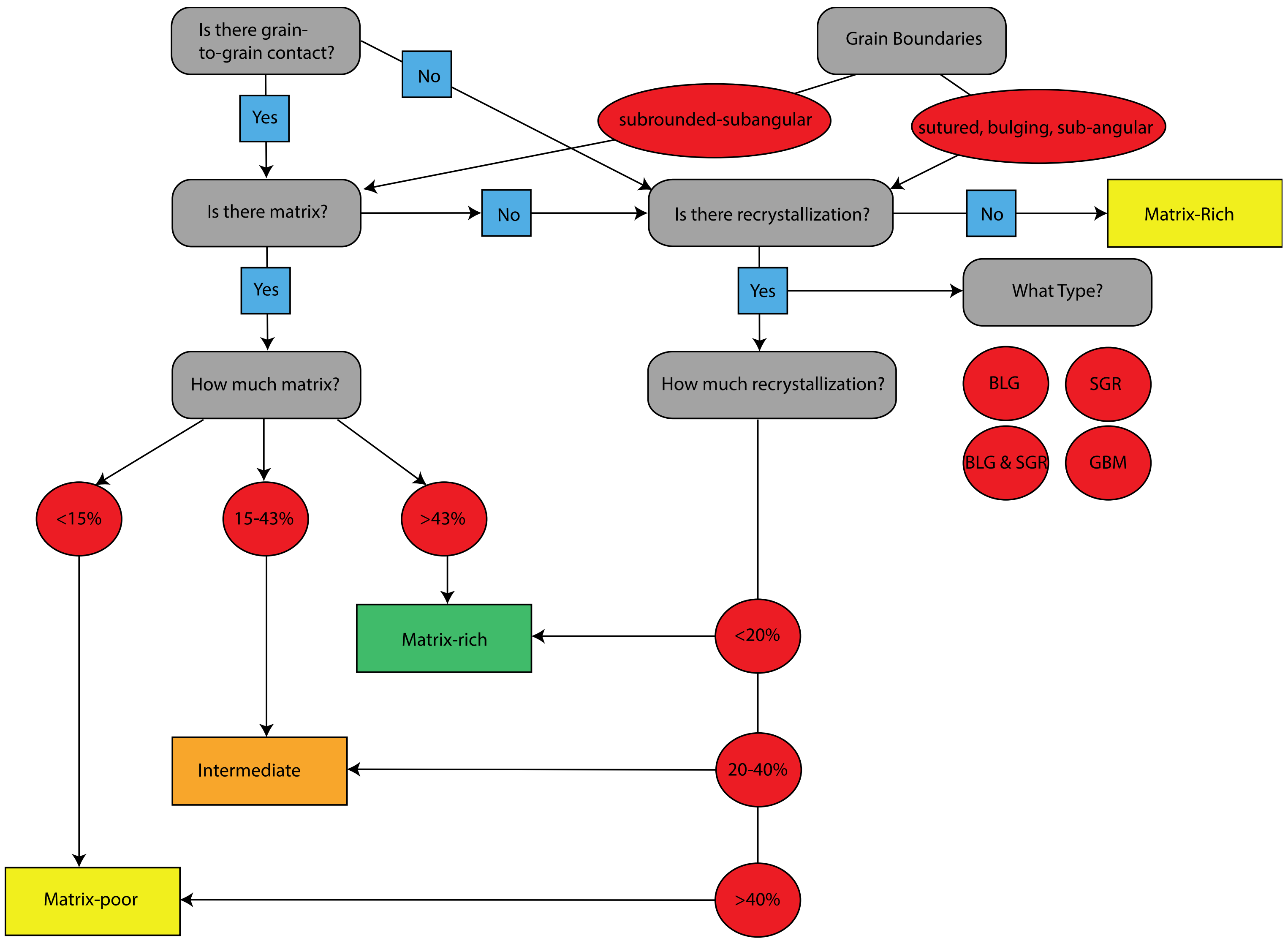

PETROGRAPHY AND POINT-COUNTING

	FRAMEWORK GRAINS			MATRIX		RECOVERY		CEMENT	TOTAL	GRAIN SIZE (mm)			SORTING	FACIES	NOTES
SAMPLE	Q	F	L/O	Q_S	M_R	SG	RX	C	T	MX	MN	AV	S/R	F	N
S6-2012	196	18	0	6	38	105	98	6	467	1.6	0.02	0.24	moderate sorting; subangular/rounded	Matrix-poor Sandstone	grain to grain contacts; minor matrix
	46%			9%		43%		1%	100%	vcu	ms	fu			
S1-2012	215	9	0	7	37	132	68	11	479	1.2	0.03	0.31	moderate to poor	Matrix-poor Sandstone	
	47%			9%		42%		2%	100%	vcl	cs	ml			
S9-2012	241	12	3	0	57	134	52	2	501	0.5	0.02	0.14	moderate sorting	Matrix-poor Sandstone	
	51%			12%		33%		0%	96%	cl	ms	fl			
S11-2-2012	228	24	8	0	33	123	86	0	502	2.1	0.01	0.33	poorly sorted	Matrix-poor Sandstone	minor matrix
	52%			7%		42%		0%	100%	gr	fs	ml			
S16-2012	344	18	3	0	12	114	61	0	552	0.9	0.03	0.22	poorly sorted; sub-rounded	Matrix-poor Sandstone	minor to rare matrix; grain to grain contacts
	66%			2%		32%		0%	100%	cu	ms	fu			
S21-2012	248	11	1	0	52	78	42	3	435	1.2	0.02	0.19	monderatley sorted; sub-rounded	Matrix-poor Sandstone	
	60%			12%		28%		1%	100%	vcl	ms	fu			
S23-2012	233	15	4	0	41	117	67	0	477	0.9	0.02	0.17	moderatley sorted; subrounded	Matrix-poor Sandstone	visually dominated by ≥0.5mm Q grains
	53%			9%		25%		0%	86%	cu	ms	fl			
S2B-2012	161	6	10	80	160	2	3	0	422	0.6	0.04	0.2	subrounded-rounded ; moderate to well sorted	Matrix-rich Sandy Claystone	clear matrix/floating grains.
	42%			57%		1%		0%	100%	cl	cs	fu			
S3B-2012	125	5	15	95	70	0	5	0	315	1.1	0.02	0.19	moderate sorting	Matrix-rich Sandy Claystone	much more concentrated/Q grains <1mm; only 4 quadrants
	46%			52%		2%		0%	100%	vcl	fs	fu			
S3T-2012	236	14	11	160	112	0	8	0	541	0.6	0.02	0.14	moderatley sorted; subrounded	Matrix-rich Sandy Claystone	grades/fines upwards...@top Qgrains <1mm
	48%			50%		1%		0%	100%	cl	ms	fl			
S5B-2012	213	21	10	115	165	0	0	0	524	0.6	0.04	0.17	sub-angular; poorly sorted	Matrix-rich Sandy Claystone	upwards becomes better sorted and fines; more porous
	47%			53%		0%		0%	100%	cl	cs	fu			
S5M-2012	165	14	16	85	117	0	4	0	401				sub -angular; moderatly to poorly sorted	Matrix-rich Sandy Claystone	
	49%			50%		1%		0%	100%						
S5T-2012	Cap is stratified; grades from vfg to silt/mud. Abrupt contact and fine sequence repeats.									0.1	0.01	0.05			
										vfu	fs	cs			
S7B-2012	73	3	3	13	103	0	0	0	195	1.1	0.05	0.22	poorly sorted; sub-rounded to	Matrix-rich Sandy	3 clasts cutting across slide;only 3 quadrants;
	41%			59%		0%		0%	100%	vcl	cs	fu			

gr=granules; vcu=very coarse upper; vcl=very coarse lower; cu=coarse upper; cl=coarse lower; mu=medium upper; ml=medium lower; fu=fine upper; fl=fine lower; vfu=very fine upper; vfl=very fine lower; cs=coarse silt; ms=medium silt; fs=fine silt

PETROGRAPHY AND POINT-COUNTING

	FRAMEWORK GRAINS			MATRIX		RECOVERY		CEMENT	TOTAL	GRAIN SIZE (mm)			SORTING	FACIES	NOTES
SAMPLE	Q	F	L/O	Q_S	M_R	SG	RX	C	T	MX	MN	AV	S/R	F	N
S7M-2012	209	11	14	18	227	0	0	0	479	0.7	0.04	0.18	sub-angular; poorly sorted	Matrix-rich Sandy Claystone	
	49%			51%		0%		0%	100%	cu	cs	fu			
S7T-2012	Cap is banded; mud/silt then abrupt contact f-vf sand w matrix overlain by mud/silt layer														
S8B-2012	252	17	8	157	41	0	0	0	475	1.3	0.05	0.24	sub-angular; moderately sorted	Intermediate Clayey Sandstone	grey/black "matrix"; looks like silt/crushed quartz? Subgrains?
	58%			42%		0%		0%	100%	vcl	cs	fu			
S8M-2012	238	7	5	119	36	0	0	6	411	0.9	0.03	0.19	sub-angular; moderately sorted	Intermediate Clayey Sandstone	grey/black "matrix"; abundant SG
	61%			38%		0%		1%	100%	cu	ms	fu			
S8T-2012	109	2	5	0	57	0	0	0	173					Intermediate Clayey Sandstone	only 2 quadrants due to clasts; fines upwards; dispersed .08-.120mm
	67%			33%		0%		0%	100%						
S10B-2012	161	5	5	4	150	0	0	2	327	0.7	0.02	0.2	sub-rounded; poorly-sorted	Matrix-rich Sandy Claystone	4 quadrants; very clear matrix
	52%			47%		0%		1%	100%	cl	ms	fu			
S10M-2012	79	3	4	4	56	0	0	1	147				sub-rounded; poorly-sorted	Matrix-rich Sandy Claystone	4 quadrants;
	59%			41%		0%		1%	100%						
S10T-2012	banded top' ml to vfl @ base, grades upwards to silt-silty/mud; overlain by vfg layer grades up to silty/mud x2														
S12B-2012	294	17	4	3	59	18	0	2	397	1.4	0.02	0.21	sub-angular; poorly sorted	Intermediate Clayey Sandstone	larger Q grains (≥1mm); visually less matrix; few 'bulging' Q grains
	79%			16%		5%		1%	100%	vcu	ms	fu			
S12M-2012	264	12	5	15	93	25	0	19	433	1.1	0.03	0.22	sub-rounded to sub-angular; moderately sorted	Intermediate Clayey Sandstone	finer than below (Q grains ≤1mm); bulging SG; towards top of slide=much cleaner
	65%			25%		6%		4%	100%	vcl	ms	fu			
S12T-2012	257	17	5	23	110	93	42	3	550	0.7	0.01	0.2	sub-rounded to sub-angular; moderately sorted	Intermediate Clayey Sandstone	dirty becomes cleaner towards the top; abundant vf-fl Q grains; abundant SG and bulging; middle of slide = 2 streaks of RXC;
	51%			24%		25%		1%	100%	cu	fs	fu			

gr=granules; vcu=very coarse upper; vcl=very coarse lower; cu=coarse upper; cl=coarse lower; mu=medium upper; ml=medium lower; fu=fine upper; fl=fine lower; vfu=very fine upper; vfl=very fine lower; cs=coarse silt; ms=medium silt; fs=fine silt

PETROGRAPHY AND POINT-COUNTING

	FRAMEWORK GRAINS			MATRIX		RECOVERY		CEMENT	TOTAL	GRAIN SIZE (mm)			SORTING	FACIES	NOTES
SAMPLE	Q	F	L/O	Q_S	M_R	SG	RX	C	T	MX	MN	AV	S/R	F	N
S13B-2012	148	3	5	60	149	20	15	3	403	0.9	0.04	0.22	sub-angular; poorly sorted	Matrix-rich Sandy Claystone	very close to being a classic waft; grains floating in places; some bulging; 5 quadrants; may be secondary matrix.
	39%			52%		9%		1%	100%	cu	cs	fu			
S13T-2012	34	1	0	19	31	2	0	0	87	0.1	0.02	0.07		Matrix-rich Sandy Claystone	1 quadrant (bottom L): m-vfg w matrix; rest of slide = silt/mud matrix with rare dispersed vfg-f grains
	40%			57%		2%		0%	100%	fl	ms	vfl			
S14B-2012	279	17	12	28	87	41	41	0	505	0.6	0.02	0.15	angular to sub-angular; poorly sorted	Intermediate Clayey Sandstone	abundant ≤0.5 Q grains; visually less matrix
	61%			23%		16%		0%	100%	cl	ms	fl			
S14T-2012	309	13	11	41	101	60	10	0	545	0.9	0.03	0.17	sub-angular; poorly sorted	Intermediate Clayey Sandstone	same as S14B-2012; dirty; abundant small grains...depo setting/flow rheology?
	61%			26%		13%		0%	100%	cu	ms	fl			
S15-2012	254	20	5	26	49	130	12	0	496	1.1	0.01	0.18	sub-rounded to sub-angular; poorly sorted	Intermediate Clayey Sandstone	minor matrix; abundant vfg straind/SG; some bulging; few pore holes
	56%			15%		29%		0%	100%	vcl	fs	fu			
S17B-2012	235	10	3	15	61	161	39	19	543	1.1	0.01	0.17	brounded; poorly sorte	Intermediate Clayey Sandstone	poorly sorted; abundant subgrains; minor matrix; towards top = bit cleaner; minor bulging
	46%			14%		37%		3%	100%	vcl	fs	fl			
S17M-2012	263	5	4	21	68	187	25	2	575	1.4	0.01	0.16	brounded; poorly sorte	Intermediate Clayey Sandstone	few patches of crc/iron oxide cement; very 'dirty' w abundant SG (smiliar to S17B-
	47%			15%		37%		0%	100%	vcu	fs	fl			
S17T-2012	222	12	4	15	68	187	43	3	554	1	0.02	0.2	sub-rounded; poorly sorted	Intermediate Clayey Sandstone	streak of RXC Q across slide.
	43%			15%		42%		1%	100%	cu	ms	fu			
S18B-2012	289	14	1	11	52	129	0	88	584	0.6	0.02	0.15	well sorted; sub-rounded	Matrix-poor Sandstone	crc/iron oxide cement concentration in the bottom 1/3 of slide; minor/rare
	52%			11%		22%		15%	100%	cl	ms	fl			

gr=granules; vcu=very coarse upper; vcl=very coarse lower; cu=coarse upper; cl=coarse lower; mu=medium upper; ml=medium lower; fu=fine upper; fl=fine lower; vfu=very fine upper; vfl=very fine lower; cs=coarse silt; ms=medium silt; fs=fine silt

PETROGRAPHY AND POINT-COUNTING

	FRAMEWORK GRAINS			MATRIX		RECOVERY		CEMENT	TOTAL	GRAIN SIZE (mm)			SORTING	FACIES	NOTES
SAMPLE	Q	F	L/O	Q_S	M_R	SG	RX	C	T	MX	MN	AV	S/R	F	N
S18M-2012	254	14	6	15	52	163	15	3	522	1.7	0.03	0.2	well-sorted; sub-rounded	Matrix-poor Sandstone	similar to S18B-2012; slightly porous
	52%			13%		34%		1%	100%	vcu	ms	fu			
S18T-2012	191	15	8	9	54	243	13	9	542	1	0.01	0.2	angular to sub-angular; poorly sorted	Matrix-poor Sandstone	towards top = abundant f-vfg subgrains
	39%			12%		47%		2%	100%	cu	fs	fu			
S19B-2012	291	15	6	0	172	48	8	7	547	1.4	0.03	0.23	sub-rounded; moderately sorted	Intermediate Clayey Sandstone	waftite; floating grains; minor Q recrystalization;
	57%			31%		10%		1%	100%	vcu	ms	fu			
S19T-2012	263	13	2	5	32	192	11	9	527	0.7	0.02	0.2	sub-angular; moderately sorted	Matrix-poor Sandstone	darker, more compact top (see macro pic); abundant
	53%			7%		39%		2%	100%	cu	fs	fu			
S1A-2013	20	1	0	0	7	31	4	13	76	1	0.02	0.22	sub-rounded to subangular; poorly	Matrix-poor Sandstone	intermediate matrix (visually)
	28%			9%		46%		17%	100%	vcl	ms	fu			
S1C-2013	71	4	1	0	30	0	0	0	106	0.2	0.01	0.07	sub-rounded; well sorted	Intermediate Clayey	no subgrains; visable matrix
	72%			28%		0%		0%	100%	fl	fs	vfl			
S1D-2013	62	0	7	37	77	0	0	0	183	0.1	0.01	0.06		Fine-Graned Banded Sandy Siltstone	
	38%			62%		0%		0%	100%	fl	fs	cs			
S2A-2013	43	1	2	0	44	0	0	0	90	0.5	0.03	0.17	sub-rounded to sub-angular; poorly sorted	Matrix-rich Sandy Claystone	
	51%			49%		0%		0%	100%	cl	ms	fl			
S2C-2013	44	0	0	41	79	0	0	0	164	0.1	0.01	0.04	sub-rounded to sub-angular; poorly sorted	Matrix-rich Sandy Claystone	
	27%			73%		0%		0%	100%	vfl	fs	cs			
S4B-2013*	45	1	0	0	11	30	2	0	89	0.8	0.05	0.24	sub-angular; poorly sorted	Matrix-poor Sandstone	
	52%			12%		36%		0%	100%	cu	cs	fu			
S4D-2013*	42	1	3	0	7	10	0	0	63	2.4	0.04	0.32	sub-angular; moderately sorted	Matrix-poor Sandstone	
	73%			11%		16%		0%	100%	gr	cs	ml			
S4E-2013	too fine to accuratley count									0.1	0.02	0.04		Fine-Graned Banded Sandy Siltstone	
										cs	ms	cs			

gr=granules; vcu=very coarse upper; vcl=very coarse lower; cu=coarse upper; cl=coarse lower; mu=medium upper; ml=medium lower; fu=fine upper; fl=fine lower; vfu=very fine upper; vfl=very fine lower; cs=coarse silt; ms=medium silt; fs=fine silt

sample	mx		mn		ave	
S1-2012	1.221962	vcl	0.034	cs	0.30644	ml
S11-1-2012	2.144706	granules	0.013463	fs	0.330981	ml
S6-2012	1.590261	vcu	0.024818	ms	0.236998	fu
S9-2012	0.506278	cl	0.01904	ms	0.139877	fl
S16-2012	0.910791	cu	0.02856	ms	0.22162	fu
S21-2012	1.207001	vcl	0.019472	ms	0.192881	fu
S23-2012	0.89445	cu	0.01904	ms	0.169277	fl
S2B-2012	0.628432	cl	0.042575	cs	0.202914	fu
S3B-2012	1.117589	vcl	0.015918	fs	0.193135	fu
S3T-2012	0.573017	cl	0.016601	ms	0.13939	fl
S5B-2012	0.581002	cl	0.03944	cs	0.174223	fu
S5T-2012	0.091606	vfu	0.010965	fs	0.053768	cs
S7B-2012	1.068771	vcl	0.051787	cs	0.220927	fu
S7M-2012	0.737429	cu	0.03944	cs	0.17848	fu
S8B-2012	1.251639	vcl	0.051267	cs	0.236863	fu
S8M-2012	0.860012	cu	0.028689	ms	0.185877	fu
S10B-2012	0.667551	cl	0.024214	ms	0.195503	fu
S12B-2012	1.43528	vcu	0.017732	ms	0.206505	fu
S12M-2012	1.11833	vcl	0.026266	ms	0.215886	fu
S12T-2012	0.740706	cu	0.01088	fs	0.199441	fu
S13B-2012	0.869376	cu	0.04039	cs	0.222507	fu
S13TA-201	0.532304	cl	0.073049	vfl	0.244668	fu
S13TB-201	0.127209	fl	0.017732	ms	0.067227	vfl
S14B-2012	0.595925	cl	0.023477	ms	0.152377	fl
S14T-2012	0.862679	cu	0.026266	ms	0.174185	fl
S15-2012	1.115824	vcl	0.013463	fs	0.184232	fu
S17B-2012	1.144995	vcl	0.01496	fs	0.170902	fl
S17M-2012	1.417788	vcu	0.00952	fs	0.158683	fl
S17T-2012	0.996131	cu	0.024818	ms	0.204387	fu
S18B-2012	0.609869	cl	0.021287	ms	0.145855	fl
S18M-2012	1.705712	vcu	0.027538	ms	0.19922	fu
S18T-2012	0.968695	cu	0.0136	fs	0.197751	fu
S19B-2012	1.433115	vcu	0.026266	ms	0.229358	fu
S19T-2012	0.703784	cu	0.015918	fs	0.197532	fu
S1C-2013	0.16864	fl	0.01496	fs	0.066618	vfl
S1D-2013	0.134613	fl	0.014711	fs	0.059274	cs
S1A-2013	1.020077	vcl	0.024214	ms	0.215766	fu
S2A-2013	0.51272	cl	0.02856	ms	0.174149	fl
S2C-2013	0.080551	vfl	0.01224	fs	0.036229	cs
S4B-2013	0.764998	cu	0.04896	cs	0.242167	fu
S4D-2013	2.365046	granules	0.039252	cs	0.318022	ml
S4E-2013	0.061547	cs	0.019233	ms	0.038068	cs

Table 1: List of maximum, minimum and average grain sizes measured for each sample.

Appendix C: Photomicrographs of Petrographic Samples

Sample	XPL 1.25 Magnification	XPL 5X Magnification
S4F-2013		
S4E-2013		
S4D-2013		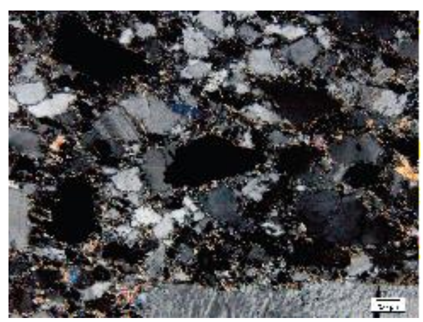
S4B-2013	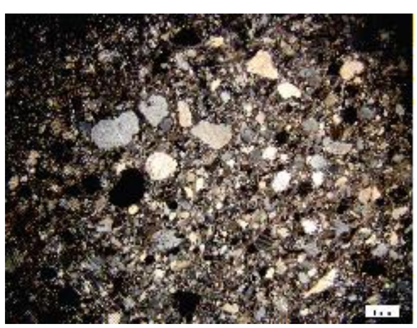	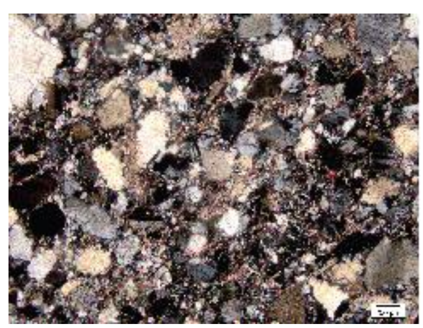

Sample	XPL 1.25 Magnification	XPL 5X Magnification
S13T-2012	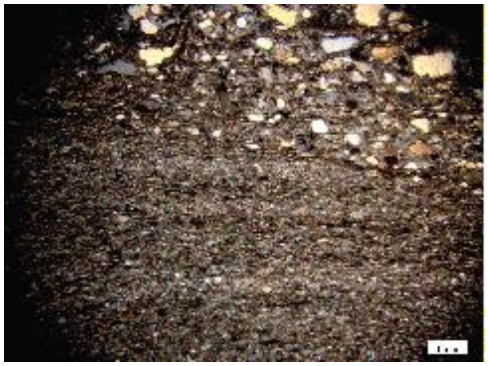	
S13B-2012		
S12T-2012	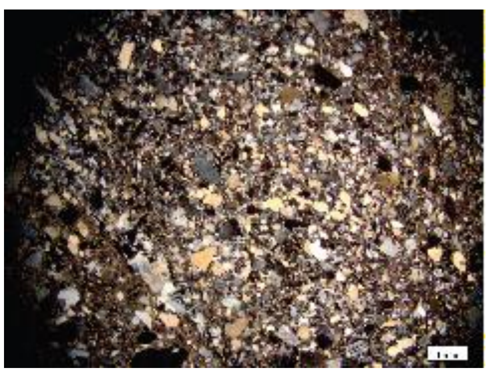	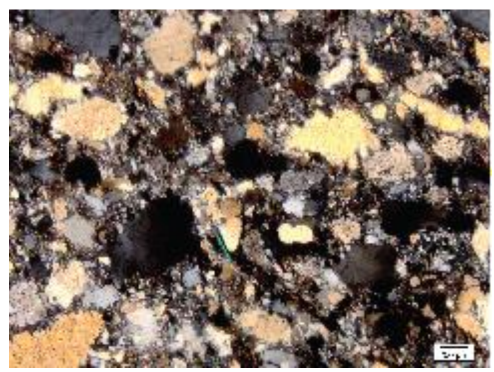
S12M-2012	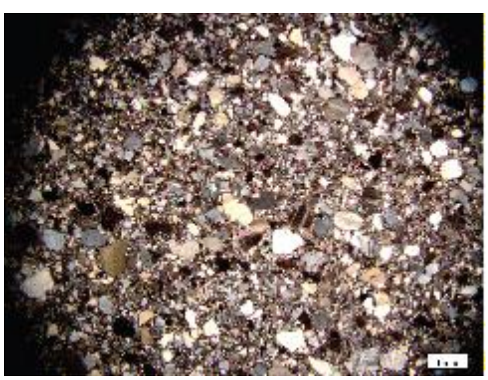	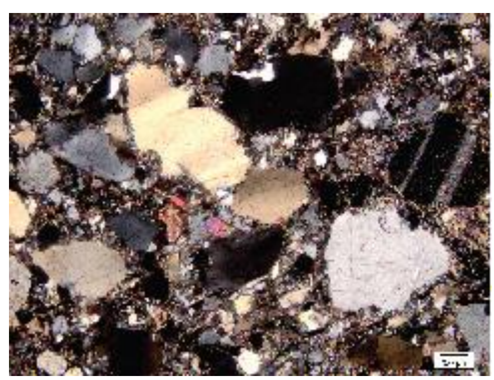

Sample	XPL 1.25 Magnification	XPL 5X Magnification
S23-2012	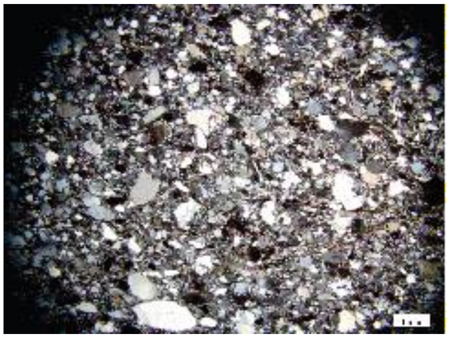	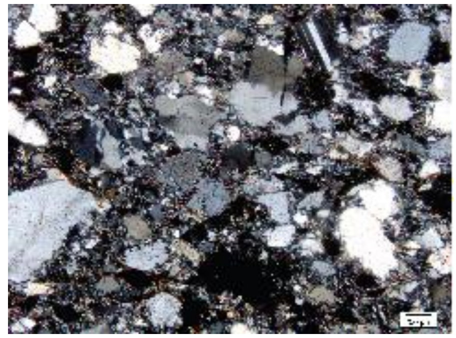
S21-2012	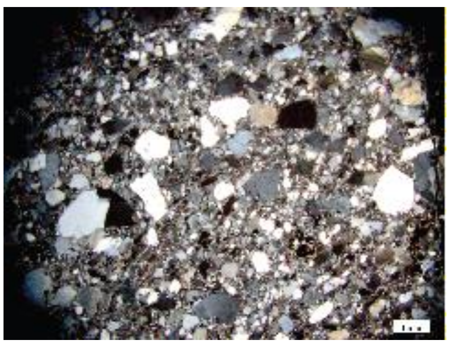	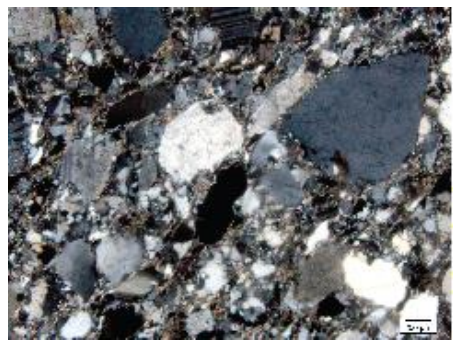
S19T-2012		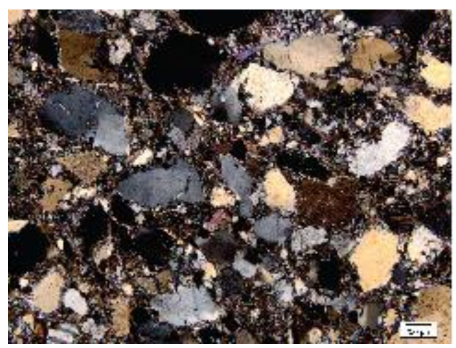
S19B-2012	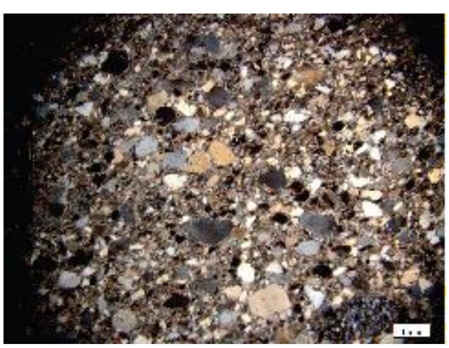	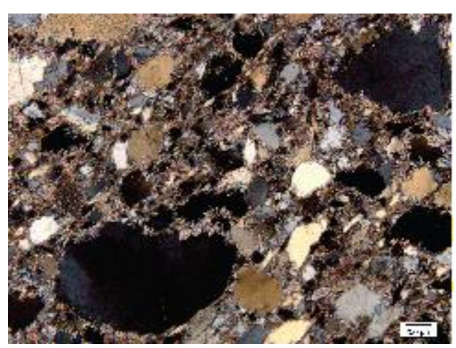

Sample	XPL 1.25 Magnification	XPL 5X Magnification
S17T-2012	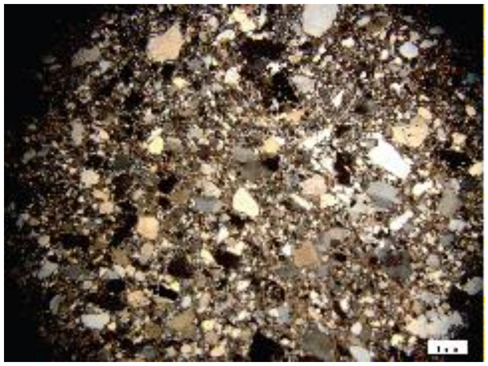	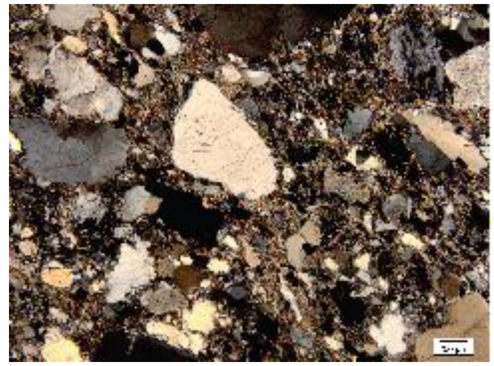
S17M-2012		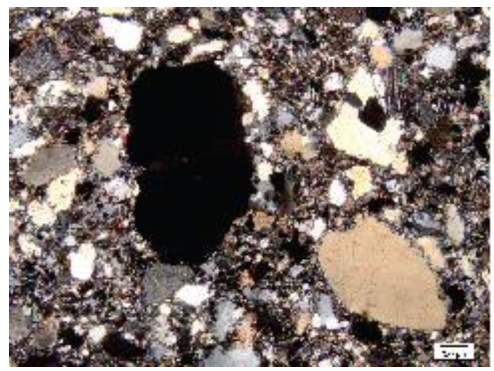
S17B-2012	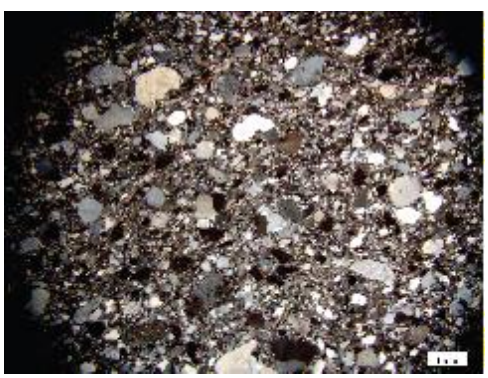	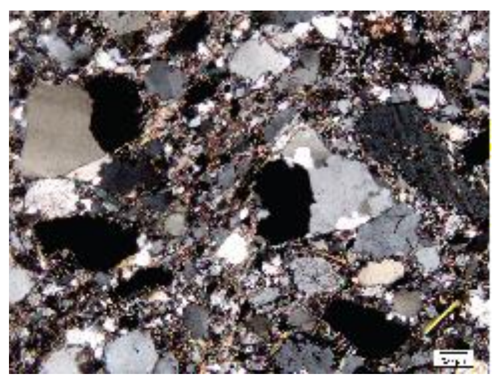
S16-2012		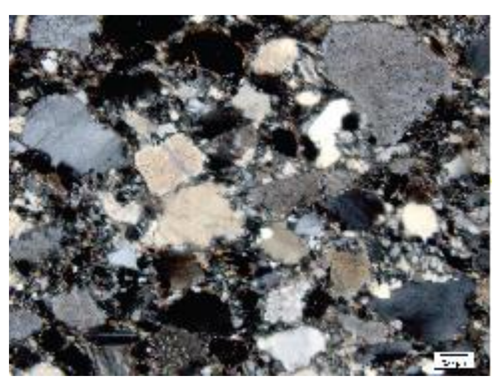

Sample	XPL 1.25 Magnification	XPL 5X Magnification
S8M-2012		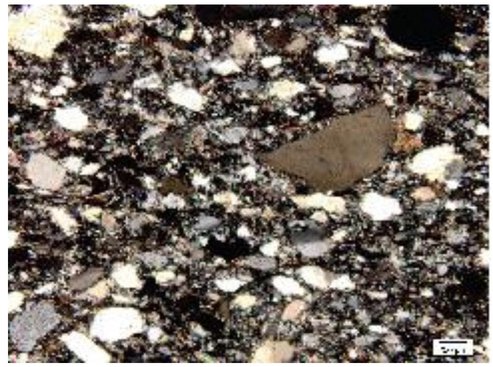
S8B-2012	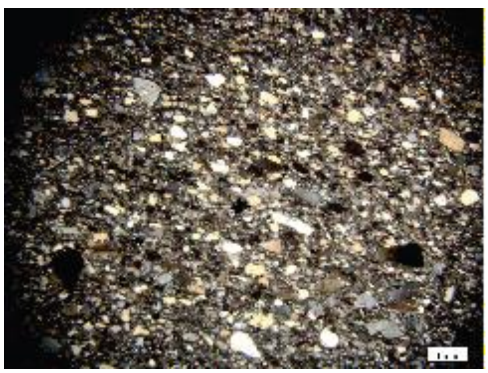	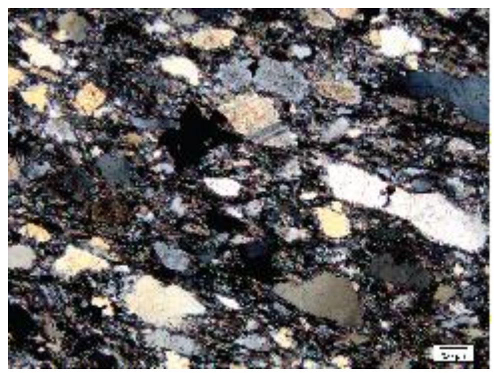
S6-2012	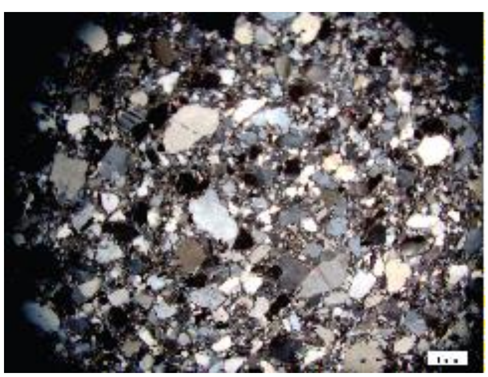	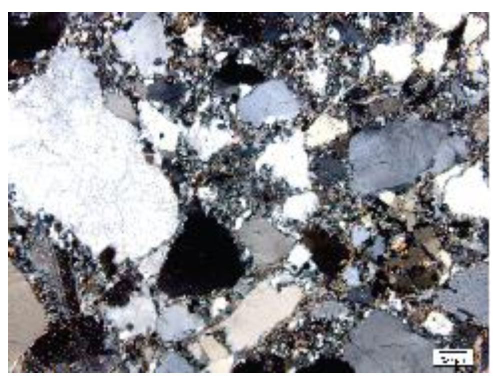

Appendix D: Lateral Facies Change Description Tables

LOG / BED	L4A-18	L3-18 – 20	L3A-26 – 28	L2-42 – 45	Truncated by scour towards L1-1 (NW)
Thick-ness	107cm	18: 23cm 20cm; 3cm [2cm dtc; 1cmC] 19: 21cm 16cm; 5cm [4cm dtb; 1cmC] 20: 23cm 20cm; 3cm [3cm dtb]	26: 12cm 6cm; 6cm [2cm dtb; 4cmC] 27: 26cm 16cm;10cm [4cmdtbc; 6cmC] 28: 32cm 24cm; 8cm [2cmdtb; 6cmC]	42: 21cm 43: 21cm (and thinner) 44: 12-24cm 45: 8cm [2cmdtb*c; 6cmC]	NA
Grain size	b: g, vc-c t: uc – um	18: vc→mu cap=fu to mud 19:cl→mu cap=fu to mud 20: cl→mu cap=fu to mud	26:mu cap= vfg to silt/mud 27mu cap=fu to mud 28:cl/mu cap=vf to mud	42:ml/mu disp cl 43: fu – silt/mud 44:mu w dis cl 45:f-vfg to mud/silt	NA

Note: the LOG / BED row content: L4A-18: matrix-poor ss; L3-18 – 20: -sandy waft+dtbc
-w+dtb
-w+dtb; L3A-26 – 28: -sandy w + dtb
-w+dtcb
-w+dtb; L2-42 – 45: ????????????
w no c, tc*de?, waft +dtbc

Notes	Large mc	18 and19 = many mc	26:mc at boundary 27:mc in ta	44 scours out tcde	NA
Trend	-From matrix-poor to sandy waft to waft w dtbc caps….beds get waftier (tj muddier) -generally, thickness of mudcap increases from L4A-L3A..thickness of dtbc stays relatively constant. Over ~250m				

LOG / BED	**L3A-42** tri-w	**L2-66** bi?-w or w+dtbc	**L1-62-64** -w+dtbc -banded dtb 5couples -w			**L1A-30-32** -w -tbt ~5sets -w+dtc		
Thick-ness	20cm ta:7cm ii:4cm dtb:8cm	19cm ta:9cm dtbc:3cm mudcap:8cm	62 23cm ta:20cm dtbc:3cm	63 34cm i:4cm[2;2] ii:6cm[2,4] iii:11cm[4,7] iv:7cm[2,5] v:7cm[2,5]	64 15cm ta:8cm dtb:2cm cap:4cm	30 18cm ta:11cm cap:7cm	31 31cm tbcde:4cm tbcde:6cm tbcde:7cm tbcde:8cm tbcde7cm	32 10cm ta:5cm dtc:2cm cap:3cm
Grain	ta:cu/cl w mu	ta:mu w cl/cu	G,vc to mu	fl-vf	ta:cl-mu	g,c disp	fu/fl	ta:mu/ml

size	ii:mu w ml-vf dtb: vfg/silt	dtbc: vfg/fl, some silt cap:mud	dtbc: fu	silt/mud	dtb:fl cap:mud/silty	mainly ml/mu cap:vfu/silt		dtc:fu cap:vfg/silt
Notes	Abrupt gs change between ta and ii (+color) and ii and dtb		L1-62 correlates to L2-66, L1-63-63 appear…most likely from opening up/expanding dtbc in L2 --64: mudclasts along boundary between ta and dtb			--30 mudclasts in upper part of ta, + trailing clasts at boundary --31 tc very thin, less than 1cm		
Trend	fg portion stays continuous or thickens; banded beds appear in L1, possibly associated with w underneath this ‘expansion’ with couplets is common throughout the study area							

LOG / BED	**L5-33** **L5-34.1**	**L4-38**	**L4A-34**	**L3-34-35**	**L2-61**	**L1-58-58i**	**L1A-26b,c**
	int.ta+dtb	int.ta+dtb cap	int.ta+dtb cap	-sandy waft? -dtb+cap	tri-w	2 w	2w

	cap									
Thick-ness	47cm ta:34cm dtb:3cm cap:10.5cm	44cm ta:34cm dtb:2cm cap:8cm	33cm ta:21cm dtb:4cm cap:8cm	17cm	12cm dtb:3cm cap: 9cm	20cm ta:4.5cm ii:4cm dtb:3cm cap:7cm	15cm ta:4cm cap:10cm	15cm ta:6cm cap:9c m	13cm ta:5cm dtb:5cm dtc:3cm cap:8cm	11cm ta:3cm cap:8cm
Grain size	ta: G,vc,c disp →to mu dtb:fu/ml cap:silty mud	ta:mu dtb:ml/fu cap:silt/ mud	ta:disp vcg/cg, mu dtb:vfg/fl cap:silty/ mud	Vc/c disp, mu	dtb:ml/fu cap:silty mud	ta:mu w some cg ii:ml/fu dtb:fl/fu cap:vfg/s ilt/mud	ta: mu, ta 2:ml caps:vfu, silt, mud --dtc at boundaries between ta and cap (very thin..less than 1.5cm)		Ta:ml/m u tbc:fu/fl cap:silt,v fg,	Ta:fu some ml cap:silt/vf g
Notes		2 mud clasts in mrta		-few mudclasts in dtb (stringy)		Stringy mudclast s at boundary	-mudclasts, many/abundant stringers		Within mrta, many wispy/elongated clasts.	
Trend	Over ~400m; obvi: intermediate ss grades into mrta; tri-w splits into two w; mud caps stay relatively even.(??); loose vcgs, cg….thickness of ta decreases, matrix content increases.									

LOG /	**L5-31**	**L4-35**	**L4A-30**	**L3-31AB**	**L3A-37**	**L2-57**	**L1-54**	**L1A-23**
BED	int TA + cap (very very dtb*	int TA + cap	int ta may be 2 beds..~67cm.. at clasts	2 int ta's no caps!	int ta + dtb and very thin cap	int ta + dtbc cap	int ta +cap	turbidite sequence TABC*DE
Thick-ness	174cm 163cm; 11cm	166cm 159cm;7cm [1cm fl; 6cm fu/vfg	116cm 112cm; 4cm dtb	A: 67cm= L3A-37 B: 40cm = L3A-38	43cm 38cm; 5cm [4.5cmdtb;0.5cmC]	59cm 42cm;13cm [11cmdtbc; 2-3cmC]	48cm 28cm;20cm	34cm ta: 18cm tbc: 11cm tde:5cm
Grain size	-Vcl → mu/cl -cap=silty mud	-g-cgs → mu -cap=fl-vfg	Vc-c →mu cap=fu/fl	g,vcg,cu→mu /cl (both)	Vc/cg→ml/fu	Cgs→ml cap=fu/fl with mud/silt 0.5cm	cgs→mu cap: LG ml/fu DG fl/vfg..silty	Ta: vc/cgs→ml Tbc: ml/fu tde:silt/mud
Notes	Very large tbt clast	Many clasts in middle of	Many clasts concentrated	Few mudclasts in		Mud clasts within	Few mudclasts in	

	232cm x 20cm	ta portion	at ~67cm	middle of beds		middle/upper portion of TA	TA portion -LGdtc, DGdtb	
Trend	Ta portion of bed decreases in thickness significantly, 'cap' portion of beds increases in thickness, from very thick ta to tbt sequence over ~400m							

LOG / BED	**L7-25** int.ta+fg cap	**L6-33A** int.ta+fg cap	**L5-34(upper)** sandy w+dtc+cap	**L4-40** tri-w	**L4A-36** w no cap, +dtc
Thick-ness	80cm ta:64cm fg cap:16cm	68cm ta:53cm cap:15cm	21cm sw:4cm dtc:4cm cap:13cm	14cm ta:3cm ii:2cm dtc:2cm cap:8cm	10cm dtc:1-2cm

Grain size	ta: mu w ml cap: vfl→silt	ta:ml w mu/cl cap:fl/vfg	sw:mu w cgs dtc:ml/fu cap:vfg/silt	ta:mu w c+vgs ii:mu dtc:fu cap:mud	Ta:ml/fu w mu,cg, dtc:fu/lighter grey
Notes	Some dtb in cap	Large elongated clast in ta, 1.5mx4cm		Abrupt colour and gs changes	Mudclasts throughout ta portion
Trend	General: from int.ta to matrix rich bed. Intermediate, sandy w, tri, classic(ish) w. Obvious decrease in thickness, and increase in mud content, and slight decrease in grain size. Over 250m				

LOG / BED	**L7-25** int.ta+fg cap	**L6-33A** int.ta+fg cap	**L5-34(upper)** sandy w+dtc+cap	**L4-40** tri-w	**L4A-36** w no cap, +dtc
Thick-ness	80cm ta:64cm fg cap:16cm	68cm ta:53cm cap:15cm	21cm sw:4cm dtc:4cm cap:13cm	14cm ta:3cm ii:2cm dtc:2cm cap:8cm	10cm dtc:1-2cm
Grain size	ta: mu w ml cap: vfl→silt	ta:ml w mu/cl cap:fl/vfg	sw:mu w cgs dtc:ml/fu cap:vfg/silt	ta:mu w c+vgs ii:mu dtc:fu cap:mud	Ta:ml/fu w mu,cg, dtc:fu/lighter grey
Notes	Some dtb in cap	Large elongated clast in ta, 1.5mx4cm		Abrupt colour and gs changes	Mudclasts throughout ta portion

Trend	General: from int.ta to matrix rich bed. Intermediate, sandy w, tri, classic(ish) w. Obvious decrease in thickness, and increase in mud content, and slight decrease in grain size. Over 250m

LOG / BED	**L10- 15** mp-ta	**L9-13** ta (int. ss)	**L8-16,17** 2 w		**L7-14,15** 2 w		**L5-18,19** 2w +dtc		**L4-20-22** 3w 21 is a baby bed			**L3-12-15** fg dtb w w		
Thick- ness	70	45	27 ta:22 cap:5	20 ta:18 cap:2	23 ta:13 dtb+cap: 10	20 ta:17 cap:3	29 ta:13 ii:3 dtc:3.5 cap:2.5	18cm ta:13 dtc:4.5 cap:<0.5	27cm ta:18 ii:4 dtc:2 cap:2	4cm ta: 3.5 cap:0.5	7cm ta:6c m cap:1c m	12cm	18cm ta:10 cap:8 14=3c mC	12cm ta:4c m cap:8 cm
Grain size	mu w disp	ml/mu w disp	Ml/fu w few	Ta:fu/m l w	Ta:fu/ml w mu	Ta:fu.m l w mu	Ta:mu w cgs	Ta:mu w cl	Ta:mu w disp	Fu/ml cap:silt	Fu/ml cap:sil	Fu	Mu w some	Ta:m u w cl

	g, +vcg, cgs	vcg,cg	cg cap:vf,silt	some mu cap: vfg,silt	cap:fl→vfg/silt	cap:vfg/silt	ii:fl dtc:fu cap:mud/silt	dtc:fu cap:silt/mud	vcg cgs ii:fl dtc:fu cap:silty		t		cl cap:vfg→mud	cap:vfg→mud
Notes	Very Zn 'cap' <0.5cm	Bluey colour					Mudclasts in mrta, elongated. ii is darker than mrta	Mudclasts in middle	Mudclasts in mrtas			12: cap is all stringy looking/mc? 13: mudclasts in mrta 14=3cmC		
Trend	From mpss to int.ss to waft-classic to waft+dtbc, can follow one waft into fg dtb., as you progress beds get muddies, and more stratified. Grain size also slightly decreases (esp from mp to mr and mr to fg) (from log 10 to log 3)													